AN EXPERIMENTAL STUDY OF FLOW AROUND BED FORMS

Cristian Filippo Giuseppe Cottino

A project report submitted to the Faculty of Engineering, University of the Witwatersrand, Johannesburg, in partial fulfilment of the requirements for the degree of Master of Science in Engineering.

Johannesburg, 1992.

DECLARATION

I declare that this thesis is my own, unaided work. It is being submitted for the Degree of Master of Science in Engineering in the University of the Witwatersrand, Johannesburg. It has not been submitted before for any degree or examination in any other University.

____

30th day of August 1993

ABSTRACT

The interaction between sedimentary dunes and turbulent flow is studied under controlled laboratory conditions. The flow of water over artificially roughened two-dimensional dunes varying in geometry and surface roughness is analyzed in a laboratory flume. Measurements of flow depth, length of separation, bed pressure and grain shear stress are recorded.

These data represent a unique set that can be used to calibrate and test present and future sediment transport models. A method for calibrating Preston tube readings is also presented.

The average flow depth over dunes can be calculated using the crest flow depth and the dune height, even under non-uniform flow conditions. The length of separation was found to be 0.25 to 0.4 times the dune wavelength. Bed pressures are at a maximum within the separation zone, decreasing from the reattachment point to a minimum at the crest.

Grain shear stress distributions show a maximum at the dune crest and a strong dependence on the combination of particle size and dune geometry rather than on the former alone.

To my father, Mario, for giving me the opportunity and the will to achieve, and to Debbie for all her love and patience.

ACKNOWLEDGMENTS

I would like to express my sincere gratitude to my supervisor, Professor C.S. James for his support, teachings and patience throughout the duration of this work and during my studies.

The work communicated in this report was funded by the Chamber of Mines Research Organisation (COMRO) and forms part of their research programme. The author wishes to acknowledge his appreciation for their permission to submit this report and for the assistance received.

Grateful acknowledgement is manifested to the technicians of the Department of Civil Engineering for their assistance in setting up the experiments.

Finally my deepest gratitude goes to my family and friends for their support during my graduate studies.

CONTENTS **Page**

LIST OF FIGURES

LIST OF TABLES

LIST OF SYMBOLS

Symbol	Definition
A	Frontal area of Preston tube
dA	Elemental frontal area of Preston tube
a	Horizontal projection of lee side of artificial dunes
C'	Chezy coefficient
c	Constant parameter
D	Depth of uniform flow
D_*	Dimensionless particle diameter
D_{50}	Representative particle size
d_i	Internal diameter of Preston tube
d_o	Outer diameter of Preston tube
Fr	Froude number
F_h	Flume height
F_l	Flume length
F_w	Flume width
f	Reading point factor
G	Geometry of artificial dunes
g	Acceleration due to gravity
H	Average flow depth
H'	Mathematical average flow depth
dH	Additional depth correction factor
H_e	Effective flow depth
h	Flow depth at a given point
h_{cr}	Flow depth at dune crest
h_{in}	Flow depth at flume inlet
k	Typical roughness length
k_s	Relative roughness of sand grains
L	Length of zone of separation
m_o	Constant parameter
n_o	Constant parameter
Q	Flow rate
R_b	Hydraulic radius related to bed geometry
Re	Reynolds number

Re_*	Shear Reynolds number
S	Roughness of artificial dunes
S_s	Specific density of sediment material
T	Transport stage parameter
t	Preston tube wall thickness
u	Point flow velocity
u_*	Bed shear velocity
$u_{*,cr}$	Critical bed shear velocity
u_*'	Bed shear velocity related to grains
v	Average flow velocity
y	Distance from theoretical bed
y_o	Distance of theoretical bed below top of channel bed surface
Δ	Average dune height
ΔP	Velocity head or dynamic pressure
δ	Dune steepness ratio
δ_s	Viscous sub-layer thickness
Z	Dimensionless variable
η	Dimensionless variable
θ	Downstream or toe angle of dunes
κ	von Karman's constant
λ	Average dune length
λ'	Horizontal projection of stoss side of artificial dunes
λ_*	Average burst length
ν	Fluid kinematic viscosity
σ	Standard deviation
T_0	Total bed shear stress
$(T_0)_{cr}$	Critical bed shear stress
T_0'	Form shear stress
T_0''	Grain shear stress
$T_0''_*$	Dimensionless grain shear stress
$T_0 V$	Stream power
X	Reynolds grain size number
Ω	Dimensionless length of separation = L/Δ
ω	Dimensionless length of separation = L/λ

Chapter 1
INTRODUCTION

1.1 General

In most streams and rivers the flow of water over a bed composed of non-cohesive sedimentary material interacts with the sediment to create a dynamic system in which a number of possible bed form configurations can arise. Turbulent flow characteristics, such as flow depth, flow velocity and fluid drag and lift on bed material, as well as transport characteristics, such as the rate at which sediment moves along the channel bed and in suspension, are influenced by bed forms. This makes bed configuration a very important parameter in the study of hydraulic and sedimentary phenomena. At the same time however, the various bed forms are in turn strongly dependent on these very same flow characteristics, as well as on sediment properties, such as particle size, particle density and relative roughness. This dynamic system is represented graphically in Figure 1.1 .

This inter-dependency is the critical distinction between alluvial channels and rigid channels: the latter are characterized by single-phase flow with the only unknown boundary being the free water surface, whereas the former display two-phase flow with the bed profile being the additional unknown boundary.

Therefore any study of alluvial channel behaviour would involve the relationship between flow parameters, fluid and sediment properties and the hydraulic roughness of the channel.

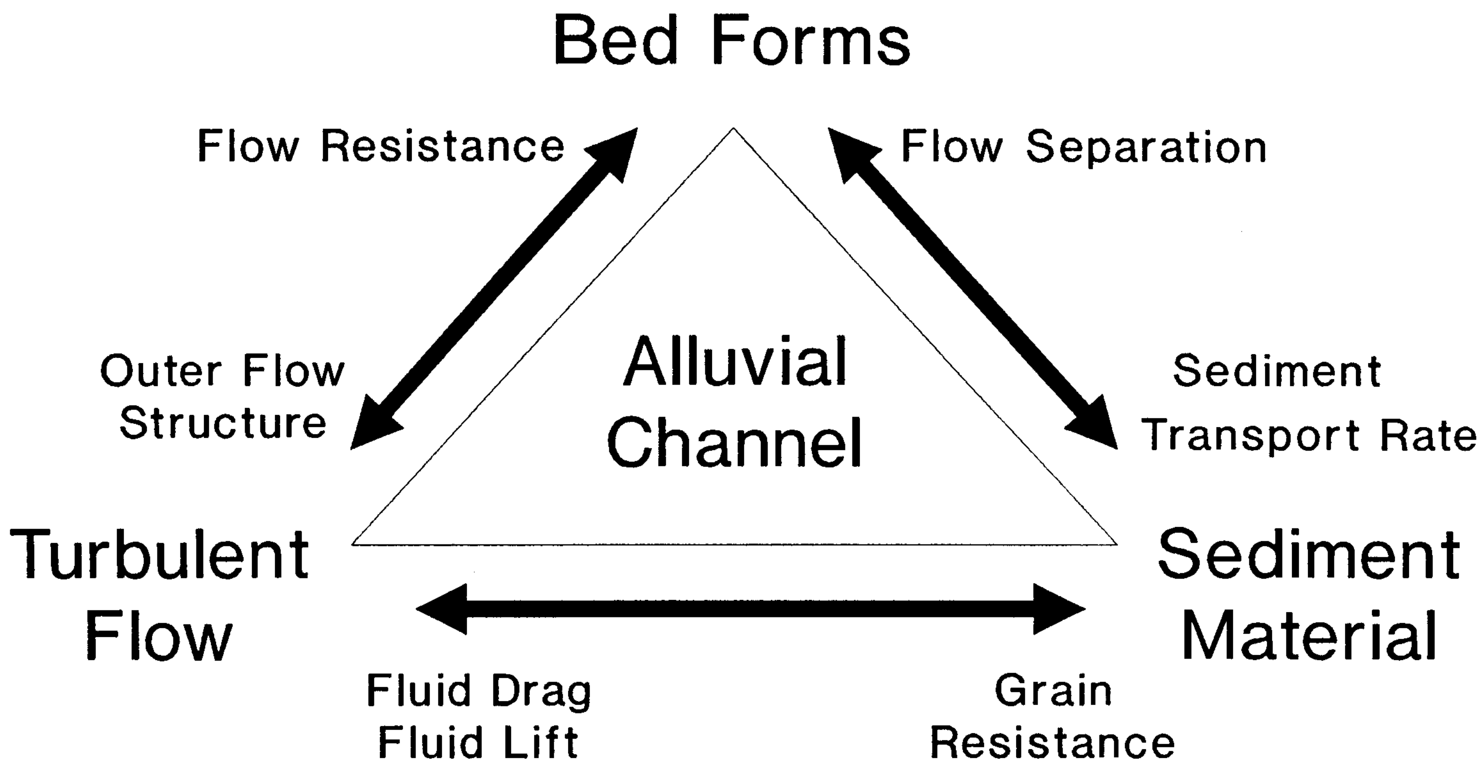

Figure 1.1 The alluvial channel: a dynamic system

Simons and Richardson (1966) presented a classification of bed forms which has become widely accepted. They identified various configurations as a function of the stream power, $T_0 v$, where T_0 is the total bed shear stress and v represents the average flow velocity. As the stream power increases, the bed forms change from very rugged arrays of ripples and dunes that are generated at lower discharges, to flat beds, antidunes and chutes characteristic of larger discharges and higher flow velocities. Among this large variety of possible bed forms, dunes have been studied the most and a number of characteristics that differentiate them from the other bed configurations have been identified.

Dunes are expected to occur in subcritical flows, where the Froude number is less than one ($Fr < 1$): this is confirmed by the fact that the dune profile and the water surface profile are found to be out of phase and the flow is thus essentially non-uniform. The dune itself, when looking in a vertical cross-section, has a quasi triangular shape with the vertex shifted forward in the downstream direction. The upstream face has a gentle slope and is often referred to as the stoss side, whilst the downstream face has a more steep slope and is referred to as the lee side of the dune and the two faces join at the crest. This geometry is shown in Figure 1.2.

As the flow of water passes over each dune, separation occurs at the crest giving rise to a wake or eddy which extends downstream from the crest, over the lee side, and ends at the reattachment point located on the stoss side of the following dune (See Figures 1.3 and 1.4). Within this zone of separation reverse circulation or back flow is present and its erosive action is of great importance to the movement of the dunes and to the preservation of their characteristic shape.

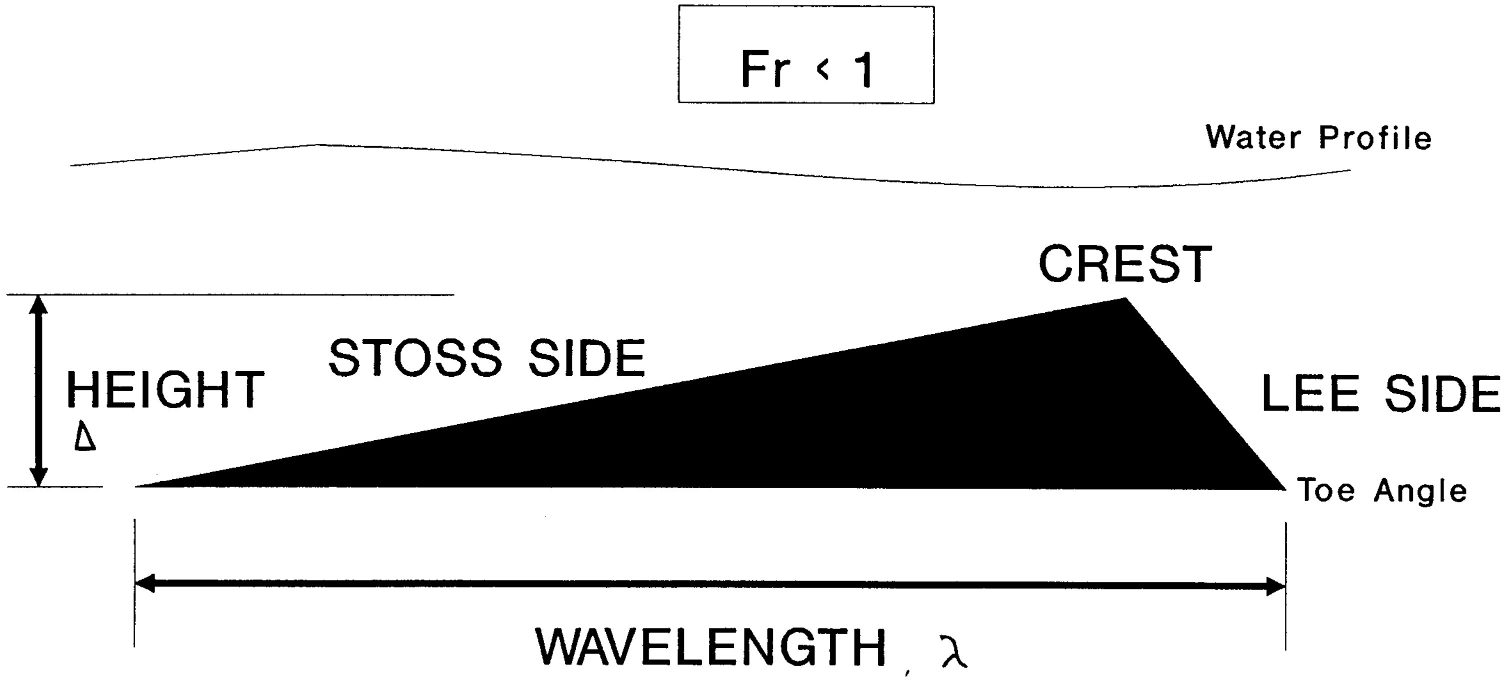

Figure 1.2 The geometry of alluvial dunes

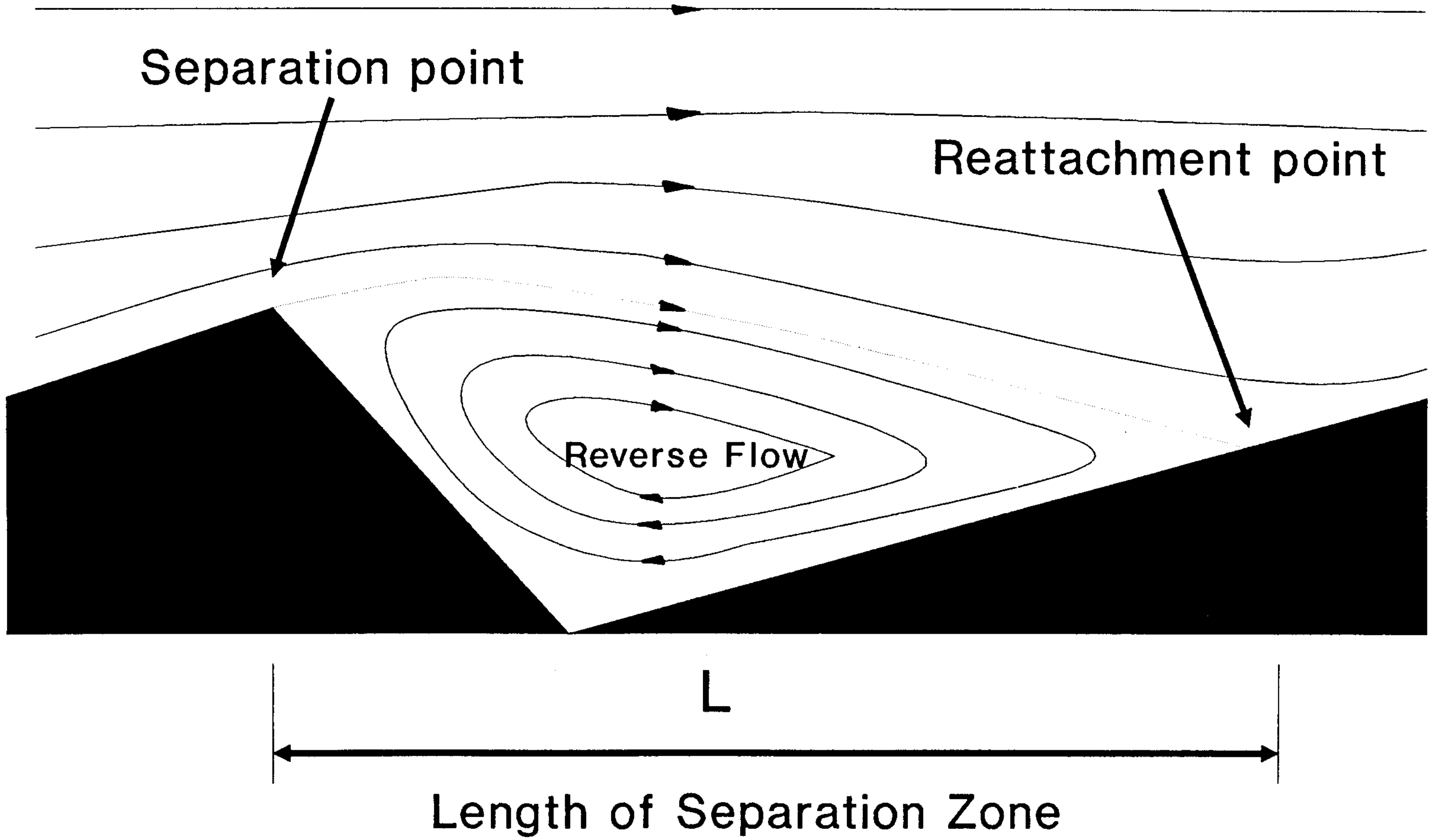

Figure 1.3 The zone of separation behind dunes

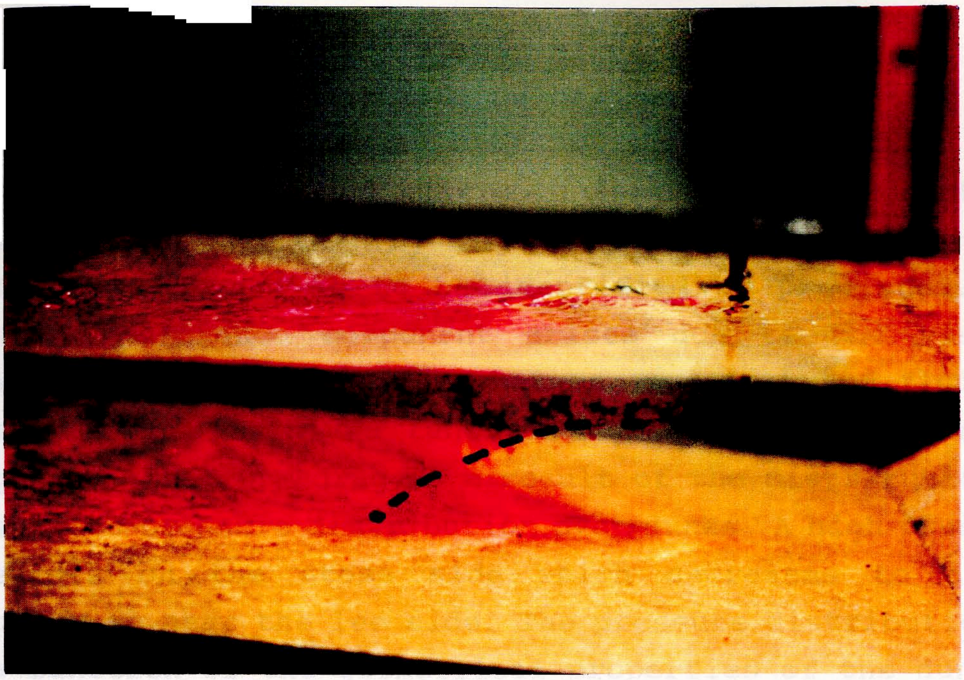

Figure 1.4 Experimental detail of the reattachment point

Dunes occur in series and form a mobile train on the bottom of an alluvial channel: sedimentary material is thus continuously transported and deposited within the dunes and therefore their presence and geometry greatly affects the transport rate of bed load material.

Research conducted by Yalin (1987) has linked the formation of dunes on an alluvial bed to the presence of turbulent flows and in particular to a cyclic bursting of cylindrical vortices associated with the physical nature of this type of flow. Therefore knowledge of the behaviour and characteristics of turbulent flow becomes essential if the interaction between dunes and the flow associated with their presence is to be studied.

The resistance to flow exerted by bed configurations can generally be divided into two components, namely:

(i) Form resistance or form drag, and
(ii) Skin resistance or grain shear.

In dunes it is found that both form and skin resistance are present and thus both must be considered if the true flow resistance is to be identified or predicted. The skin resistance component arises due to the viscous stresses at the interface between sediment and fluid, and is thus mainly a function of the properties of the grains. The form drag is a result of the distribution of surface pressure distribution over dunes. A high pressure exists on the stoss side which decreases to a low pressure near the lee side. The pressure distribution is a function of the geometrical properties of the dune.

The total bed shear stress can be represented by

$$T_0 - T_0' + T_0'' \qquad \ldots(1.1)$$

where T_0 = Total bed shear stress
T_0' = Form shear stress
T_0'' = Grain shear stress

In studying the interaction between sedimentary dunes and turbulent alluvial channel flows, three aspects were identified as being a potential source of problem, namely:

(i) The effect of sediment particles being transported by the flow,
(ii) the dynamic nature of the dunes in that their

geometrical properties and position are varying with time and

(iii) the availability of equipment that would enable measurements of shear stress and pressure distributions over a mobile dynamic bed.

These problems were overcome by considering the idealized situation of having clear water, free of sediment in suspension, flowing over a train of artificially roughened, uniform, stationary dunes. These simplified conditions can be justified by the fact that the dune velocity along the bed of alluvial channels, is considerably less than the streamline velocity of the flow (Mendoza-Cabrales, 1987). The geometrical parameters of a number of dunes present in an alluvial channel are very similar and therefore the artificial dunes making up the train can all have an identical geometry.

The fact remains however that a dynamic system represented by turbulent flow and by constantly moving and evolving sedimentary dunes has been simplified as the dunes are now fixed and cannot interact freely with the flow. This aspect must be considered when interpreting the experimental results.

1.2 Overall aims of the study

The interaction between bed dunes and turbulent flow is an important aspect in the mechanisms and behaviour of alluvial channels, particularly in channel geometry changes, variations in flow depths under different flow conditions, and where the effects of channel roughness and resistance to flow are concerned. Studying this interaction is also useful in understanding sediment transport mechanisms and thus in the development and testing of sediment transport models.

The basic structure of a sediment transport model is shown in Figure 1.5 . Given certain known initial flow conditions (discharge) and the initial channel geometry parameters, a flow analysis module determines the resulting hydraulic properties of the flow (total bed shear stress, bed pressure distribution, bed velocity, flow velocity, flow depth). These in turn are used by the sediment transport module to determine the transport rates of the bed material.

To date, research concerning the interaction between turbulent flow and sedimentary dunes has been conducted by a number of researchers such as Raudkivi (1963), who reported an experiment of flow over a ripple that had been allowed to form naturally and then stabilized. Rifai and Smith (1971) conducted experiments with open channel flow over an idealized dune bed composed of a series of triangular elements whilst Vittal et al (1974) performed experiments on water as well as air flowing over a series of smooth and sand coated, two dimensional sharp crested triangular elements.

McLean (1976) carried out experimental measurements of natural sand waves in the Columbia River and Fehlman (1985) continued the series of idealized investigations by conducting experiments in a laboratory flume.

Further information and research is however required, in order to improve our understanding and to provide additional data with which to test the accuracy and validity of current and future sediment transport models (Mendoza-Cabrales, 1987).

This study is a contribution to the development of sediment transport models as it looks at the hydraulic properties of the turbulent flow that form the input to the flow analysis module. The properties studied and presented herein are:

(i) water profiles,
(ii) average flow depth,
(iii) length of separation,
(iv) bed pressure distribution and
(v) grain shear stress distribution.

Previous research has been directed to the analysis of one or two of these properties at any given time. The results of this study provide a unique set of data and information in that all these properties are, for the first time, studied simultaneously under the same dune geometry, bed roughness and flow conditions.

The effect of variations in these three parameters is carefully monitored, and the data presented herein results in a detailed experimental study of the interaction between turbulent flow and sedimentary dunes.

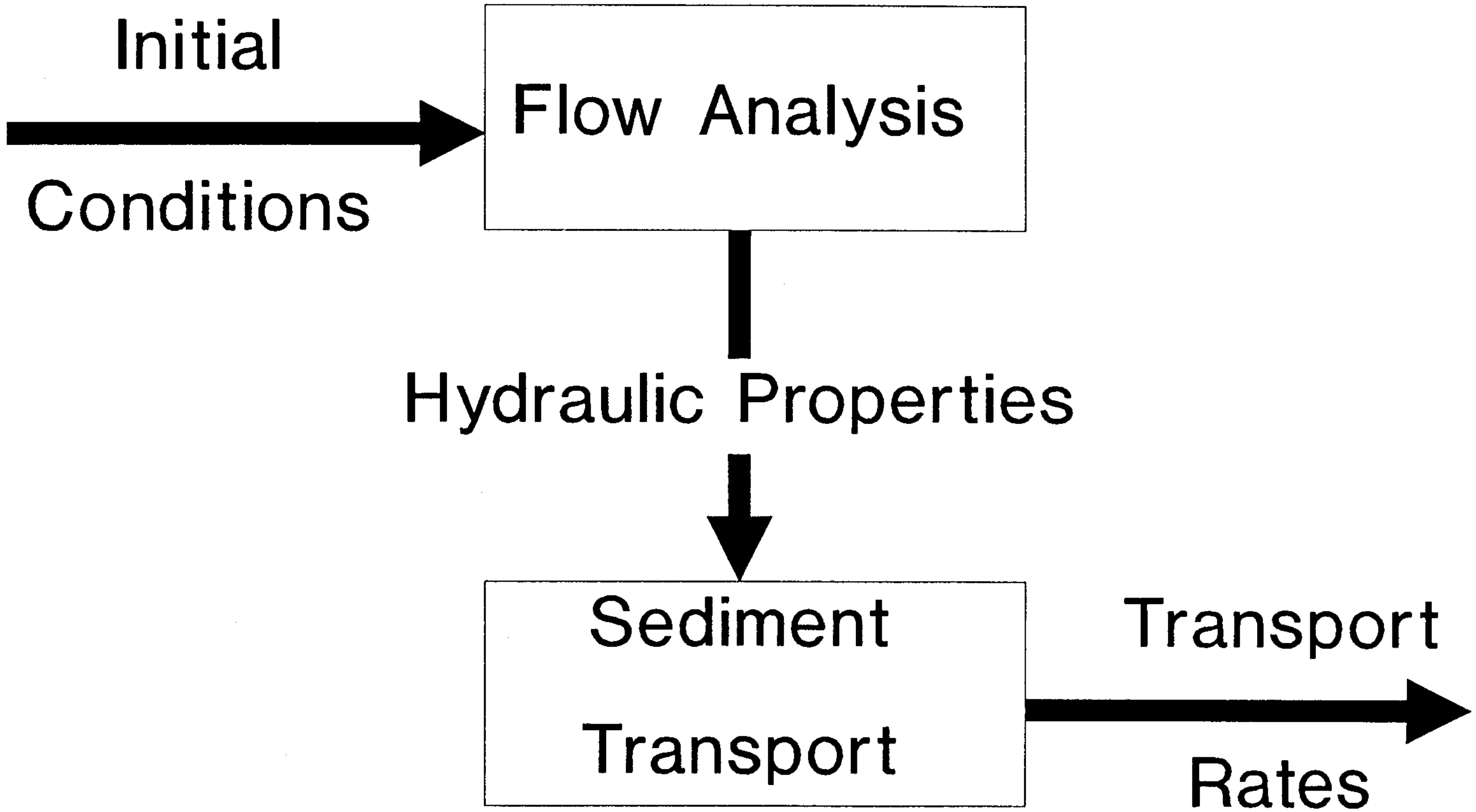

Figure 1.5 Structure of sediment transport models

Chapter 2
FORMULATION OF PROBLEM

2.1 Review of Previous Work

2.1.1 Structure of Turbulent Flow

Why turbulent flow ?
Turbulent flow has been identified with the presence of bed forms in an alluvial channel in most of the literature available on the subject. Jackson (1976), Leeder (1983) and Yalin (1987) in particular have put forward a theory linking the presence and dimensions of bed forms in subcritical flow (i.e. ripples and dunes) to turbulence and suggested that they are in fact a direct result of the eddy and streak bursting phenomenon characteristic of the turbulent flow boundary layer.

Eddy or streak bursting occurs when low-momentum fluid at the bed is periodically gathered into cylindrical vortices which are then thrust and pulled up into the faster outer current, were they eventually burst causing a sudden rush of fluid towards the bed. Yalin (1987) showed that the average burst length, λ_*, and the average dune length, λ, were given by the same product, (6-7)*H, H being the average flow depth, and therefore concluded that the dune length was in fact the impression of the burst length on the deformable, mobile bed surface.

It is therefore important to understand the complex nature of turbulent flow if the interaction between dunes and the flow associated with their presence is to be studied.

Turbulent flow

Turbulent flow is associated with fluid moving in irregular paths and with the presence of eddies which aid the mixing of the fluid. For practical purposes it can be sub-divided into three classes, the subdivision being dependent on whether the roughness elements on the bed boundary are protruding out of the viscous sublayer found near the boundary or not.

Given k_s = roughness height of the grains,
δ_s = viscous sub-layer thickness,
u_* = bed shear velocity and
ν = fluid kinematic viscosity

then if $k_s > \delta_s$ the viscous sub-layer is destroyed and we have fully rough turbulent flow;
if $k_s < \delta_s$ the viscous sub-layer is present and we have smooth turbulent flow.

The boundary layer thickness δ_s is related to the bed shear velocity by the following

$$\delta_s = \frac{c\nu}{u_*} \qquad \text{...(2.1)}$$

where c = constant found to be 11.6 .

Based on the these considerations a dimensionless parameter known as the Reynolds shear number has been developed :

$$Re_* = \frac{k_s u_*}{\nu} \qquad \text{...(2.2)}$$

Re_* is then used to identify the nature of the turbulent flow in that

if	$Re_* < 5$	the flow is smooth,
if	$5 < Re_* < 70$	the flow is transitional and
if	$Re_* > 70$	the flow is fully rough.

Velocity profiles in turbulent flows

Prandtl's mixing length theory (with von Karman's constant $\kappa = 0.4$) has been used to develop the velocity profile equations in turbulent flows, and it has been found that these profiles are logarithmic in nature. If y is the distance from the theoretical bottom and u the flow velocity at that point, then

$$\frac{u}{u_*} = fnct \log(y) + Correction\ factor \qquad \ldots(2.3)$$

The correction factor has been found to be a function of the Reynolds shear stress and therefore of the relative grain roughness and bed shear velocity. The equations developed by Nikuradse (1950) and Einstein (1950) are valid for fully rough, transitional as well as for smooth turbulent flow, and the correction factors are obtained from charts.

Turbulent flow over a rough surface

In turbulent flow over a rough, rigid surface or boundary the turbulence itself is affected by forces which result from the flow around the roughness elements, and in an alluvial channel these are represented by the sedimentary particles.

It has now been accepted that the structure of turbulent flow can be divided into two distinct regions (Hinze, 1975; Leeder, 1983; Nezu and Rodi, 1986; Cardoso et al, 1989; Graf, 1989):

(i) an Inner Region where the wall stress and wall roughness are the important parameters and

(ii) an Outer Region where the wall stress is the important parameter.

The inner region is also called the wall or near-wall region and the outer region is referred to as the core or near-water surface region.

Graf (1989) found that the logarithmic velocity profile was valid within the inner region but that in the outer region the conditions that led to the logarithmic velocity profile were no longer valid in that additionally a non-zero wake component was observed. This was also confirmed by Cardoso et al (1989), thus strengthening the idea of a new relationship, incorporating this non-zero wake component, already put forward by Hama (Hinze, 1975, p. 631) and by Nezu and Rodi (1986).

Graf (1989) also found that, if D represents the uniform flow depth, then :

(i) The limit of the separation between the inner and outer regions fluctuates between $0.13 < y/D < 0.2$ being on the average comparable to $y/D = 0.15$, as given by Hinze (1975),

(ii) the position of the theoretical bed below the top of bed surface, represented by the symbol y_o, varies between $0.3 < y_o/k_s < 0.4$, being on the average comparable to the values given by Zippe and Graf (1983) as $y_o/k_s \simeq 0.5$ and by Hinze (1975) as $y_o/k_s \simeq 0.25$.

Spatially accelerating turbulent flow

The flow field moving over the stoss or upstream side of dunes undergoes spatial acceleration, comparable to a large extent with the converging flows in nozzles installed downstream from long prismatic pipes. Very few studies have been carried out on the detailed structure of the flow field along a contracting discontinuous boundary such as that represented by a dune in an alluvial channel.

One such study is that presented by Cardoso et al (1989) in which a fully developed uniform flow underwent spatial acceleration by placing a smooth triangular element on the bottom of the flume. The experimental details are shown below in Table 2.1 .

Table 2.1 Details of accelerating flow experiments (Cardoso et al,1989)

Runs	Δ (mm)	λ (mm)	h_{in} (mm)	Q (l/s)
1	190	2500	368	255
2	190	2500	356	226

The symbol h_{in} represents the flow depth at the flume inlet.

The results of the study show that:

(i) The velocity profiles become fuller (increasingly more uniform) in the downstream direction,

(ii) there is an increase in the bed shear stress and shear velocity along the inclined plate and

(iii) the inner logarithmic layer, although reducing in size, is nevertheless retained along the inclined section of the channel. This inner layer is a dominant characteristic, whereas the outer layer represents a decaying remnant of the uniform flow.

2.1.2 Properties and Characteristics of Sedimentary Dunes

Formation of dunes

At extremely low velocities the critical shear stress of the bed particles, $(T_0)_{cr}$, is not exceeded and sediment motion does not occur. An increase in the velocity may result in sediment movement when the bed shear stress, T_0, has exceeded the particle critical shear stress. Kennedy (1969) believes that bed forms are the consequence of an instability phenomenon. Under specific conditions a small disturbance on an initially flat bed will affect the flow and local sediment transport rate in such a way, that deposition and scour occur over the crest and troughs respectively. This leads to an increase in the amplitude of the initial bed undulation, and as the bed profile disturbance increases in amplitude it further perturbs the local sediment transport rate. This in turn increases the rate of local scour and deposition and thereby further enhances the growth rate of the bed forms. This continues until factors associated with the increased amplitude of the bed waves intervene, limiting their growth and fixing their equilibrium amplitude.

The common bed forms occurring in the lower regime, $Fr < 1$, have a characteristic dune pattern in that they are triangular shaped elements with steep downstream slopes (lee) and gentle upstream slopes (stoss).

The downstream angle is generally close to the angle of repose of the material (Karahan and Peterson, 1980; Haque and Mahmood, 1986), and the lee side is associated with a separation zone, in which reverse flow occurs. This separation zone plays a fundamental role in the evolution of ripples and dunes as it helps the bed form to move in a downstream direction.

The spacing and the geometry of the dune patterns is uniform from a statistical sense. This has been of great help to researchers in that a series of dunes present on the bottom of an alluvial channel could be represented for experimental and theoretical purposes by an idealized dune defined by a few basic parameters.

Individual dune patterns are referred to as either ripples or dunes, with ripples being small bed features and dunes being rather larger and out of phase with the water surface. It is not uncommon to find ripples superimposed on the stoss side of dunes.

As mentioned earlier, the total flow resistance and bed stress, T_0, is composed of the form roughness, T_0', and the grain roughness, T_0'', and are both components of importance in the study of turbulent flow over dunes. This was first suggested by Einstein (1950) and more recently was confirmed experimentally by Shen et al (1990).

Steepness of sedimentary dunes

Considerable work has gone into studying the shape and dimensions of sedimentary dunes, and in particular in determining the steepness of dunes under varying flow conditions.

One of the most important pieces of literature available on this subject is that presented by Yalin and Karahan (1979). The authors characterize the steepness of sedimentary dunes in terms of the ratio of the dune height to the dune length, so that

$$\delta = \frac{\Delta}{\lambda} \qquad \ldots(2.4)$$

and they subsequently determine δ by the dimensionless variables η and Z which are given by

$$\eta = \frac{T_0}{(T_0)_{cr}} \quad ; \quad Z = \frac{h}{D_{50}} \qquad \ldots(2.5)$$

At they same time they also made use of the Reynolds grain size number

$$X = \frac{u_* D_{50}}{\nu} \qquad \ldots(2.6)$$

The most relevant findings were that:

(i) If $X > \approx 25$ then the steepness of the dunes forming on the initially flat bed surface does not depend on X any longer and the ripples superimposed on them are either insignificant or nonexistent (Yalin, 1977),

(ii) the influence of Z on the dune steepness progressively decreases with its increasing values and that when $Z > \approx 100$ then δ becomes a function of η only, and

(iii) the maximum steepness of sedimentary dunes is

$$\delta_{max} = 0.06$$

This maximum value had already been put forward by Yalin (1964 and 1977). It was also confirmed by Haque and Mahmood (1985) as well as by Fredsøe (1982). Rifai and Smith (1971) conducted visual observations of sand beds in flumes finding that not only did well-formed dunes develop, with their typical gentle upstream slope and steep downstream face, but also that between such well defined features, part-size dunes and chance irregularities often occurred. The result was that the average steepness ratio computed from the longitudinal trace of a typical dune bed is usually of the order of 0.05 to 0.07. Finally, Jonys (1973) conducted a series of tests over mobile beds and found that the average value for δ was 0.06 .

Other dune geometry parameters

The steepness of the dune is not the only parameter of interest when analyzing dunes and van Rijn (1984-b) carried out extensive work in this respect by analyzing flume and field data.

Assuming that the dimensions of the bed forms are controlled by the bed load transport, van Rijn (1984-a) showed that the bed load transport can be described by a dimensionless particle parameter, D_*, and a transport stage parameter, T, as follows :

(i) particle diameter,

$$D_* = D_{50} \left[\frac{(S_s-1)\, g}{\nu^2} \right]^{1/3} \qquad \ldots(2.7)$$

in which D_{50} is the median grain size and S_s is the specific density of the sedimentary bed material.

(ii) transport stage parameter,

$$T = \frac{(u_*')^2 - (u_{*,cr})^2}{(u_{*,cr})^2} \qquad \ldots(2.8)$$

in which u'_* is the bed shear velocity related to grains and is calculated using the following expressions:

$$u_*' = \left(\frac{g^{0.5}}{C'}\right) v \qquad \ldots(2.9)$$

$$C' = 18 \log \left(\frac{12\ R_b}{3\ D_{90}}\right) \qquad \ldots(2.10)$$

where C' = Chézy-coefficient related to grains,
R_b = hydraulic radius related to the bed according to Vanoni and Brooks (1957),
D_{90} = particle diameter of bed material,
v = mean flow velocity and
$u_{*,cr}$ = critical bed shear velocity according to van Rijn (1984-b).

Van Rijn assumed that the dimensions and migration of the bed forms are mainly determined by the value of the bed load transport rate. Using simple kinematic considerations and the continuity equation he arrived at the following functional relationships:

$$\frac{\Delta}{H} = fnct\left(\frac{D_{50}}{H}\ ,\ D_*\ ,\ T\right) \qquad \ldots(2.11)$$

$$\frac{\Delta}{\lambda} = fnct\left(\frac{D_{50}}{H}\ ,\ D_*\ ,\ T\right) \qquad \ldots(2.12)$$

In the above expressions H represents the average flow depth.

To determine these relationships van Rijn (1984-b) analyzed a large quantity of experimental data on bed form dimensions. In all, 84 flume experiments with particle diameters in the range 190-2300 μm were used and only experiments in the lower and transitional flow regime with dune type bed forms were considered, with the exclusion of ripple data as ripples are supposed to be independent of the flow depth.

For the large majority of the data, a clear correlation between the bed form dimensions and the D_*-parameter could not be detected. Therefore the D_* influence was neglected and the bed form dimensions were related to the particle size, the transport stage parameter and the mean flow depth in the following way,

$$\frac{\Delta}{H} = 0.11\left(\frac{D_{50}}{H}\right)^{0.3}(1-e^{-0.5T})\,(25-T) \qquad \ldots(2.13)$$

$$\frac{\Delta}{\lambda} = 0.015\left(\frac{D_{50}}{H}\right)^{0.3}(1-e^{-0.5T})\,(25-T) \qquad \ldots(2.14)$$

The parameter T lies between $0 \leq T \leq 25$, as $T = 25$ corresponds to the change from lower flow regime to upper flow regime. These functions were verified against flume and field data and showed an excellent correlation (van Rijn, 1984-b).

An expression for the bed form length was then derived by using the above two functions,

$$\lambda = 7.3\, H \qquad \text{...(2.15)}$$

which indicates that the dune length is related only to mean flow depth. This has also been reported by Yalin (1977, p. 242), in that, by using theoretical analysis, he arrived at a similar result,

$$\lambda = 2\pi H \qquad \text{...(2.16)}$$

Another parameter that deserves special attention is the downstream angle of the sedimentary dunes, θ (this is the angle between the lee side of the dune and the horizontal). This angle has been found to be close to the value of the angle of repose of the material, ϕ (Haque and Mahmood, 1986) and the value adopted by most researchers for both analytical as well as experimental purposes (Engel, 1981; Rifai and Smith, 1971; Vittal et al, 1977; Fehlman, 1985) has been $\theta = 30°$.

2.1.3 Flow Over Sedimentary Dunes: Related Experimental Studies

Velocity, pressure and grain shear stress distribution

Given the difficulties in conducting experiments over real dunes in alluvial channels, researchers have concentrated on conducting experiments under controlled laboratory conditions.

The first reported study of flow over artificial dunes was made by Laursen et al (1962). Detailed measurements of velocity, pressure and grain shear stress distributions were obtained for the flow of air over triangular bed forms placed on the bottom and top faces of a closed conduit. Measurements indicated that the shear stress increased almost linearly from a value close to zero at the flow reattachment point to a maximum at the dune crest.

Raudkivi (1963,1966) reported an experiment of flow over a ripple that had been allowed to form naturally and then stabilized. The details of the experiment are shown in Table 2.2 . The flume geometry parameters of length, width and height are represented by the symbols F_l, F_w and F_h respectively.

Table 2.2 Details of Raudkivi's experiments (1963)

F_l (mm)	F_w (mm)	F_h (mm)	D_{50} (mm)
2440	76.2	152.4	0.4
Δ (mm)	λ (mm)	δ	H (mm)
22.4	386	0.058	

Velocity distributions were measured using the van Essen differential manometer, grain shear stress was assessed by means of a Preston tube and pressure distributions were measured using pressure tappings. It is interesting to note that two different Preston tubes were used ($d_{i,1}$ = 1.44 mm, $d_{o,1}$ = 1.59 mm , $d_{i,2}$ = 2.72 mm and $d_{o,2}$ = 3.53 mm. The subscripts i and o denote inner and outer respectively), and they had not yet been calibrated at the time the paper was published. The results obtained with these two Preston tubes were identical within a small experimental scatter.

The results for turbulence intensity show that maximum turbulence energy is reached at a point close to the reattachment point and decreases towards the crest. From the evaluated grain shear stress distribution Raudkivi concluded that entrainment and sand transport over the ripple surface were not uniquely related to either the mean grain shear stress or to the mean velocity.

Vanoni and Hwang (1967) found that for open channel flows of a constant depth over a stabilised ripple bed, both the normalised velocity distribution and the normalised piezometric head distribution remain unchanged with variation in flow velocity.

Rifai and Smith (1971) conducted experiments with open channel flow over an idealized dune bed composed of a series of triangular elements. These elements were made of brass which resulted in a very smooth surface, and were positioned on the bottom of the flume extending for the latter's full width and length. A number of experiments were conducted where the geometry of the elements was kept constant and the flow conditions were varied. (See Table 2.3)

Table 2.3 Details of Rifai and Smith's experiments (1971)

F_l (mm)	F_w (mm)	Δ (mm)	λ (mm)
6400	380	51	510

The downstream angle of the elements was 30°.

Point velocities were measured with a Preston tube connected to a differential manometer which used water and a coloured fluid of specific gravity 0.78 . The longitudinal component of turbulence was measured using quartz-coated parabolic hot film sensors.

Some preliminary experiments were carried out to see to what extent the structure of the flow had become fully developed over the triangular elements. For example the velocity profiles over the fourth and fifth elements differed by only 2 to 3 % and it was concluded that the turbulence generated by the triangular elements caused a rapid development of the flow structure in the flume.

Based on their experiments they found that the flow over triangular elements reproduces, in idealized form, a number of characteristics of flow over dunes. They also indicated that a relatively uniform velocity profile formed above the crest of the elements as a result of the flow contraction along the upstream slope. The turbulence intensities measured were higher than for flow in a corresponding channel with a rigid plane bed and were high near the bed form surface but diffused rapidly towards the free surface.

Naturally developed, unstabilised dunes in a laboratory flume were studied by Jonys (1973). The dune grain shear stress was calculated from the measured velocity profiles and found to increase from a value of zero at the reattachment zone, reaching a maximum at a point located approximately one-fourth of the bed form length upstream from the dune crest. The maximum and minimum piezometric heads were found to occur at one-tenth of the dune length, downstream from the reattachment point and at a point slightly upstream of the crest respectively.

Vittal et al (1977) performed experiments on water as well as air flowing over a series of smooth and sand coated, two-dimensional sharp crested triangular elements. In the open channel flow experiments the elements spanned the entire width and length of the flume (See Table 2.4).

Table 2.4 Details of Vittal et al experiments (1977)

FLUME DETAILS			SAND DETAILS	
F_l (mm)	F_w (mm)	F_h (mm)	D_{50} (mm)	σ
12500	600	600	0.6	1.5
DUNE DETAILS				
Δ (mm)	λ (mm)	δ		
30	600	0.05		
30	450	0.067		
30	306	0.098		
30	150	0.2		

The lee angle of the elements was kept at 30° throughout the study. To measure pressure distribution, taps having a 3 mm outer diameter were located on the upstream and downstream faces at several points along the centre line of two triangular elements. Readings were taken using an inclined manometer. The grain shear distribution on the stoss side of the dunes was measured using a Preston tube with an outer diameter d_0 = 6.35 mm which had been specially calibrated for use on the sand-coated surface.

The main findings were that the bed grain shear on the upstream face of the triangular elements increases continuously from a value of zero at the reattachment region to a maximum at the crest of the elements. The pressure measurements indicated low pressures at the upstream end and at the crest, with the maximum pressure occurring somewhere between these two sections.

Fehlman (1985) investigated the velocity distributions of open channel flow over dunes by using idealized bed form experiments in a laboratory flume. Tests were conducted involving identical artificial triangular dunes, both smooth and artificially roughened. The downstream angle of the elements was kept at 30°. The dune geometry remained constant for all the experiments, whilst the flow conditions were altered so as to obtain Froude numbers in the range $0.1 \leq Fr \leq 0.4$ for the smooth elements and $0.1 \leq Fr \leq 0.3$ for the sand coated elements (See Table 2.5).

Measurements of local grain shear stress and pressure distribution on the dune surface were used to determine the characteristics of skin and form resistance.

Table 2.5 Details of Fehlman's experiments (1985)

Δ (mm)	λ (mm)	δ	D_{50} (mm)
137.5	914.4	0.15	1.75

The numerical investigation of the experiments revealed that the magnitude of the velocity close to the water surface does not change significantly with the streamwise position, contrasting with the behaviour of the velocity near the dune surface. Velocity profiles away from the dune surface are not influenced by the surface roughness. Downstream of the reattachment point measurements showed a steadily increasing grain shear stress, the magnitude of the stress thus being dependent on position along the dune, with a maximum coinciding with the crest. About halfway up the stoss side the grain shear stress exceeded the Shields critical shear stress, emphasizing the role played by turbulence in the transport of sediment grains over the dune surface. The pressure distribution curves were consistently found to be bell- shaped, concave downward, with skewness dependent on the position of the maximum and minimum pressure relative to the dune geometry. The maximum pressure occurs at the reattachment point, and the minimum pressure occurs at a point just downstream of the dune crest.

Mendoza-Cabrales (1987) subsequently used his theoretical model to extend the grain shear distribution measurements of Fehlman into the zone of separation. Here flow reversal gives rise to negative grain shear stresses of very small value.

Length of separation

A review of the available literature has showed that attempts have been made to obtain the length of separation, L, for various bed form configurations. Research carried out to date (See Table 2.6) has focused on relating flow separation length to the height of stabilized or artificial dunes and of rearward facing steps.

Table 2.6 Research on length of separation.

REFERENCE	DETAILS	$\Omega = L/\Delta$
Raudkivi (1963,1976)	Stabilized ripple	5 to 8
Walker (1961)	Rearward step (rectangular)	≈ 5
Tani (1957)	Rearward step (rectangular)	≈ 6
Etheridge and Kemp (1979)	Rearward step (rectangular)	5 to 7
Chang (1970)	Single cast iron angle	5 to 8
Knoroz (Engel,1981)	Analytical analysis	10
Jonys (1973)	Non-stabilized dunes	4.2 (*)
Karahan and Peterson (1980)	Artificial dunes	5.33 (at $Fr > 0.2$)

(*) = The data by Jonys (1973) was examined by Engel

(1981) who arrived at this value by estimating the distance from the dune crest to the point of zero shear stress on the stoss of the next dune.

Karahan and Peterson (1980) conducted a study of the flow pattern over smooth dune shaped beds by making use of streaming bi-refringence. By this visual observation, qualitative measurements were carried out and the variation of the separation zone length in terms of the Froude and Reynolds numbers was established. The dune geometry was kept constant whilst the flow conditions were varied to obtain a good range of Froude ($Fr < 1.0$) and Reynolds numbers. Discharges were measured using an underflow gate (See Table 2.7).

Their experimental data showed that at low Fr values the length of the separation zone is proportional to the inverse of the Froude number, $L \propto 1/Fr$. If the Froude number is greater than 0.2 then there is no significant change in the separation zone length with Fr, and the dimensionless separation zone length, $\omega = L / \lambda$, is almost constant and has a value of 0.32 . In the laminar boundary layer, ω is a function of the flow Reynolds number and decreases with increasing Re.

Table 2.7 Details of Karahan and Peterson's experiments (1980)

F_l (mm)	F_w (mm)	δ	θ (°)
600	150	0.06	45

In the case of the turbulent boundary layer ω is independent of the Reynolds number. Furthermore it was found that the ratio of separation length to dune height remained constant with varying flows and had a value of 5.3 .

The results from the literature survey indicate that the length of the separation zone behind dunes may vary from five times to ten times the dune height. Unfortunately, the information is too limited to determine a general relationship between the separation length, bed form shape, sand grain roughness and flow conditions (Engel, 1981). Although the results from measurements over dunes, ripples and rearward facing steps appear to be similar, it is doubtful that this similarity can be taken to be general, especially when the sand waves have steep upstream faces.

In view of the above considerations, Engel (1981) conducted a series of experiments in an attempt to obtain a comprehensive relationship between the length of separation over dunes and certain pertinent independent variables. The relationship sought by Engel was :

$$\frac{L}{\Delta} = fnct\left(\frac{\Delta}{\lambda}, \frac{D_{50}}{\Delta}, \frac{H}{\Delta}, Fr\right), \quad for\ \Delta > 0 \qquad \ldots(2.17)$$

The bed forms used varied in geometry (four different steepness ratios) and surface roughness (smooth and three different particle sizes) as shown in Table 2.8 . The bed forms, represented by triangular elements fabricated from plywood and covered with sand, were placed over the full length of the flume.

A special set of tests was conducted in which a rearward facing step with horizontal upstream and downstream boundaries was used. The height of the step was the same as that of the dunes and this configuration was tested both with a smooth surface and with a sand coating, D_{50} = 1.2 mm. This set of tests was done to provide data for comparing the length of the zone of separation behind dunes and such a step.

Table 2.8 Details of Engel's experiments (1981)

DUNE DETAILS			ROUGHNESS DETAILS	
Δ (mm)	λ (mm)	δ	D_{50} (mm)	D_{50}/Δ
30	1500	0.02	0.0	0.0
30	900	0.033	0.62	0.021
30	600	0.05	1.20	0.040
30	430	0.07	2.60	0.087

FLUME DETAILS	
F_l (mm)	F_w (mm)
20000	1000

The flow separations were measured using a Potassium Permanganate solution as a visual aid: a 100 ml hypodermic syringe with a needle 450 mm long and 1 mm inside diameter, attached to a traversing mechanism, was used to inject the dye close to the dune surface at right angles to the flow.

In all, data for 291 runs were obtained in which dune length, flow depth, sand size and discharge were varied. The downstream angle of the dunes was kept constant at 30° and the flows were always uniform with $Fr < 0.5$.

The experimental results revealed that the length of the flow separation behind dunes is virtually independent of the flow depth for $Fr < 0.5$ and values of $H/\Delta > 5$, but that it is dependent on the sand grain roughness when the dunes are flat. If the dunes are steep ($\Delta/\lambda > 0.05$) then the effect of the sand grain roughness is virtually negligible and in fact for steep dunes

$$L \approx 4\Delta \qquad ...(2.18)$$

The experiments with the reverse step showed that the rectangular step can be considered to be a special case of dunes with infinite wave length ($\delta = 0$). The largest attainable flow separation occurred for this case and Engel concluded that it is therefore not correct to compare flow separation lengths behind dunes ($\delta > 0$) directly with those behind a reverse step.

For a given sand roughness L increases significantly for decreasing values of $\delta < 0.05$. This variation was found to be most significant for values of $D_{50} \approx 0$. As D_{50}/Δ increases and the steepness decreases, the rate of change in length of flow separation reduces.

Engel provided a graph that could be used to determine estimates of L for most situations with dunes, provided Δ, λ and D_{50} are known.

Müller and Gyr (1982), developing the concepts put forward by Engelund and Fredsoe (1982), studied the formation of vortices within the flow separation region and found that these tube vortices developed out of the initial shear layer and contributed to preserving the shape of the dune.

2.1.4 Calibration of the Preston Tube

The Preston tube technique, first introduced by Preston (1954), has been generally recognised as a convenient and reliable method for measuring the grain shear stress on smooth and rough boundaries. However, doubts have been expressed about the existence of a universal calibration for rough boundaries, particularly when quantitative measurements of shear stress are needed (Hwang and Laursen ,1963).

The Preston tube is a combined total pressure or total head and piezometric head tube which is placed on the boundary facing the flow. The velocity head or dynamic pressure, ΔP, obtained from this tube is correlated to the boundary grain shear stress T_0'' : this correlation is based on the existence of the law of the wall, discussed earlier, and which is known apply to turbulent boundary layers.

For smooth boundaries, based on the law of the wall and using dimensional arguments, it can be shown (Hollingshead and Rajaratnam, 1980) that:

$$\Delta P = fnct\ (T_{0*}'') \qquad \ldots(2.19)$$

with ΔP_*, the dimensionless dynamic pressure, and T_{0*}'', the dimensionless grain shear stress, given by

$$\Delta P_* = \frac{\Delta P\, d_o^2}{4\rho v^2} \qquad T''_{0*} = \frac{T''_0\, d_o^2}{4\rho v^2} \qquad \ldots(2.20)$$

Preston evaluated the relationship between ΔP and T_0 by calibrating his Preston tubes in fully developed turbulent pipe flow and his work was subsequently reinforced by Head and Rechenberg (1972) with Patel (1965) developing a rather definitive and widely used calibration curve for the use of Preston tubes over smooth boundaries.

If the boundary is hydrodynamically rough, Preston (1954) himself suggested that for a Preston tube resting on it

$$\frac{\Delta P}{T''_0} = fnct\left(\frac{d_o}{k}\right) \qquad \ldots(2.21)$$

where k is some typical roughness length. Ippen et al (1960) calibrated a Preston tube on a rough bed in an open channel and found that for one roughness size and for a small range of flow depths, $\Delta P / T_0'' = 47.6$.

Hwang and Laursen (1963) conducted a series of pipe experiments using four different roughness sizes and four Preston tubes with inside to outside diameter ratios of 0.64 to 0.78 . Most measurements were made in turbulent flows that fell in the transitional region discussed earlier. Assuming that

$$\Delta P = \int_A \frac{\rho\, u^2}{2}\, dA \qquad \ldots(2.22)$$

where A is the frontal area of the Preston tube with dA being an elemental area and u is given by the Karman-Prandtl equation

$$\frac{u}{u_*} = 5.75 \log\frac{y}{k_s} + 8.5 \qquad \text{...(2.23)}$$

Hwang and Laursen (1964) obtained an expression relating dynamic pressure and grain shear stress in terms of the internal radius of the Preston tube, the relative roughness of the bed and the distance from the geometric centre of the Preston tube to the line of zero datum.

The equation can be used directly for fully rough flows, whereas for transitional flows a correction factor must be applied, as the factor 8.5 is no longer constant under these flow conditions. For problems where a quantitative measure of the grain shear stress is required the authors recommend that experiments similar to the ones they conducted should be carried out in order to develop a correction factor chart for the particular roughness involved. This, and the fact that this solution is dependent on the choice of a suitable value of k_s, make this method not universally acceptable.

Ghosh and Jena (1971) arrived at very similar relationships for both the smooth and the fully rough turbulent flow cases which they then used in their study of boundary shear distribution in open channels.

Hollingshead and Rajaratnam (1980) developed analytically a Preston tube calibration chart for the measurement of shear stress on smooth as well as uniformly rough boundaries. They then conducted a series of tests in a flume, involving the use of grains and hemispheres on rectangular and trapezoidal channels using four different sized Preston tubes, to verify their chart. They found that a fair correlation existed between their results and those of other researchers, in particular Hwang and Laursen (1963), but recommended that further experiments should be conducted before the chart could be used with confidence.

Preston tube readings can be calibrated for any specific roughness if quantitative measurements of grain shear stress are required (Hwang and Laursen, 1964). Velocity profiles are measured and plotted on semi-log paper. From the plot the slope is calculated and the grain shear stress can then be determined.

2.1.5 Relative grain roughness, k_s

The very first experiments conducted in order to determine the effects of various sand grain roughnesses were performed by Nikuradse (1950) as early as 1933 and in fact the term k_s is often referred to as Nikuradse's sand grain roughness.

In his experiments Nikuradse used sand to roughen the inside of pipes of varying internal diameters. He assumed that the height of the roughness was equal to the diameter of the sand grains he used. Over the years criticism has been expressed about the fact that the gluing procedure adopted by Nikuradse was not very good by today's standards, but more importantly that pouring thick lacquer over the grains after the initial gluing process may almost certainly have affected his results especially for very small sand particle sizes (Hwang and Laursen, 1963; Kamphuis, 1974).

Table 2.9 Relative roughness experiments

REFERENCE		k_s (mm)
Ackers and White	(1973)	$1.25*D_{35}$
Einstein and Barbarossa	(1953)	D_{65}
Engelund and Hansen	(1967)	$2*D_{65}$
Hey	(1979)	$3.5*D_{84}$
Kamphuis	(1974)	$2*D_{90}$
Mahmood	(1971)	$5.1*D_{84}$
van Rijn	(1982)	$3*D_{90}$

Although Nikuradse's sand grain roughness became a standard method of describing the roughness of a boundary in both pipes and open channels, research was still directed at finding a better way of relating the relative roughness of an alluvial bed to some representative bed particle size. Usually k_s has been related to the largest particles present in the bed, D_{65}, D_{84} and D_{90} with the gradation of the bed material, shape of particles and flow conditions being disregarded.

Table 2.9 shows the wide range values that are used to define k_s, confirming that the definition of the relative roughness of the sedimentary bed in an alluvial channel still remains a rather obscure and subjective concept.

2.1.6 Average flow depth

In the analysis of flow over a series of bed forms, in this instance over alluvial dunes, the concept of an average flow depth becomes important in determining a number of parameters (e.g Froude number and average flow velocity). Past researchers have related the average flow depth to the flow depth at the crest of the artificial dune, in that (Engel and Lau, 1980; Engel, 1981; Engelund and Fredsoe, 1982; Fehlman, 1985; Shen et al, 1990):

$$H = h_{crest} + \frac{\Delta}{2} \qquad \ldots(2.24)$$

Pillai (1979) put forward the concept of an effective flow depth for channels having bed undulations. The average flow depth was shown to account only for the roughness of the elements whilst the form effects were not considered. Pillai argued that the effective flow depth, H_e, might not always be equal to the average flow depth, but that it would in fact be less when the crests of the dunes were closer together and greater when the crests were further apart.

He thus proposed an additive correction factor, d(H), and after conducting experiments involving turbulent flow over small bed undulations, he arrived at the following empirical equation,

$$d(H) = \frac{\Delta}{m_0}\left(\frac{\Delta}{\lambda}\right)^{-n_0} \qquad \ldots(2.25)$$

for which m_0 and n_0 were found to be constants, equal to 3 and 0.3 respectively. Therefore the effective depth would be given by

$$H_e = H + d(H) \qquad \ldots(2.26)$$

Using this approach Pillai obtained a better correlation with his experimental data than he did by using the average flow depth as given by equation (2.24) .

2.2 Specific aims

In order to improve our understanding of the interaction between alluvial channel bed forms and turbulent flow and at the same time provide a unique set of data which can be used to develop and test sediment transport models, the following hydraulic properties were simultaneously investigated:

(i) water profiles and effective flow depth,
(ii) length of the zone of separation,
(iii) bed pressure distribution,
(iv) grain shear stress distribution.

In particular the effects of different dune geometry, surface roughness and flow conditions on these properties will be investigated by means of laboratory experiments, and the resulting data were analysed and compared with previous research results.

CHAPTER 3
EXPERIMENTAL EQUIPMENT

3.1 General

The experiments were carried out in a recirculating system comprising a tilting flume, overhead water tank and Venturi flowmeter located in the Lower Laboratory of the Department of Civil Engineering.

The overhead tank allowed the experiments to be conducted under a constant head condition and the Venturi meter was used to measure the inlet flow rate. The accuracy of the meter was established by comparing readings against volume and time measurements at the flume outlet. The flume used is a glass walled flume 15 m long, 380 mm wide and 1000 mm high. The tilting section is 9000 mm in length and the slope can be adjusted by using an electrically powered jack.

The flume walls are equipped with rails enabling a movable carriage and a traversing mechanism to move along its entire length. Therefore a number of measuring devices, after being attached to this mechanism, can be positioned anywhere within the experimental sections.

A smaller re-circulating flume was used for the calibration of the Preston tube. This glass sided flume has a length of 3000 mm, a width of 100 mm and an operating height of 300 mm. The entire unit is made up of a pump, small tank and flowmeter. The slope of this flume could also be altered as needed.

3.2 Preston Tube and Flow Transmitter

In order to measure point velocities within the flow, use was made of a flow transmitter unit connected to a Preston tube. The latter consists of two concentric tubes: the one tube measures the static head and the other tube measures the total head (static head plus velocity head) at any point in a fluid. Dimension details of the Preston tube are given in Table 3.1 . The velocity head, ΔP, also referred to as dynamic pressure, is given by

$$\frac{\Delta P}{\rho g} = \frac{u^2}{2g} \qquad \ldots(3.1)$$

Thus $$\Delta P = \frac{\rho u^2}{2} \quad , \textit{but as} \quad \rho = 1000 \ \frac{kg}{m^3}$$

$$\Delta P = 500\ u^2 \qquad \ldots(3.2)$$

A Fuji FJQ FC Series flow transmitter was coupled to a Fuji PGK self-balancing recorder (Shown in Figure 3.1) in order to obtain direct point velocity readings. The flow transmitter has a measuring range of between 20 and 100 mm of H_2O (where a reading of 100 % at a setting of 50 mm of H_2O corresponds to 490 N/m^2 differential pressure or 1.0 m/s point velocity), an accuracy of ± 0.25 % and a zero adjustment which must be set to give an output current of 4 mA for a 0 % reading.

The output is displayed both on the flow transmitter and on the recorder, and is in terms of a percentage of the maximum point velocity which can be measured for that particular setting. In these experiments the setting was 50 mm H_2O resulting in u_{max} = 1.0 m/s.

Table 3.1 Preston tube dimensions

Inner diameter, d_i	1.0 mm
Outer diameter, d_o	2.3 mm
Wall thickness, t	0.65 mm
d_i/d_0	0.44

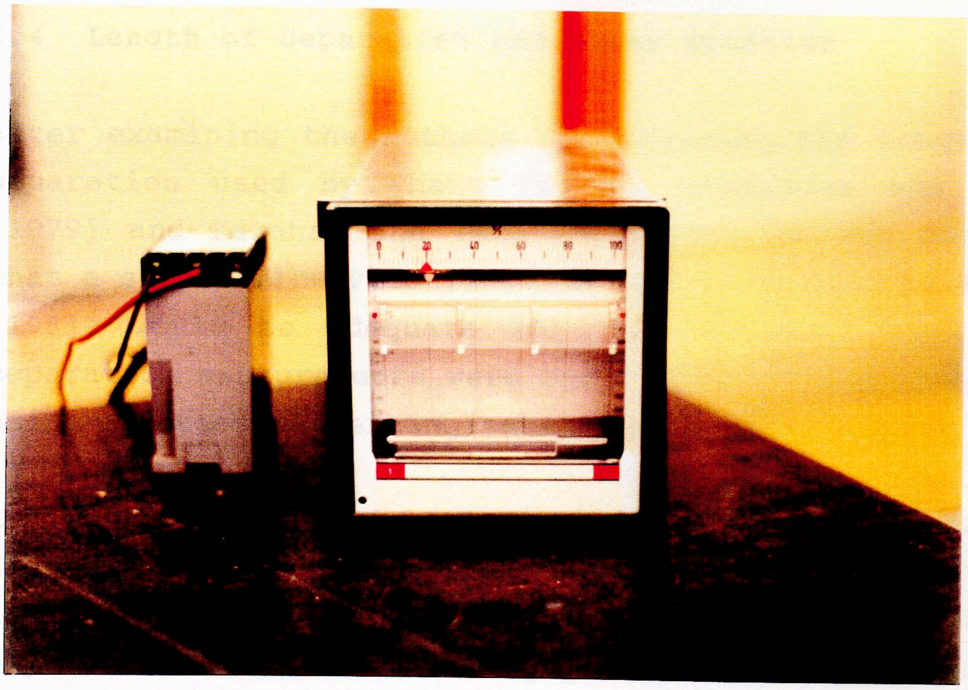

Figure 3.1 Fuji PGK self-balancing recorder

3.3 Pressure Manometer

A standard vertical pressure manometer was used to measure the pressure on the bed of the test dunes. Pressure measurements were taken by connecting the manometer to two different measuring tubes having internal diameters of 2.5 mm and 0.6 mm respectively. The tubes enabled measurements to be taken close to the surface of the bed. In order to eliminate the effects of the velocity head and hence to measure the static pressure only, the openings on the tubes were positioned at 90° to the direction of the flow.

The fluid used in the manometer was ordinary water mixed with a little Fluorescene dye. The chemical gave the fluid a bright green colour and this made changes in pressure readings easier to detect and record.

3.4 Length of Separation and Water Profiles

After examining the methods of measuring the length of separation used by Chang (1970), Etheridge and Kemp (1979) and Karahan and Peterson (1980) it was decided that a simple flow visualization method as used by Engel (1981) would be adequate for this project. The flow separation measurements were carried out in all cases by using a Potassium Permanganate solution as a visual aid.

A pipette with an internal diameter of 1 mm and an outer diameter of 3 mm was mounted on the traverse mechanism and a hypodermic syringe was placed at the top end of the pipette. The combination of pipette and syringe allowed the dye to be injected at right angles to the flow and slow enough so as not to impart a momentum to the solution in the streamwise direction, and therefore influence the measurements.

The water profiles for the various flow conditions were measured using a depth gauge connected to the flume's traverse mechanism, shown in Figure 3.2.

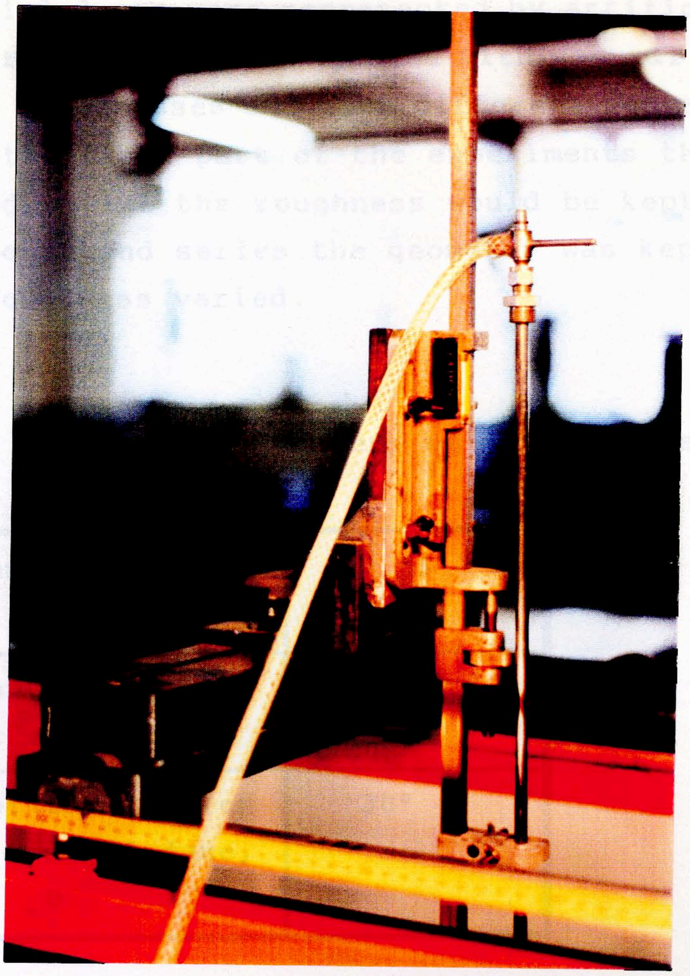

Figure 3.2 Details of the flume's traverse mechanism

3.5 Artificial Dune Trains

After examining the work carried out by various researchers as presented in 2.1.3 it was decided that a series of artificial dune trains, varying both in geometry and in roughness, would allow a meaningful investigation of grain shear stress, pressure distribution and length of separation. Table 3.2 shows the fixed parameters used to determine the geometry of the dunes.

The alluvial dunes were represented by artificial dunes, triangular in shape and roughened with natural sand. Four different roughnesses and four different geometries were used. In the first part of the experiments the geometry was varied whilst the roughness would be kept constant, and in the second series the geometry was kept constant and the roughness varied.

Table 3.2 Constant parameters of experimental dunes

Maximum steepness ratio δ_{max}	0.06
Constant dune height Δ	45 mm
Angle of inclination of lee side of dune, θ	30°

The letter G and the steepness ratio were used to represent the various geometries, whereas the letter S and the D_{50} of the coating sand identify the various roughnesses used. The sand used was a washed silica sand available in various pre-packed size ranges from a nearby quarry. A representative sample was obtained from each batch and a sieve analysis conducted in order to determine the particle size dimensions required. Appendix A contains the particle size distributions and photographs of the sand grains used.

Table 3.3 shows the dune geometries and artificial roughnesses used in the experiments: each set of dunes consisted of six identical elements that made up the train along the tilting flume bed, as shown in Figure 3.3.

The artificial dunes were made of 0.6 mm thick galvanised steel sheet. The width of the dunes was 380 mm and therefore they covered the flume width leaving only a couple of millimetres on either side to simplify their installation.

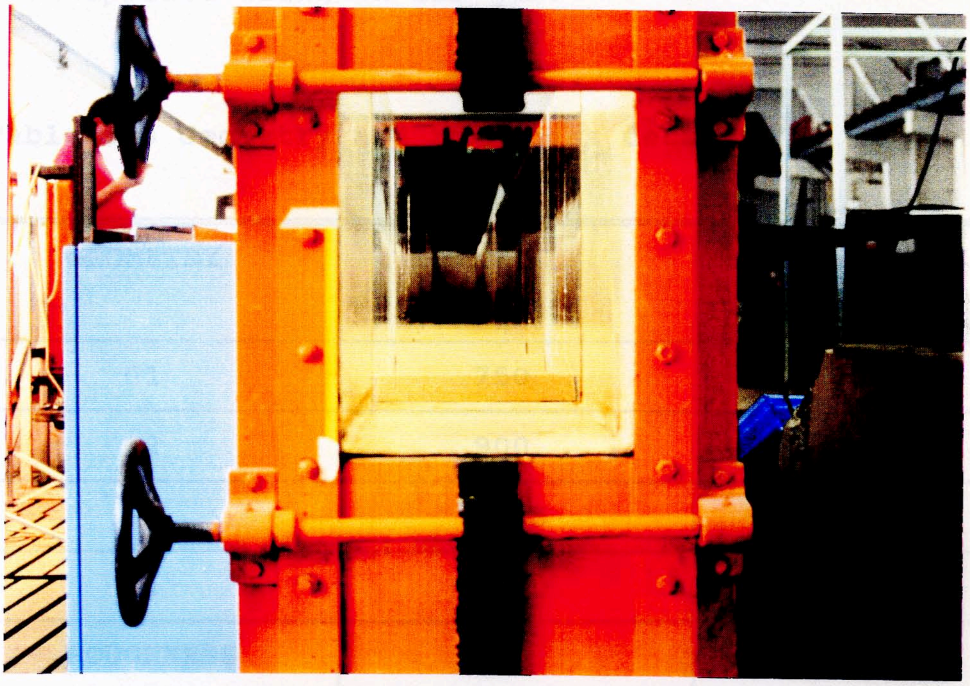

Figure 3.3 Details of dune train placed in experimental flume

To create a solid structure that would withstand the action of water, each element had three wooden supports, placed on the underside, and treated to prevent their deterioration. The dunes were fixed to the flume bed by means of silicone sealant as this proved to be strong enough to hold the dunes in place during the experiments, but at the same time allowed for their quick removal at the end of the runs.

A coat of Glatex-8 Primer was applied to the top surface of the elements and allowed to dry. The next step involved applying Glatex-8 Plascodure by brush, and whilst the paint was still wet, the sand was sprinkled gently until a thick layer covered the entire surface. The paint was allowed to dry and the excess sand was blown and brushed off. To render the elements more durable a very thin layer of Glatex-8 Matt Varnish was then applied using an air gun.

Table 3.3 Geometry and roughness details

GEOMETRY	λ (mm)	δ
G1	750	0.06
G2	900	0.05
G3	1125	0.04
G4	1500	0.03
ROUGHNESS	D_{50} (mm)	RANGE (mm)
S1	0.5	0.3 to 0.65
S2	0.93	0.6 to 1.2
S3	1.6	0.8 to 1.8
S4	3.05	2.4 to 5.8

At the same time a series of four different flat strips, with the four different roughnesses, were prepared in exactly the same way (See Figure 3.4). These would be used for the calibration experiments.

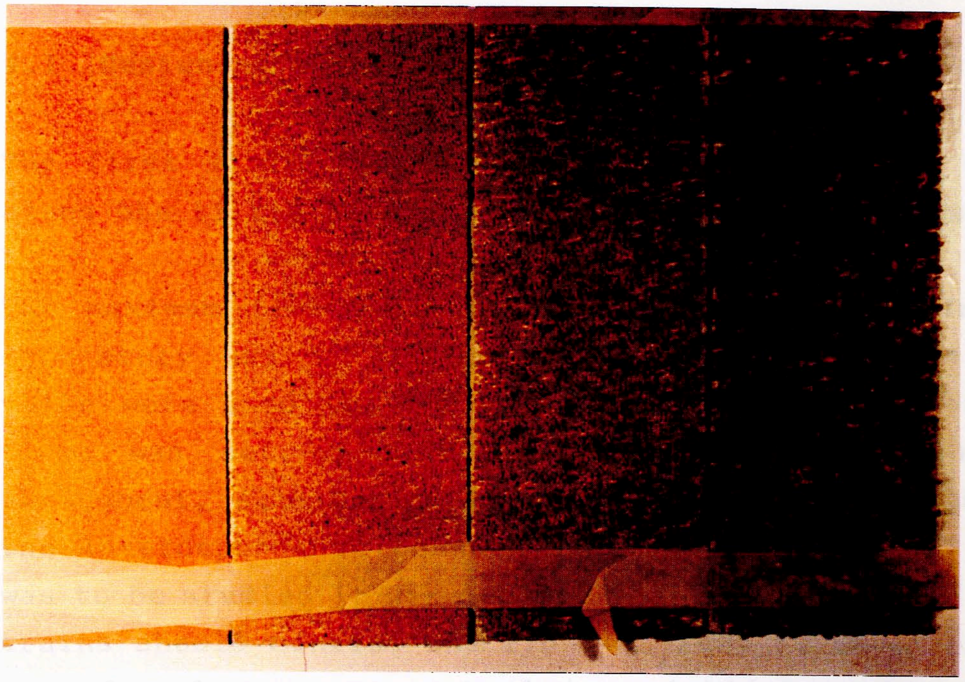

Figure 3.4 Flat strips used in calibration experiments

CHAPTER 4

EXPERIMENTAL PROCEDURE AND DATA PROCESSING

4.1 Design of experiments

The first train of dunes was positioned in the flume along the tilted portion. All the equipment was tested.

The maximum flow rate that could be obtained in the laboratory was 52 l/s and therefore flows below this value were used for the experiments. The slope of the flume was set at 1:500 and this was kept constant throughout, eliminating possible bed slope effects. As the interdependence between the flow and the bed forms was to be studied it was decided that the artificial dune trains should control the flow, thereby eliminating the use of a downstream control to establish various flow patterns and conditions.

Each set of dunes was subjected to the same range of flows to provide a common base for the comparison of the results. Figure 4.1 shows the combination and order of the main experiments and Table 4.1 gives the details of the flow ranges used.

At the beginning of each experiment the system was flushed to eliminate any air pockets trapped in the pipes. The venturi meter was bled and its zero setting checked. After the required flow rate was set using the control valves and the venturi meter, the flow was allowed time to interact with the artificial bed and thus establish itself. This was subsequently confirmed when measurements of flow depth, taken at two points along the flume section (one at the flume inlet and the other upstream of the experimental section), showed no variation. These flow depths were carefully recorded on the data collection sheets for future reference (h_{in}).

Temperature readings were then recorded and measurements of the various hydraulic properties were taken. Measurements were taken along the centre line of the third artificial dune of each train, as initial checks had shown that the flow was fully established by this stage, and that tailing effects from the end of the train would be eliminated. During the experiments some measurements were taken along the centre line of the fourth dune to monitor any potential problems.

Table 4.1 Flow ranges used

RANGE	MEASUREMENTS
10 - 35 in 5 l/s	Shear stress and bed pressure
10 - 45 in 5 l/s	Length of separation and water profiles

Measurements for all the experiments were conducted in a systematic way, always following this order:

(i) Water surface profile,

(ii) Length of separation,

(iii) Bed pressure distribution and

(iv) Grain shear stress distribution.

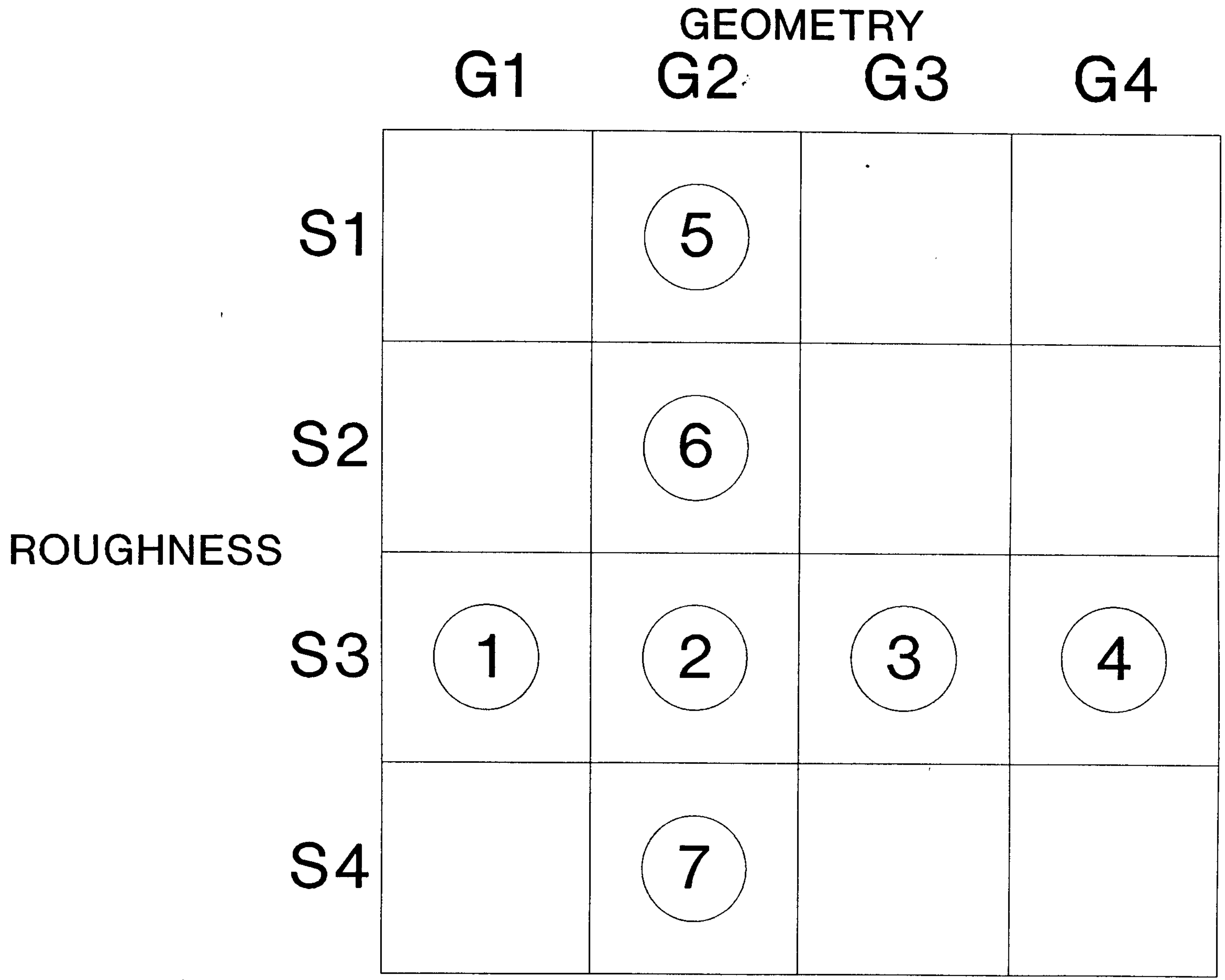

Figure 4.1 Combination and order of experiments

To facilitate the collection of experimental data, and to allow comparison of data from dunes with different geometry, reading points were defined in terms of the dune wavelength as shown in Figure 4.2 .

Figure 4.2 shows that x has its origin at the crest of the previous dune and all positional measurements were taken with this point as the zero reference.

Defining $$\lambda' = \lambda - a \qquad \text{...(4.1)}$$

and $$x = a + (f) * \lambda' \qquad \text{...(4.2)}$$

where f is the proportional length, as defined in Table 4.2 . The reading points for each geometry were then marked on the horizontal scale of the flume wall. It should be noted however that measurements were taken at intermediate points as well (See Table 5.5).

4.2 Water surface profiles

Flow depths were measured at all points along the centre line of the third dune, as well as at point 1, the crest and toe along the centre line of the fourth dune. This was done to ensure that the flow had established itself and that the readings for dune 3 would be representative of the whole train. At lower flow rates the difference between readings for the two dunes remained negligible (± 2-3 %), but as the flow approached 50 l/s the disparity became very evident (± 10 %).

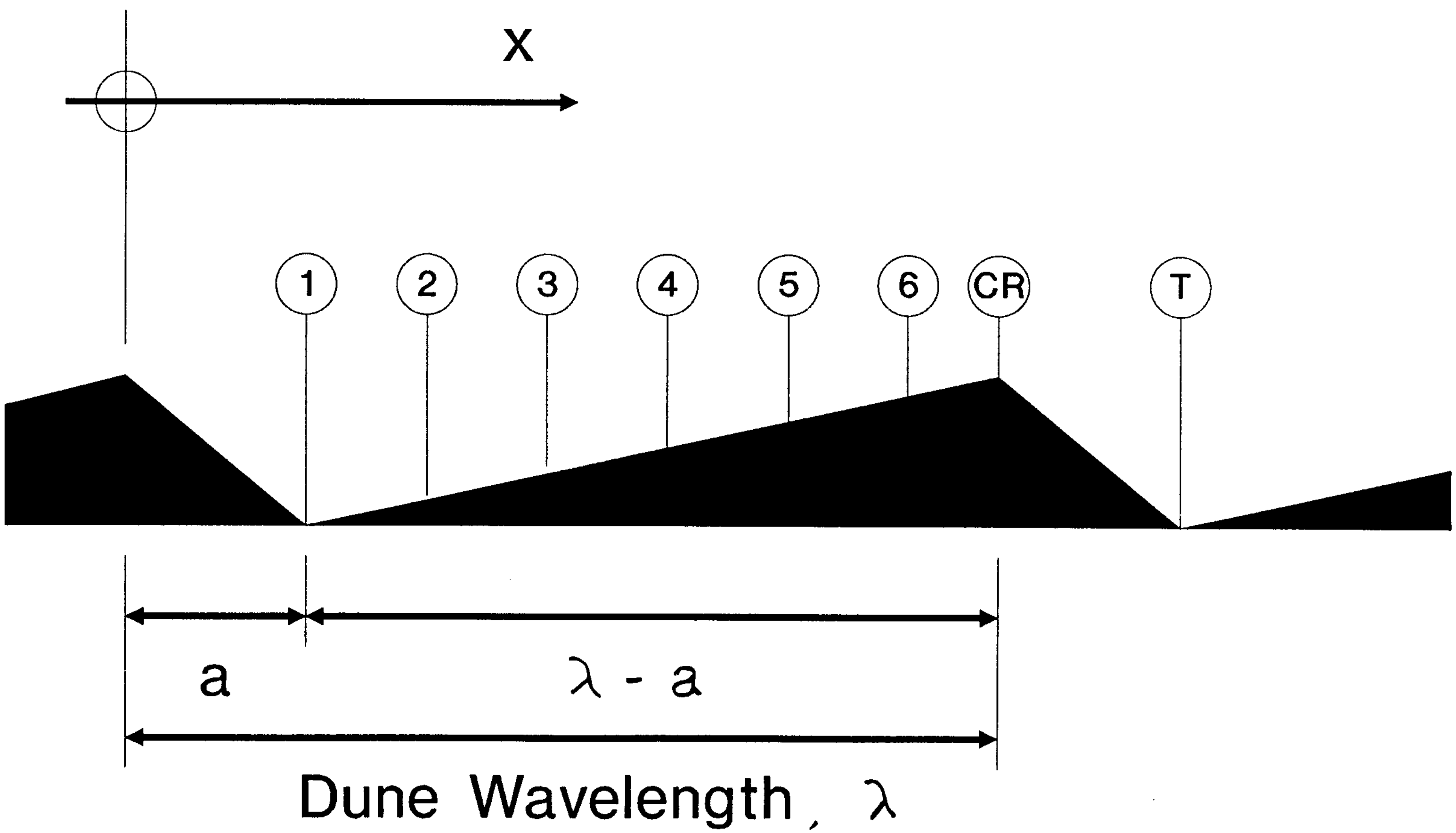

Figure 4.2 Definition sketch for reading points

Table 4.2 Definition of the reading points

POINT	f
1	0/6
2	1/6
3	1/3
4	1/2
5	2/3
6	5/6
CR	1

Furthermore as the flows approached the upper limits standing wave effects became evident. These conditions are not only unrealistic for dunes, but also indicated that, even if higher flows could be achieved, the data collected at this level would be unreliable.

A vernier scale on the depth gauge, mounted on the traverse mechanism, was used to determine the bed level and then the water level, the difference between them representing the flow depth at that point.

4.3 Length of separation

To measure the point of reattachment of the separation zone, a two step procedure was followed. In both steps the dye was allowed to enter the flow very close to the boundary and its direction of motion was observed. In the first step the pipette was positioned well upstream of the expected reattachment zone, so that there was a clear movement of the dye upstream. The pipette was then moved in small 2-3 mm increments until a point was reached were the dye seemed to hang in the fluid for a brief moment and then flowed mainly in the downstream direction. This point was taken as the upstream boundary of the reattachment zone.

The pipette was now moved downstream of this region, well beyond the zone of separation, to a point were the dye clearly moved only downstream. In small increments it was now moved upstream until a point was reached where the dye again remained still for brief moments, as shown in Figure 4.3 below. This was recorded as the downstream boundary of the region.

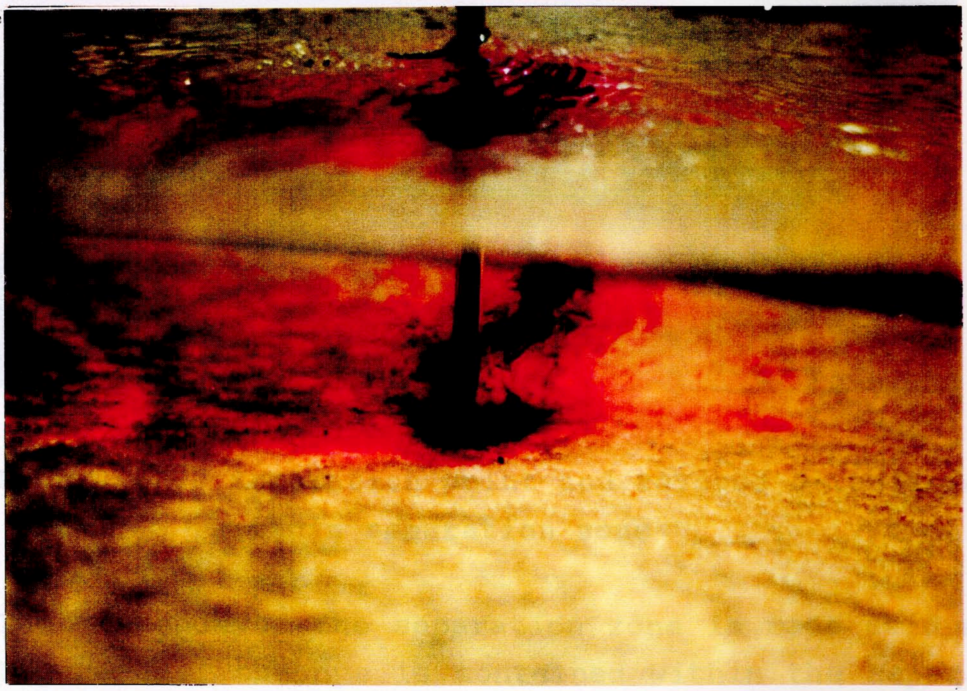

Figure 4.3 Downstream boundary of the reattachment region

The concept of the region is not new and was introduced by Engel (1981). Due to the turbulent fluctuations identified by Etheridge and Kemp (1979) it would not be possible to define a precise reattachment point but rather an averaged position. The same technique was applied to the fourth dune to ensure a reasonably reliable position for the point of reattachment. The length of separation for any particular combination of flow, geometry and roughness was then taken as the average of the four measurements.

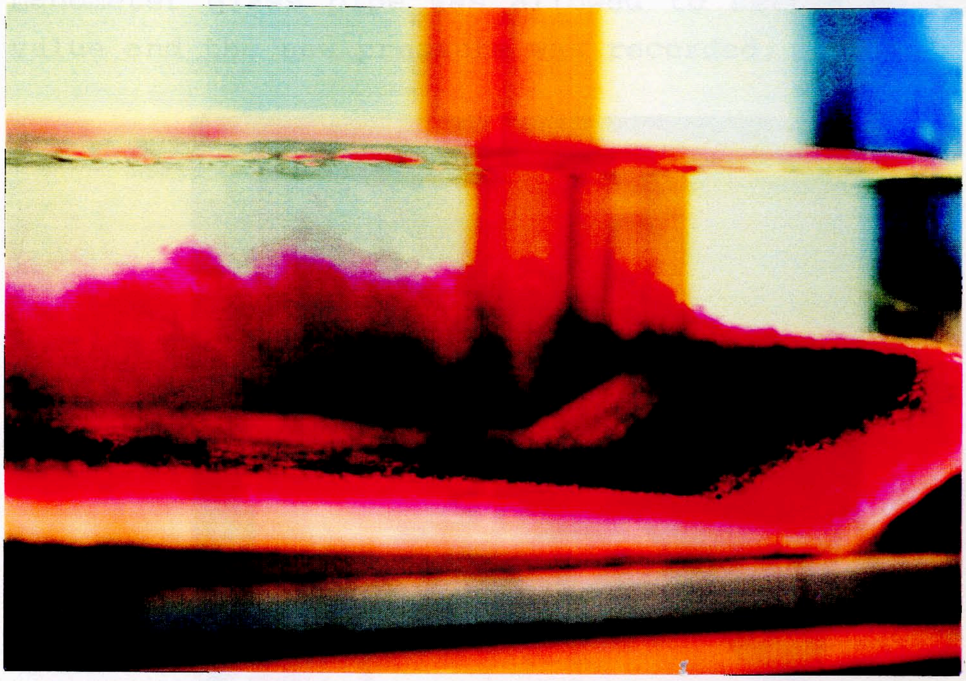

Figure 4.4 Separation point and reverse circulation within separation zone

The presence of the separation zone is made evident by Figure 4.4: the dye is contained within the separation zone by the recirculating flow, and there is a clear boundary between the latter and the outer flow.

4.4 Bed pressure distribution

Two tubes were used on the bed surface because firstly a smaller tube was needed to measure the pressure along the steep face of the dunes, and secondly to provide a check on the readings obtained using the larger tube. Both tubes were attached to the traversing mechanism using appropriately made connections as shown in Figure 4.5. They were then moved into position, the fluid in the manometer glass pipe was allowed to settle to the new value and the new pressure was recorded.

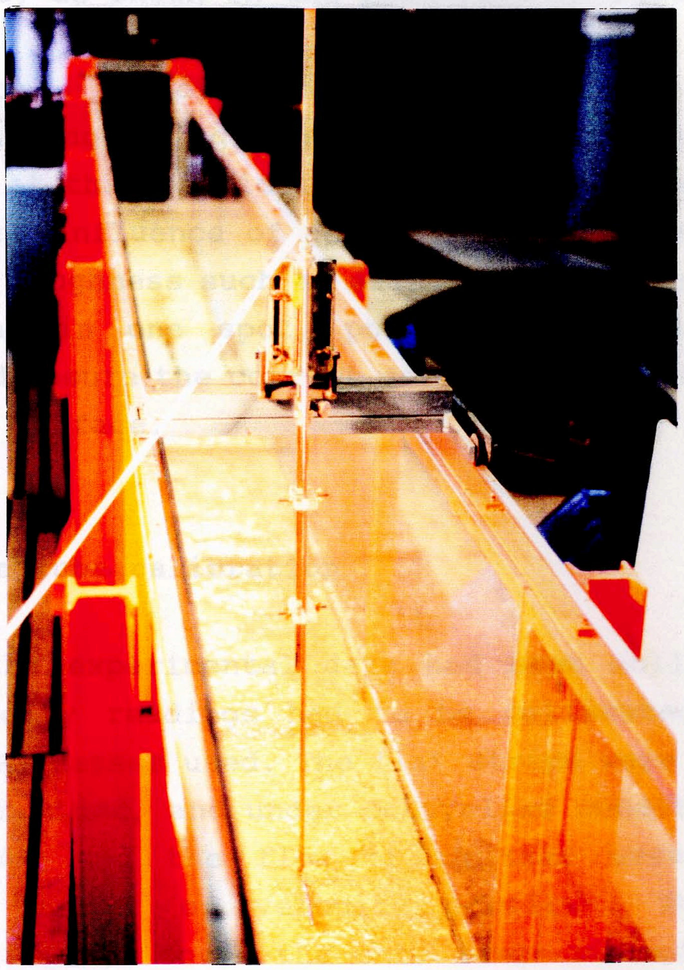

Figure 4.5 Bed pressure measurements in progress

4.5 Grain shear stress

The use of the Preston tube provided a further check on the location of the point of reattachment in that in the reattachment region the readings on the recorder and flow transmitter should be zero. The tube was connected to the traverse mechanism by clips and elastic bands, holding it in place so that the tube openings faced directly upstream and at 90° to the flow. Measurements were taken along the centre line (A) as well as along two other parallel lines (B and C) located 10 mm to the left and right of it, as shown on the plan view in Figure 4.6 .

Three readings for every point were obtained and these were then averaged to give a value for the point velocity on the bed at that particular position. This was done to minimize the influence of any localized problems of the artificial roughness such as excessive concentrations of sand grains in one spot, possible scratches in the surface and ensure the correct positioning of the tube on the dune's surface.

4.6 Preston tube calibration

Once all the experimental data had been collected the point velocity readings had to be calibrated for the various roughnesses used. The flat strips were placed in the smaller flume, and under controlled conditions, the Preston tube and the flow transmitter were used to measure a number of velocity profiles. These were selected so as to cover the same range of bed velocity conditions recorded during the main experiments.

4.5 Grain shear stress

The use of the Preston tube provided a further check on the location of the point of reattachment in that in the reattachment region the readings on the recorder and flow transmitter should be zero. The tube was connected to the traverse mechanism by clips and elastic bands, holding it in place so that the tube openings faced directly upstream and at 90° to the flow. Measurements were taken along the centre line (A) as well as along two other parallel lines (B and C) located 10 mm to the left and right of it, as shown on the plan view in Figure 4.6 .

Three readings for every point were obtained and these were then averaged to give a value for the point velocity on the bed at that particular position. This was done to minimize the influence of any localized problems of the artificial roughness such as excessive concentrations of sand grains in one spot, possible scratches in the surface and ensure the correct positioning of the tube on the dune's surface.

4.6 Preston tube calibration

Once all the experimental data had been collected the point velocity readings had to be calibrated for the various roughnesses used. The flat strips were placed in the smaller flume, and under controlled conditions, the Preston tube and the flow transmitter were used to measure a number of velocity profiles. These were selected so as to cover the same range of bed velocity conditions recorded during the main experiments.

Temperature and flow depth details were recorded, thereafter bed velocities were taken at three different positions and a velocity profile was measured above the centre line of the strip.

The slope of the smaller flume was kept at 1:500, the same as that of the large tilting flume.

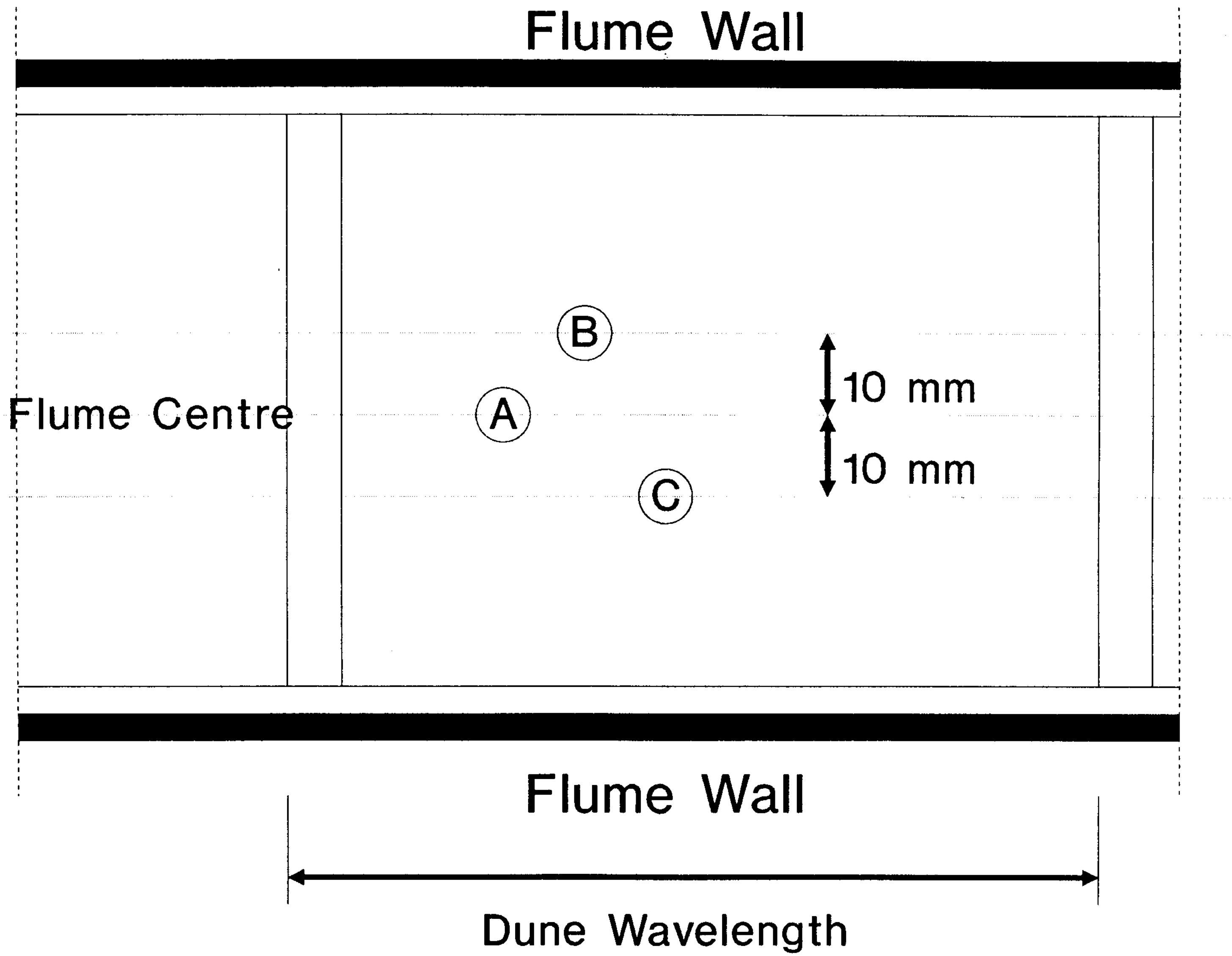

Figure 4.6 Plan view of dune train (Lines A,B,C)

Chapter 5
RESULTS AND DISCUSSION

5.1 Calibration experiments

To ensure that the Preston tube and flow transmitter combination was working correctly an independent test was carried out using a propeller meter. The flow transmitter was set by the suppliers to read a maximum velocity of 0.7 m/s and then of 1.0 m/s. For each setting simultaneous velocity measurements were taken in the small tilting flume using the flow transmitter and the propeller meter, the latter acting as the common reference.

A plot of the velocity measurements obtained using the Preston tube and the flow transmitter for the two different settings is shown in Figure 5.1 . The result is a straight line with a correlation coefficient r^2 of 1.0 . The straight line is a near perfect 45° line confirming that the instrumentation was working correctly.

A summary of the calibration experiments is presented in Table 5.1 . A total of 30 runs were conducted in which the bed velocities varied from a minimum of 0.12 m/s to a maximum of 0.55 m/s .

These velocities translate into differential pressures ranging from about 7 N/m^2 to a maximum of 140 N/m^2 , effectively covering the range recorded during the main experiments. Appendix B contains a summary of the results as well as the velocity profiles measured.

One of the profiles is presented in Figure 5.2 . The profiles are plotted on semi-log graph paper and generally show three very distinct regions:

(i) an initial curve between 1 and 3-3.5 mm depth followed by

(ii) a straight line portion between 3.5 and 30 to 35 mm depth and finally

(iii) an almost vertical line resulting from constant velocity readings above a depth of 35 mm.

The initial curve is due to the fact that the level of zero velocity is not known, i.e. the measuring datum is arbitrary. The straight line portion of the profile is consistent with the inner region velocity distribution, and its slope is used to determine T_o'', as discussed in Section 2.1.4. The measurements above a depth of 35 mm are in the outer region of the flow, and are consistent with the discussion on profiles presented in Section 2.1.1.

Table 5.1 Summary of calibration experiments

ROUGHNESS	D_{50} (mm)	RUNS
S1	0.50	C8 to C15
S2	0.93	C16 to C23
S3	1.60	C1 to C7
S4	3.05	C24 to C30

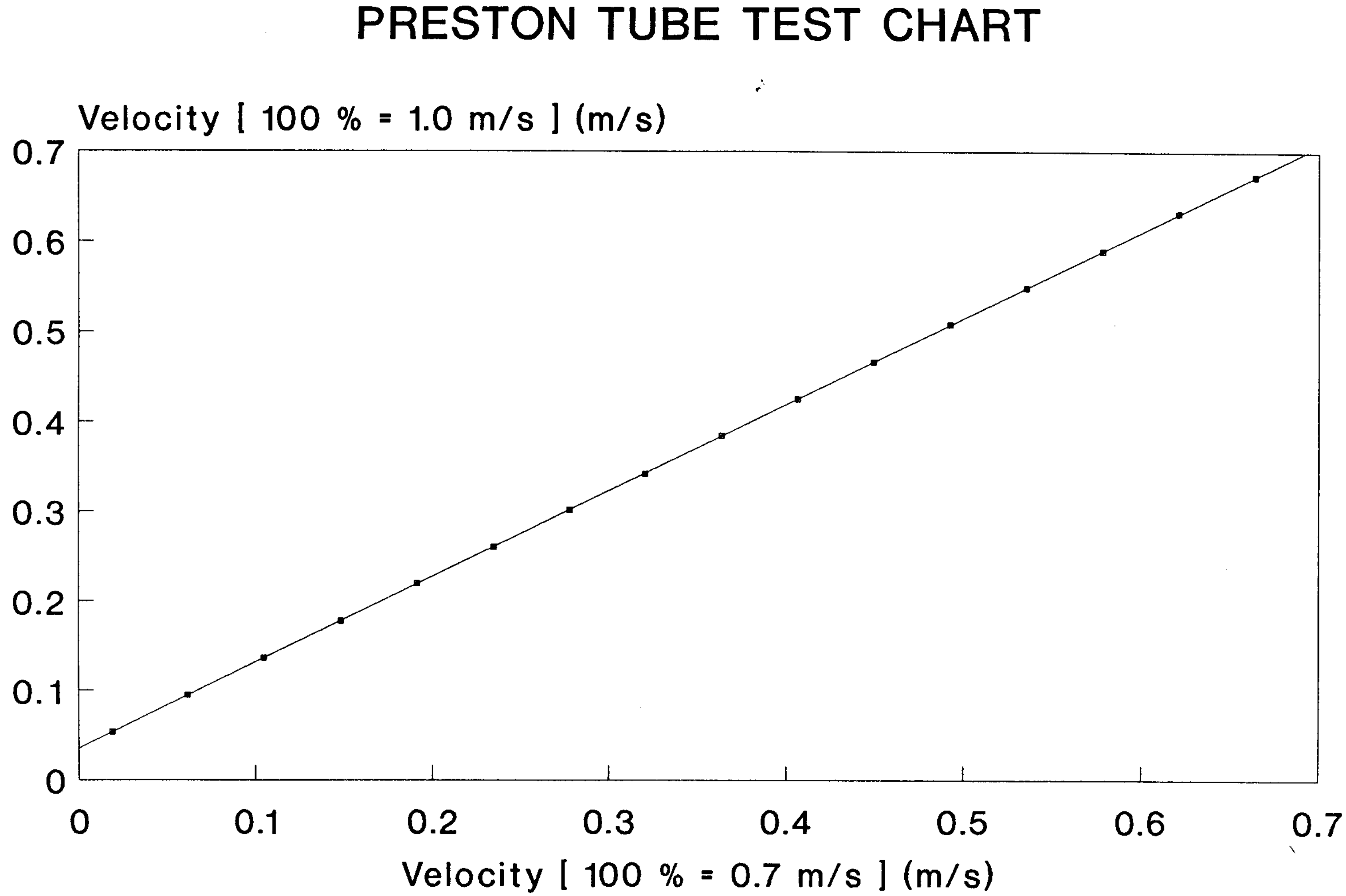

Figure 5.1 Results of the Preston tube and flow transmitter tests

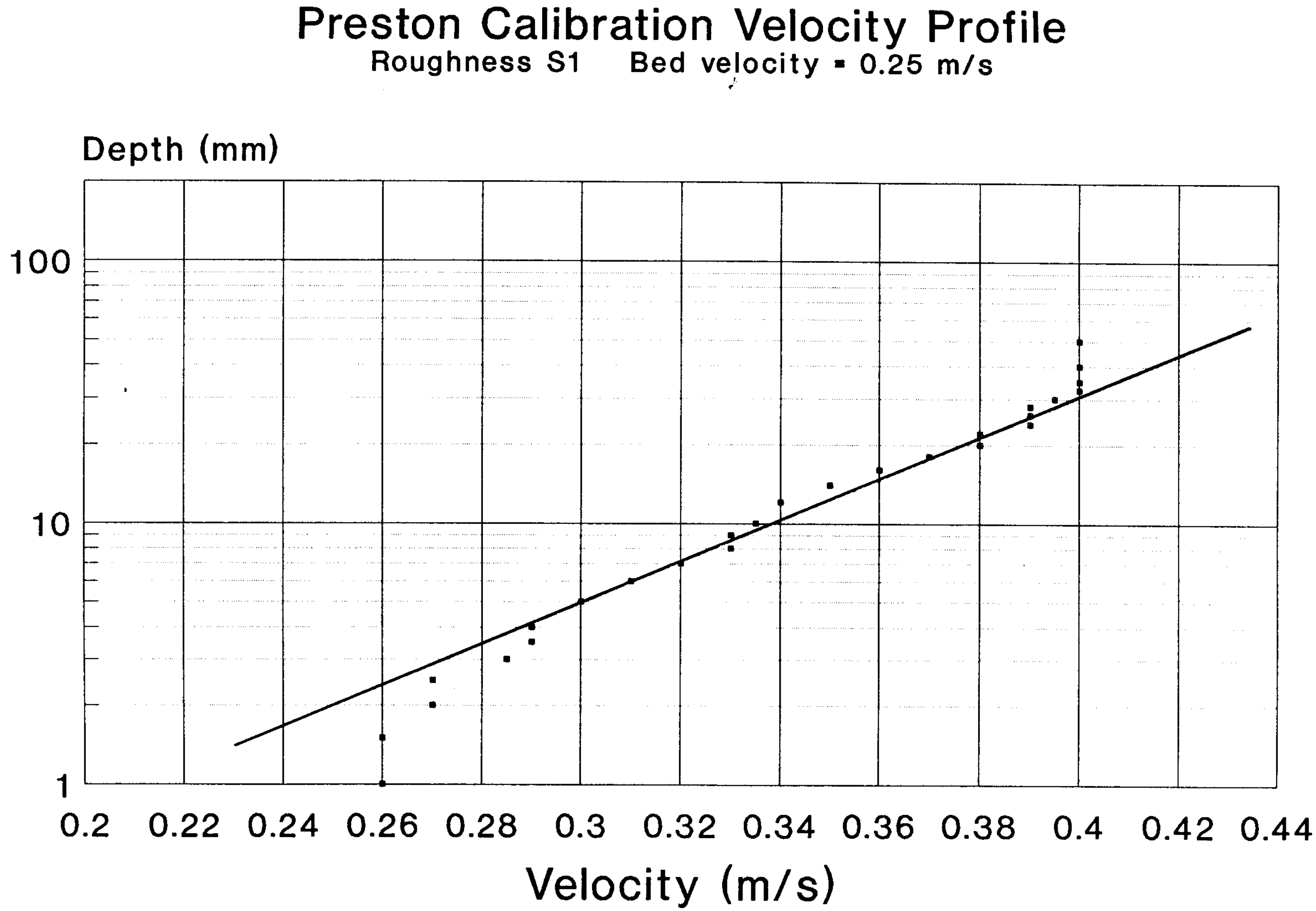

Figure 5.2 Typical velocity profile

PRESTON CALIBRATION CHART

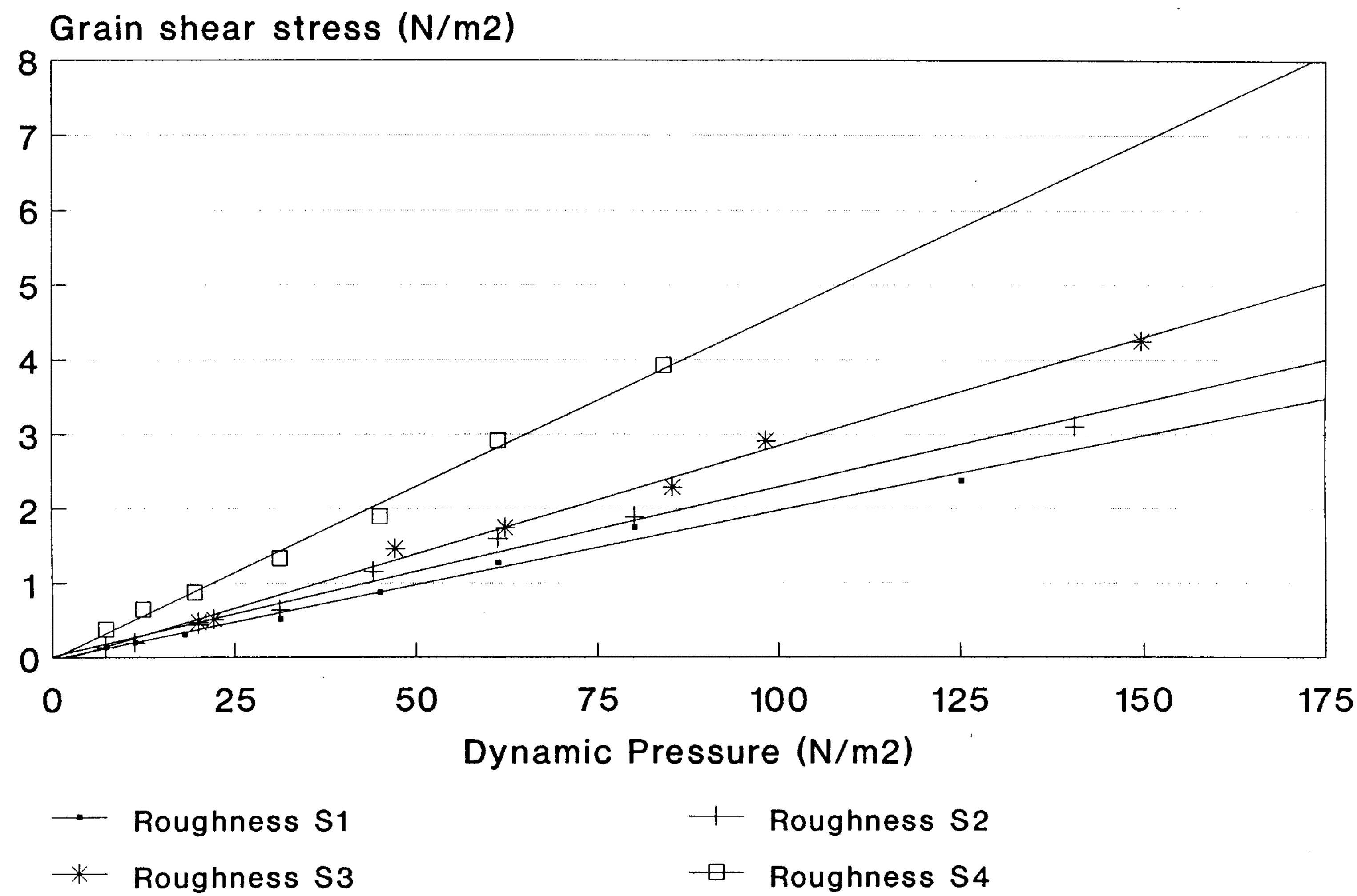

Figure 5.3 Preston calibration chart

Figure 5.3 shows a plot of grain shear stress, T_0'', versus differential pressure, ΔP, for the four different roughnesses used in the experiments. This is the calibration chart used to obtain the grain shear stress values for the main experiments.

From the chart it is evident that there is a linear relationship between dynamic pressure and grain shear stress. All four lines could be said to pass through the origin and there is an increase in grain shear stress with increasing dynamic pressure and bed velocity.

The straight lines were obtained by least squares regression, and the correlation coefficient for each was 0.99. The equations defining the lines are listed in Table 5.2 .

For dynamic pressure values below 25 N/m^2 the values of grain shear stress for roughnesses S1, S2 and S3 are almost identical, and after 25 N/m^2 the difference becomes increasingly more evident.

Table 5.2 Preston tube calibration equations

Roughness	Straight Line Equation
S1	$T_0'' = -0.02609 + 0.02006\ \Delta P$
S2	$T_0'' = 0.01517 + 0.02280\ \Delta P$
S3	$T_0'' = -0.06934 + 0.02914\ \Delta P$
S4	$T_0'' = -0.01751 + 0.04628\ \Delta P$

The value of grain shear stress for a given value of dynamic pressure increases with increasing bed roughness. The grain shear stress is thus dependent on the bed particle size, as would be expected. In this case the steepest line is that corresponding to a bed having the largest representative particle size, i.e. 3.05 mm.

Looking at the equations presented in Table 5.2 ,and ignoring the constant terms as they are very close to zero, we obtain the direct relationships between ΔP and T_0'', as listed in Table 5.3.

The results of Table 5.3 show that for any given particle size the ratio of dynamic pressure to grain shear stress, over a wide range of flow depths, is constant. Ippen et al (1960) arrived at a similar conclusion, and for their roughness the ratio was 47.6. This ratio however is not the same for all particle sizes as it decreases with increasing grain size.

Table 5.3 Simplified Preston tube relationships

ROUGHNESS	$\Delta P/T_{0''}$
S1	49.9
S2	43.9
S3	34.3
S4	21.6

5.2 Main experiments

5.2.1 General

A total of 55 experiments involving artificial dunes were conducted and are summarized in Table 5.4 . The geometry code, G, and the roughness code, S, are those described earlier in Table 3.3 , whereas D_{50}/Δ represents the dimensionless dune particle size proposed by Engel (1981).

Table 5.5 shows the position of the various reading points used during the experiments. The dimensions listed represent the distance in millimetres of the point from the crest of the previous dune. This table should be used in conjunction with the various graphs when interpreting the experimental results. All the main reading points are consistant with those listed in Table 4.2 and shown on Figure 4.2.

The additional reading points, denoted by an alphabetical subscript, were introduced to obtain measurements at important positions on the dune surface, e.g. on the lee side of the dunes or close to the reattachment point, as well as to provide a check on other measurements and confirm a particular trend.

Table 5.4 Summary of experimental runs

RUNS	G	S	D_{50}/Δ	Δ/λ
1 - 6B	1	3	0.04	0.06
7 - 13	2	3	0.04	0.05
14 - 21	3	3	0.04	0.04
22 - 29	4	3	0.04	0.03
30 - 37	2	1	0.01	0.05
38 - 45	2	2	0.02	0.05
46 - 53	2	4	0.07	0.05

5.2.2 Water profile and average flow depth

The water profiles measured during the experiments showed them to be out of phase with the dune profile, confirming this phenomenon as a typical characteristic of dunes. The profiles however deteriorate with increasing flow as higher flow rates give rise to standing waves, as shown in Figure 5.4 . The profiles are such that at higher flows there is a very sharp reduction in the flow depth at the dune crest.

Associated with this reduction in depth is a sharp increase in grain shear stress towards the crest of the artificial dunes, as discussed in section 5.2.5 . The flow is therefore interacting with the given geometry conditions in an attempt to alter the bed configuration.

Directly related to the water profile is the concept of an average flow depth over the dunes. The use of the average flow depth is important in determining the average flow velocity and the Froude number for a given flow condition.

As discussed in Section 2.1.6, there exist a number of different ways of determining the average flow depth. The water profiles measured in the experiments would suggest at first that calculating the average flow depth, H, by simply adding half the dune height to the crest flow depth is not satisfactory. For this reason the flow depths used to determine the water profiles were also used to calculate a mathematical average flow depth over the dune, H', and a comparison was then made between the two.

Table 5.5 Position of reading points

POINT	G1 (mm)	G2 (mm)	G3 (mm)	G4 (mm)
1	78	78	78	78
1_a	136	95	100	100
1_b		125	137	157
1_c		170	195	236
2	190	215	253	315
RP_b		320	387	494
3	302	352	427	552
3_a	328		485	
3_b	345	421	515	
3_c	358		544	
3_d	368			
3_e	380			
4	414	489	602	789
4_b				
5	526	626	776	1026
5_b			864	
6	638	763	951	1263
6_b		831	1038	1382
CR	750	900	1125	1500
CR_a		930	1155	1530
CR_b		960	1185	1560
T	828	978	1203	1578

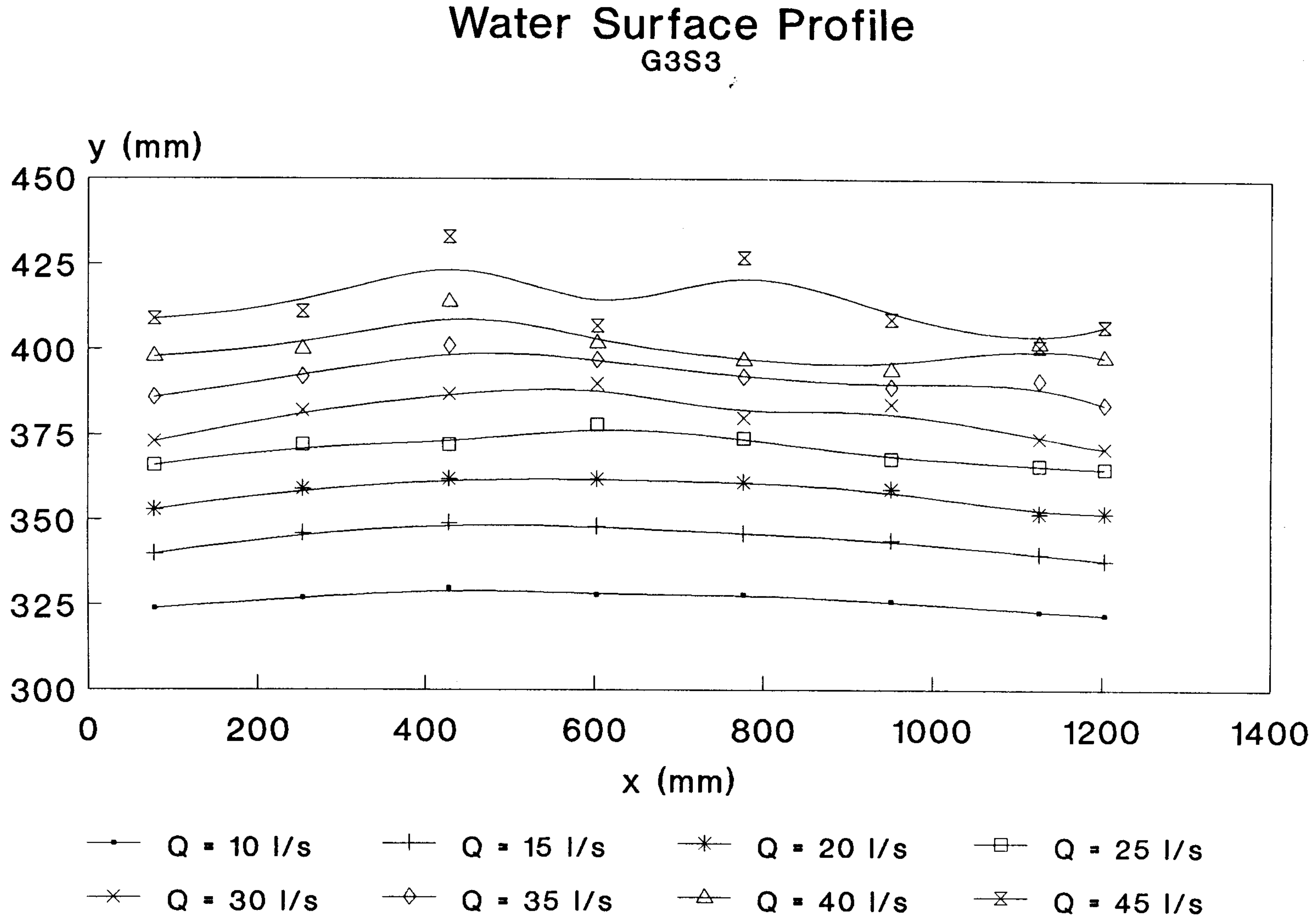

Figure 5.4 Typical water surface profile

$$H = h_{crest} + \frac{\Delta}{2} \qquad \ldots(5.1)$$

$$H' = \frac{\Sigma_{i=0}^{N} h_i}{N} \qquad \ldots(5.2)$$

The results presented in Appendix C show that differences between the average depths calculated in this way varied from a minimum of - 1.14 % to a maximum of 6.42 % of the value of H, the difference being 2.8 % on average. These discrepancies fall well within acceptable limits indicating that the average flow depth over a dune can be calculated by knowing the crest flow depth and the dune height. The average depth calculated using Equation 5.1 was then used to determine the relevant Froude numbers for each run.

Pillai's (1979) correction factor (Section 2.1.6) was also used to determine an effective flow depth, but in this instance differences varying between 20 % and 55 % were encountered. Pillai's equation for effective flow depth was derived from deep flows over small bed undulations and hence it should not be used when the dune height is significant in terms of the channel flow depth.

The variation in average flow depth for each geometry-roughness combination is presented in Table 5.6 .

The smallest average flow depth was 78.5 mm and the maximum recorded was 163.5 mm, thus ranging from 1.7 to 3.6 times the dune height. There is little difference in the flow depth for the various combinations at low flow velocities, but with increasing dune size and higher flow rates there is a tendency to have deeper flow. This is natural as there is an increase in the resistance to flow and more energy is required to overcome this.

Table 5.6 Range of average flow depths

COMBINATION	H_{min} (mm)	H_{max} (mm)
G1S3	78.5	136.5
G2S3	80.5	140.9
G3S3	79.5	158.5
G4S3	82.5	163.5
G2S1	81.5	160.5
G2S2	84.5	161.5
G2S4	84.5	163.5

A change in the bed roughness does not result in a marked change in flow depth except for the combination G2S3 which has a maximum average flow depth considerably lower than that of the other roughnesses. Appendix C also contains plots of the water profiles and the data recorded. The curves were plotted using least squares regression.

5.2.3. Length of separation

A summary of the length of separation measurements is shown in Figure 5.5 , where the length of separation is plotted against varying flow rates, and in Figures 5.6 and 5.7 where the plot is against varying Froude numbers.

From Figure 5.5 it is evident that initially the length of separation decreases with increasing flow until a minimum value is reached, thereafter increasing gradually. This trend is evident in both the varying geometry and varying roughness experiments.

The length of separation values are greater for the larger dunes and they decrease as the dunes reduce in size, as expected. The length of separation also varies with the size of the bed particles: the smaller the particle size the longer the separation length under identical flow and geometry conditions. In this instance however the curves converge onto one line after the minimum value has been reached. The separation length appears to be dependent on the surface roughness at low flow rates, but as these increase particle size would appear to lose its influence.

In Figures 5.6 and 5.7 the length of separation is plotted against Froude number, as the latter is considered to be a more meaningful flow parameter. The length of separation measurements were all taken in a range between 0.34 and 0.60 of the Froude scale. For varying bed particle sizes and different dune sizes the same trends described previously are confirmed and in fact become more evident as, for instance, after the minimum value is reached there is a clear convergence of the four varying roughness curves onto one line.

Throughout the experiments the reattachment point was always located between the second and third reading points, in other words between 0.25 and 0.4 times the dune wavelength.

$$0.25\lambda \le L \le 0.4\lambda \qquad \ldots(5.3)$$

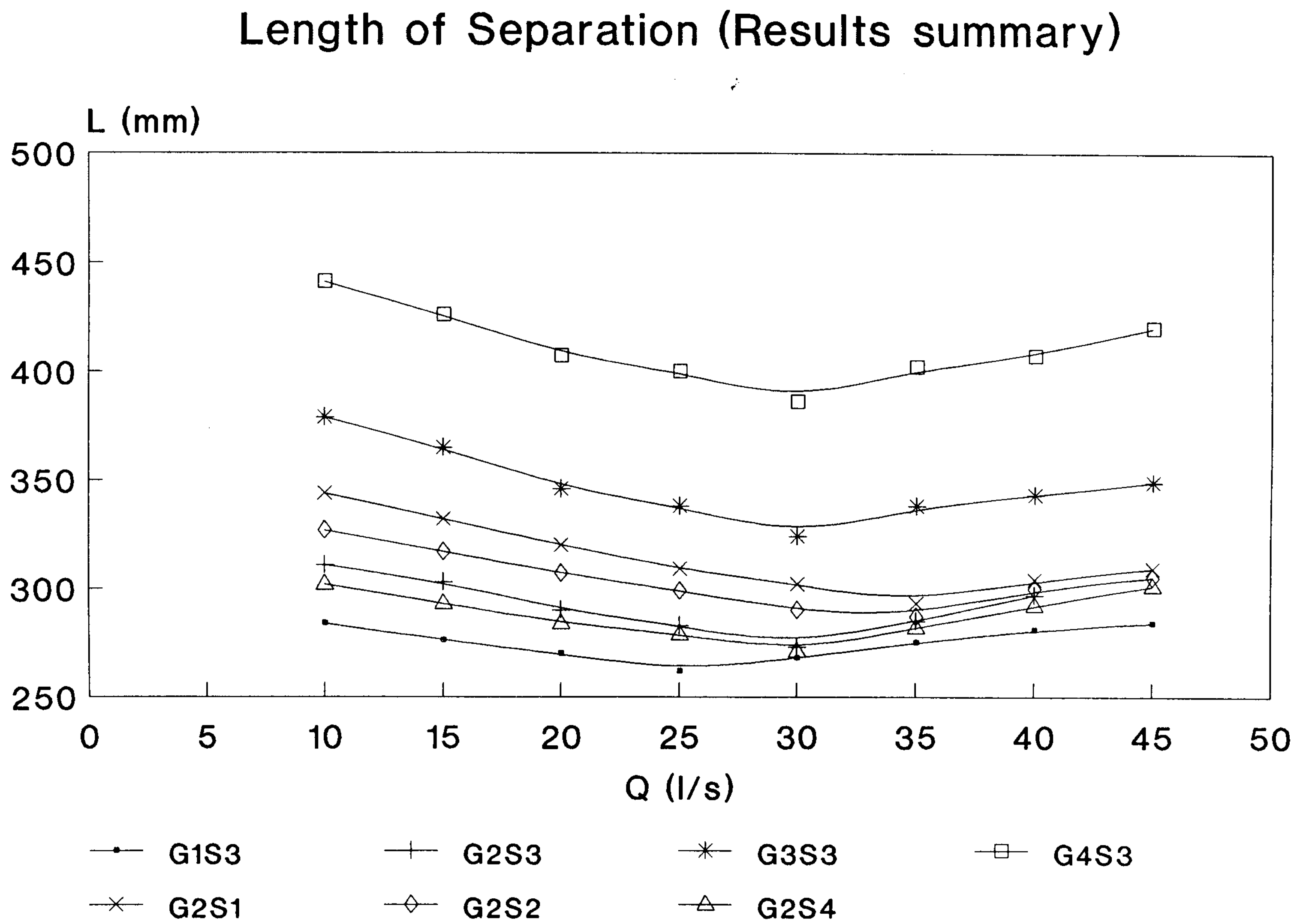

Figure 5.5 Length of separation measurements

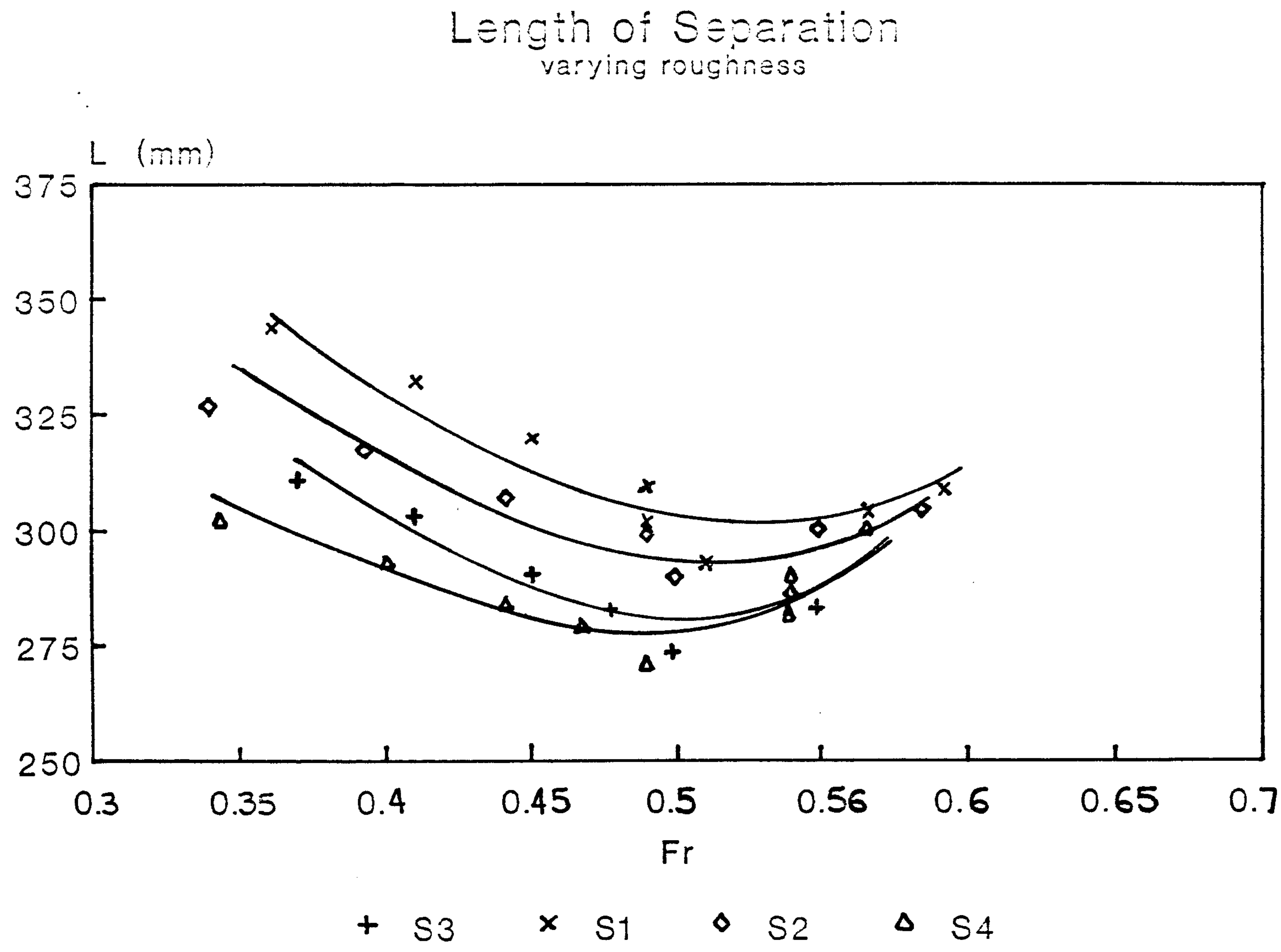

Figure 5.6 Length of separation for varying roughness

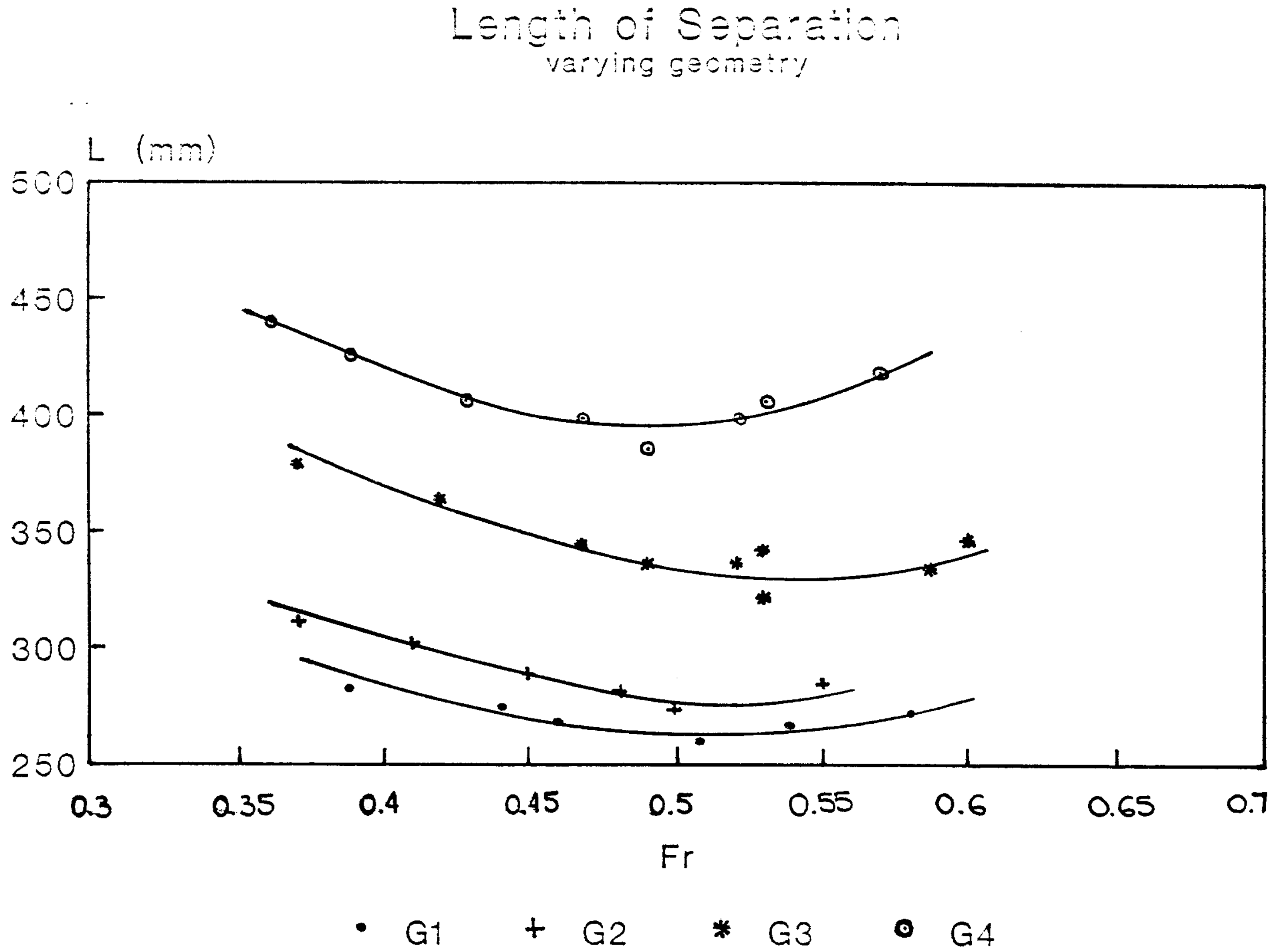

Figure 5.7 Length of separation for varying geometry

The effect of geometry and roughness on the separation length becomes clearer when looking at Figure 5.8 . The results for different roughnesses all fall onto one line showing very little variation in the magnitude of the separation length, whereas the results for the different geometries fall onto four different lines. The slopes of the lines also increase with increasing dune wavelength. Likewise, the length of separation increases in magnitude with increasing dune wavelength, but in relative terms the smaller dunes have a greater area in which reverse flow takes place. All the relevant graphs and summaries are in Appendix D.

Table 5.7 shows the average ratio of separation length to dune height and to dune length, for the various roughness and geometry combinations used.

Table 5.7 Average dimensionless length of separation

<table>
<tr><th>COMBINATION</th><th colspan="2">$\omega = L/\lambda$</th><th colspan="2">$\Omega = L/\Delta$</th></tr>
<tr><td>G1S3</td><td colspan="2">0.37</td><td colspan="2">6.11</td></tr>
<tr><td>G3S3</td><td colspan="2">0.31</td><td colspan="2">7.73</td></tr>
<tr><td>G4S3</td><td colspan="2">0.27</td><td colspan="2">8.02</td></tr>
<tr><td>G2S1</td><td>0.35</td><td rowspan="4">0.33</td><td>6.98</td><td rowspan="4">6.7</td></tr>
<tr><td>G2S2</td><td>0.34</td><td>6.76</td></tr>
<tr><td>G2S3</td><td>0.32</td><td>6.48</td></tr>
<tr><td>G2S4</td><td>0.32</td><td>6.4</td></tr>
</table>

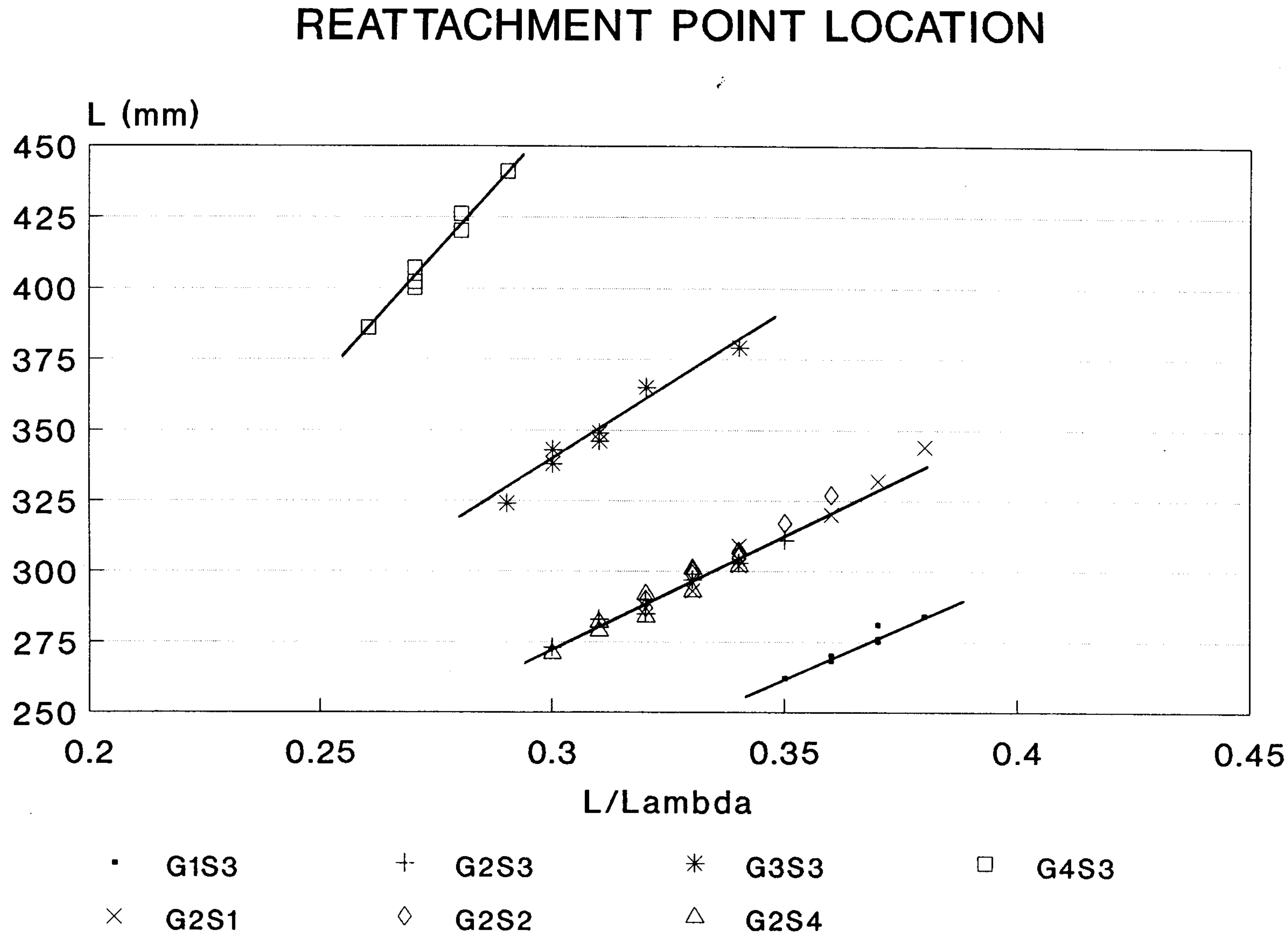

Figure 5.8 Reattachment point location

The values of Ω compare favourably with those of previous researchers, as presented in Table 2.6 . There is little variation due to changes in roughness, whereas changes in dune length affect the separation length considerably.

The value of Ω for geometry G1 is comparable with that of 5.3, obtained by Karahan and Peterson (1980) in their experiments, involving dunes having an identical steepness ratio of 0.06 (See section 2.1.3).

The results for Ω , however, are consistently higher than the values put forward by Engel (1981). Given the similar experimental conditions and the method of measurement adopted (See section 2.1.3), a good correlation with Engel's results would have been expected.

The one significant element that could explain the difference in the results is the fact that in these experiments a dune height, 1.5 times that used by Engel, was adopted. As the range of Froude numbers obtained were similar, the height of the dunes must therefore have an influence on the separation length. The values of ω confirm that the smaller dunes have, in relative terms, a larger separation zone and that roughness has a negligible effect on separation length. The average value of 0.33 compares favourably with Karahan and Peterson's value of 0.32 (1980).

5.2.4 Bed pressure distribution

The bed pressure distribution profiles have proven to be constant in nature and in magnitude through the changes of roughness and dimension of the dunes. In Figure 5.9 a typical plot of bed pressure against position along the dune surface is presented.

The bed pressure increases with increasing flow conditions and flow depth as expected. The curves all have an initial plateau of almost constant values even though at this stage the flow depth is already decreasing with distance. The pressure then starts to decrease at a point somewhere between reading points 2 and 3, coinciding with the location of the reattachment point (See section 5.2.2). The bed pressure continues to decrease until it reaches a minimum value at the dune crest, thereafter increasing rapidly over the lee side of the dune. This coincides with the sudden increase in flow depth and the bed pressure now reaches its original values so as to repeat the pattern over the following dune (See Appendix E).

Comparison of the bed pressure values under varying flow conditions is made possible by using a bar chart such as the one shown in Figure 5.10 (Q = 35 l/s). The bed pressure shows very little variation in magnitude under varying roughness conditions as would be expected. At times the values of pressure for roughness S3 are lower than for the others, particularly at lower flow rates. Under varying geometry conditions the difference in pressure readings is more evident, with the pressure increasing in magnitude with increasing dune length.

Pressures recorded varied from a minimum of 150 to a maximum of 265 mm of water.

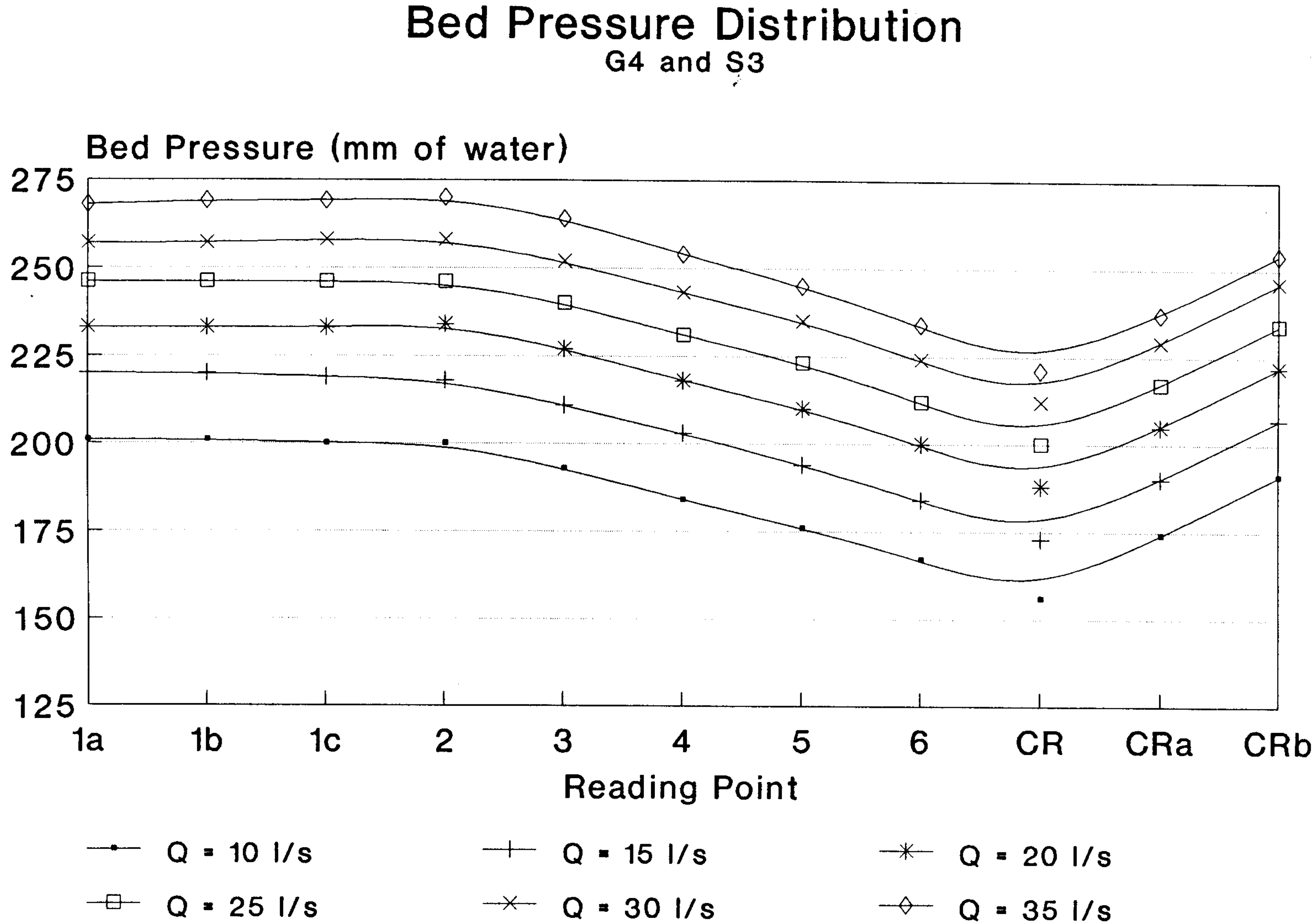

Figure 5.9 Typical bed pressure distribution

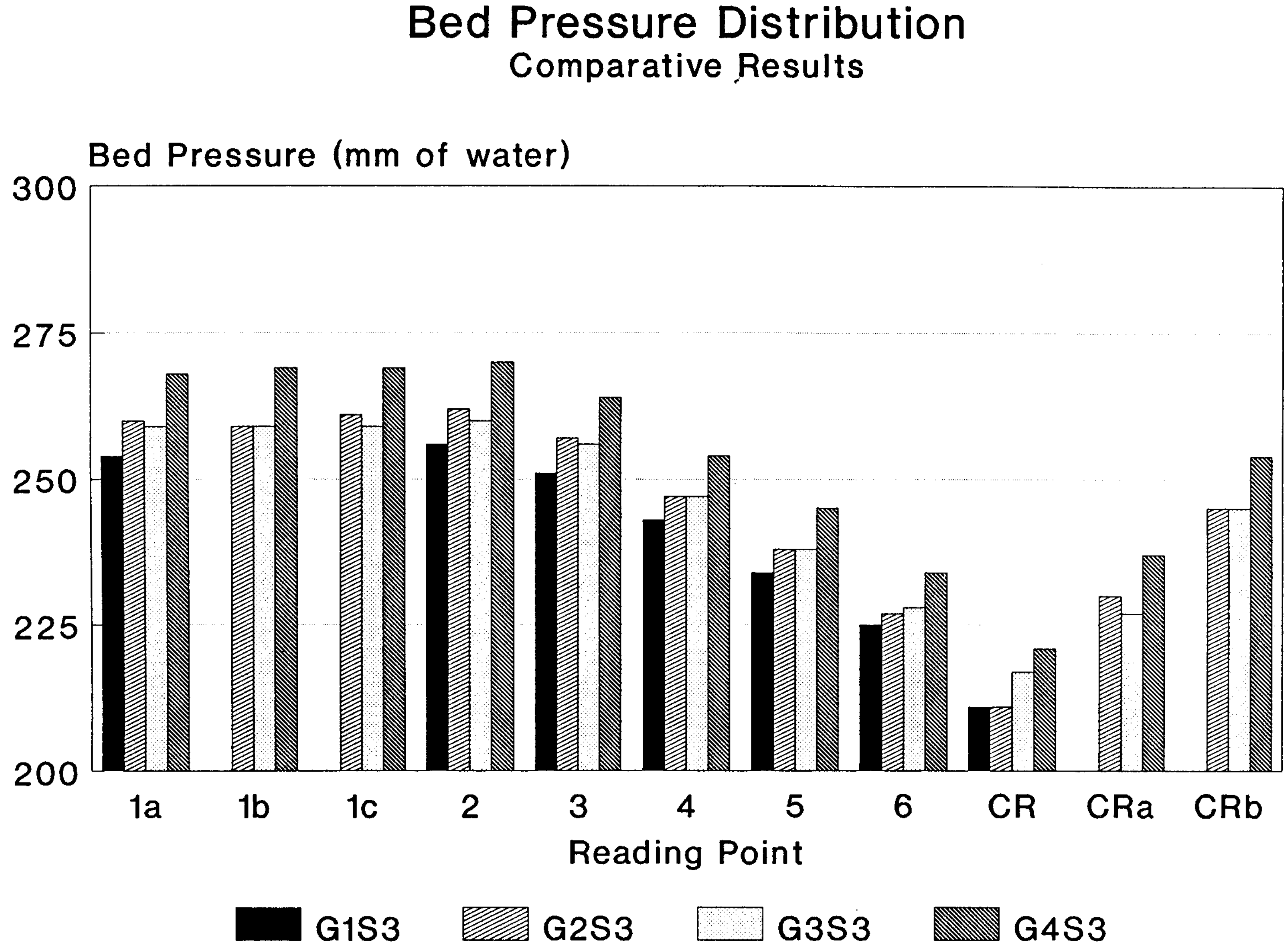

Figure 5.10 Comparative analysis of bed pressure distribution

5.2.5 Grain shear stress

In general the plot of grain shear stress along the dune surface starts from a value of zero at the reattachment point and increases to a maximum at the crest. This is in line with the findings made by Jonys (1973), Vittal et al (1977) and Fehlman (1985). The curve profile varies with increasing flow conditions starting almost as a straight line under the initial flow rates and progressively becoming more parabolic in shape, starting with a rapid increase from zero and then flattening out.

However the curves do not gradually flatten out to a maximum at the crest as expected, but instead, from about the 6^{th} reading point, or $5/6^{ths}$ of the stoss side length, there is a final rapid increase in the grain shear stress values. This increase becomes more evident as the flow conditions increase, and readings taken between the sixth reading station and the crest confirm this phenomena.

Thus three distinct regions can be identified when studying the grain shear distribution along the surface of a dune (See Figure 5.11 and those in Appendix F):

(i) An initial region of rapid development of grain shear stress between the reattachment point (grain shear stress value of zero) and a point half way along the stoss side.

(ii) An intermediate region of constant development in grain shear stress starting half-way along the stoss face up to $5/6^{ths}$ of the stoss.

(iii) A final region of rapidly increasing grain shear stress culminating in a maximum value at the crest.

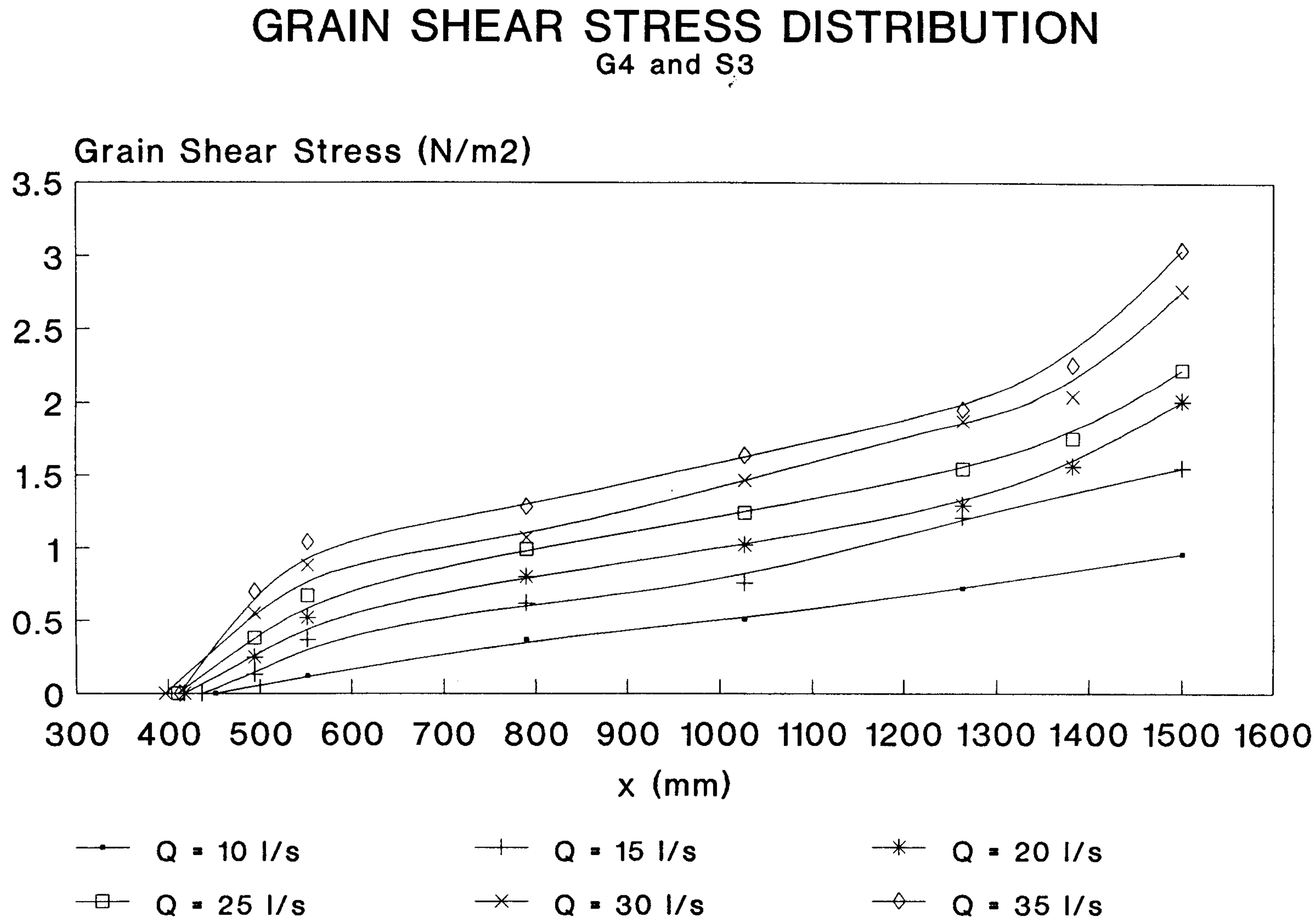

Figure 5.11 Typical grain shear stress distribution

This peculiar distribution can be explained if we look at the shape of dunes found in nature. The artificial dunes used were triangular in shape with a fairly sharp crest, whereas in nature dunes are almost parabolic in shape with a flat plateau leading to the crest, not too dissimilar to the grain shear stress distribution obtained in these experiments. The artificial dunes do not flatten out towards the crest and the system is therefore reacting to this in an attempt to reach a state of equilibrium. The grain shear stress increases thus, attempting to erode the crest and give the dunes a more natural shape.

The shear stress distribution on a natural equilibrium dune would be similar to the distributions obtained in these experiments. The significant difference however, would be the absence of the final region of rapidly increasing shear stress, and the distribution would gradually flatten out to a maximum value at the crest.

Varying geometry conditions

The grain shear stress has a value of zero, or close to zero, in the separation zone extending from the crest to the reattachment point on the following dune. No measurements could be taken within the separation zone to confirm this but there exists sufficient evidence (Mendoza-Cabrales,1987) that points to this.

The bar charts, such as the one in Figure 5.12, show a comparative analysis of grain shear stress values at the same geometrical points for the four geometries used, under the same flow conditions.

The maximum crest grain shear stress value was always recorded for the steepest dune (i.e. the dune with the shortest wavelength). This value was significantly higher

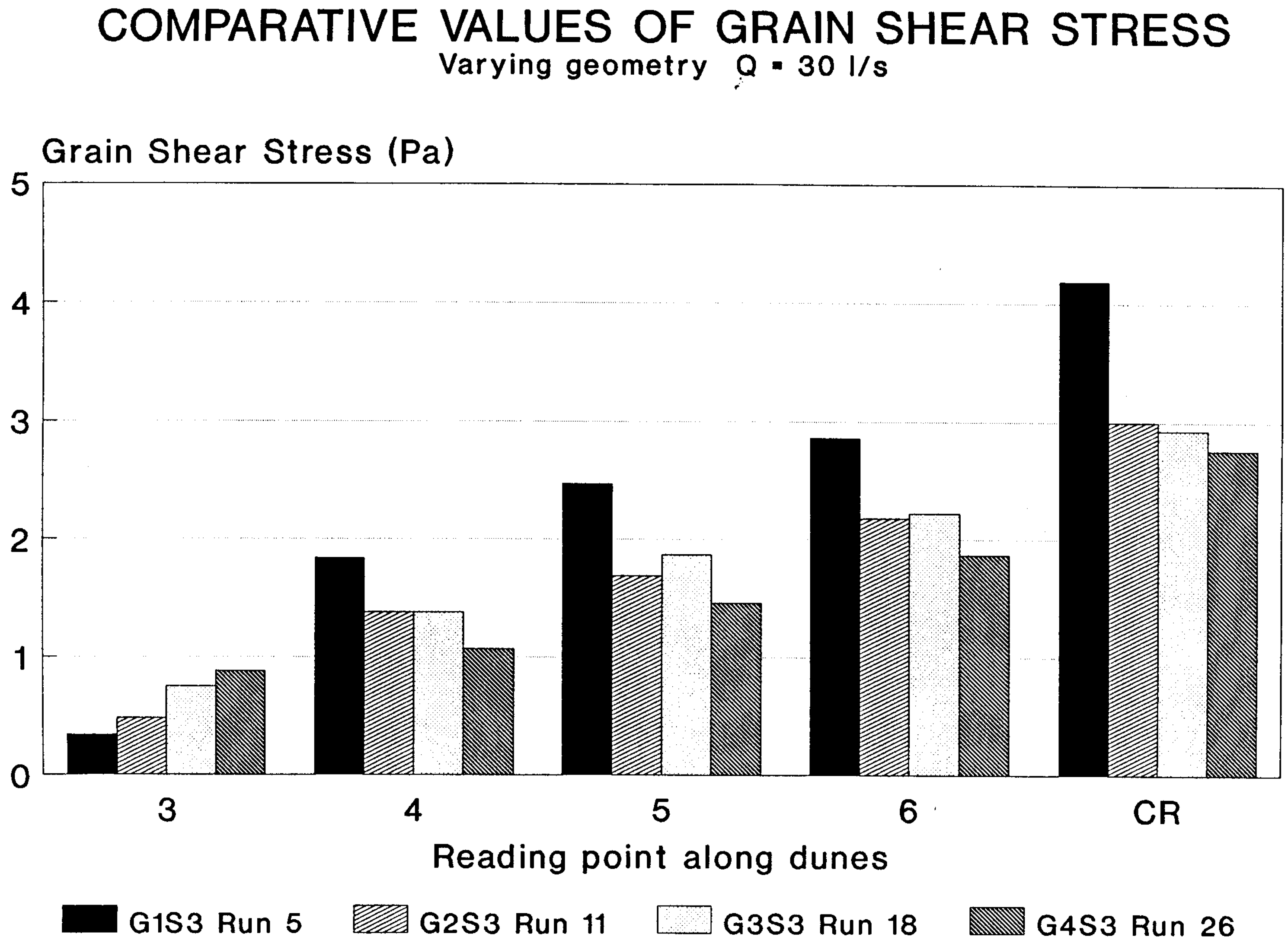

Figure 5.12 Grain shear stress (varying dune geometry)

than the measurements on the other dunes. The measurements for these latter in fact never differed significantly in magnitude. In general it appears that the flatter/longer the dunes the lower the maximum/crest grain shear stress.

The grain shear stress next to the reattachment points is higher for the flatter dunes and in general increasing flow conditions result in an evening out of the grain shear stress values for the varying geometries. These results thus indicate that at low to intermediate Fr values (0.3 to 0.6), the geometry of the dunes has an influence on the magnitude of grain shear stress.

Varying roughness

The same comments made for the varying geometry results hold true, with one notable exception in the fact that for the largest bed particle size tested, S4, there are only two distinct regions:

(i) The initial region described earlier, with the rapid development of grain shear stress,

(ii) and then a second region in which the grain shear stress increases steadily to a maximum at the crest.

This profile, shown in Figure 5.13, could be the result of a wrong geometry-roughness combination resulting in the system reacting to the initial conditions by trying to drastically alter the dune profile.

The comparative analysis of the bar charts, shown in Figure 5.14, reveals that again the maximum grain shear stress is measured at the crest of the dunes, and in these experiments the largest values were recorded for the largest bed roughness, S4.

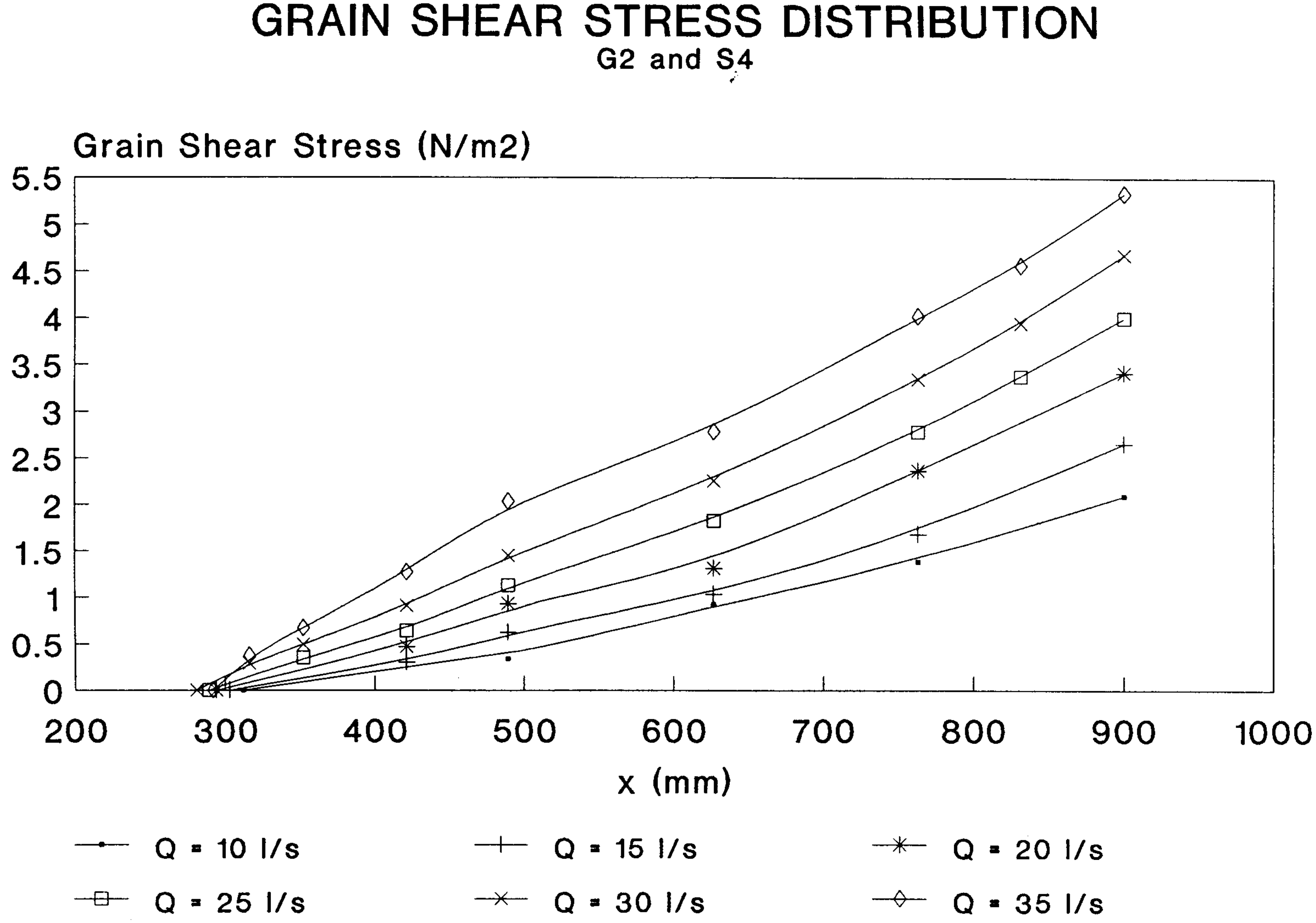

Figure 5.13 Grain shear stress for roughness S4

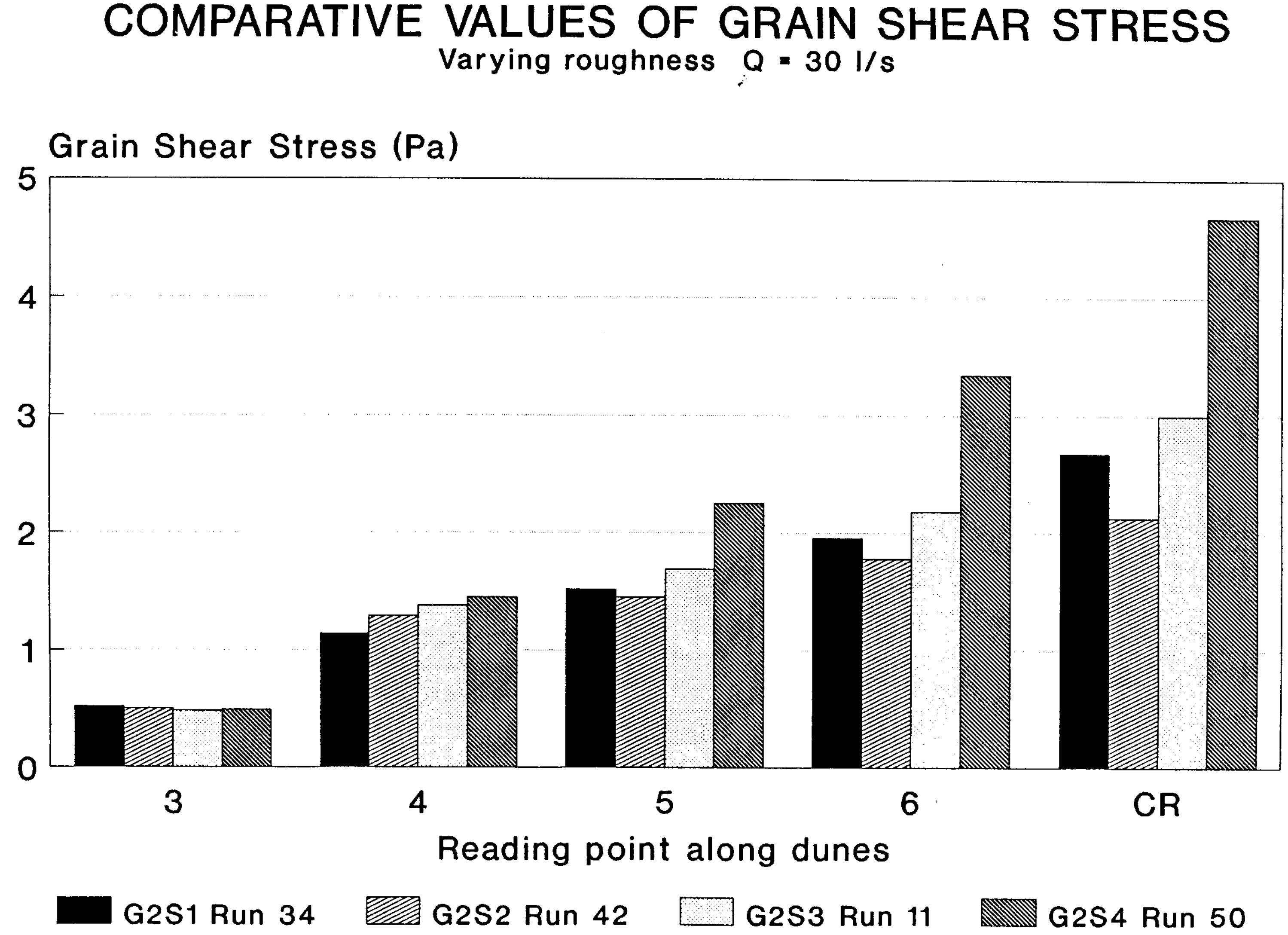

Figure 5.14 Grain shear stress (varying dune roughness)

The order of magnitude however reveals that the smallest values were measured for roughness S2, in that:

S4 > S3 > S1 > S2

This could be the result of the best geometry-roughness combination for the given flow conditions, with the system showing the least reaction to it. This was already reported in section 5.2.2 when looking at the flow depths and water profiles over the artificial dunes.

The grain shear stresses recorded for roughness S4 clearly stand out in magnitude whereas those for the other three surfaces remain fairly close to one another throughout the experiments. The larger particle size has therefore a marked influence on the grain shear stress.

It can thus be concluded that grain shear stress is not dependent on particle size alone, but that the combination of dune geometry and particle size will determine the grain shear stress magnitude and distribution over the bed of an alluvial channel under specific flow conditions.

Chapter 6
SUMMARY, CONCLUSIONS AND RECOMMENDATIONS

6.1 Summary

Alluvial channels are dynamic systems composed of constantly moving and evolving sedimentary bed forms and turbulent flow. In this study a simplified system is used under controlled laboratory conditions to measure specific hydraulic properties. These properties represent a unique set of data in that they are all measured simultaneously under varying geometry, roughness and flow conditions, for the first time.

The data can be used to improve the understanding of alluvial channel behaviour and to test and calibrate the accuracy and validity of current and future sediment transport models.

The flow of water over artificially roughened dunes at intermediate Froude numbers is studied using a combination of four bed particle sizes and four dune sizes placed in a laboratory flume. Measurements of flow depth, length of separation, bed pressure and grain shear stress are recorded using depth gauges, potassium permanganate as a visual aid, a pressure manometer and a Preston tube coupled to a flow transmitter respectively. The results are then presented and discussed by means of tables, graphs and charts.

In addition secondary experiments are conducted in order to calibrate the Preston tube and flow transmitter for the various roughnesses. A calibration chart, which relates the grain shear stress to the bed pressure differential, is included.

6.2 Conclusions

6.2.1 Calibration experiments

* There exists a linear relationship between grain shear stress, T'_0, and dynamic pressure, ΔP.
* Calibration charts of grain shear stress against pressure differential can be prepared for the different bed particle roughnesses.
* Grain shear stress increases in magnitude with increasing bed particle size.

6.2.2 Water profile and average flow depth

* The water profiles measured were out of phase with the dune profile.
* There is a sharp reduction in the flow depth at the dune crest.
* The average flow depth over a dune can be calculated knowing the crest flow depth and the dune height by using Equation 5.1 .

6.2.3 Length of separation

* At intermediate Fr values (between 0.34 and 0.60) the length of separation is strongly dependant on the size of the dunes and on the flow conditions. The length of separation at first decreases with increasing Froude number until a minimum is reached, thereafter increasing again.
* The bed particle size shows some effect on

length of separation, for Fr values less than 0.50. Thereafter its effect rapidly decreases with increasing Froude number.

* In relative terms the smaller the dune the greater the separation zone area.
* The reattachment point is always located at a distance of 0.25 to 0.4 times the dune wavelength, measured from the crest of the previous dune.

6.2.4 Bed pressure

* The bed pressure is at a constant maximum within the separation zone and it is at a minimum at the dune crest.
* The pressure distribution begins to decrease at a point coinciding with the reattachment point of the separation zone.
* Dune roughness has very little effect on bed pressure, whilst dune geometry has a more marked effect.

6.2.5 Grain shear stress

* The grain shear stress distribution starts from a value of zero at the reattachment point and increases to a maximum at the dune crest.
* The geometry of the dunes has an effect on grain shear stress at lower Fr values. The longer the dunes the lower the maximum grain shear stress.
* The grain shear stress is strongly dependent on particle size as would be expected. The larger the bed particles the higher the measured grain shear stress.

* An optimum combination of dune geometry and bed roughness (G2S2) resulted in a decrease in the grain shear stress values. This indicates that these two parameters act together in determining the grain shear stress distribution over the dunes.

6.3 Recommendations for future study

* Extensive Preston tube measurements using different particle sizes and shapes should be carried out to obtain a general calibration chart. These experiments would also provide an insight into the correct use and limitations of this instrument.

* The information presented in this study should be used to test present transport models and in the development of future models.

* Further experiments should be undertaken to obtain more information on the interaction between dunes and turbulent flow in alluvial channel. Areas of particular interest are:
  (i) flows at higher Froude numbers,
  (ii) effect of different dune heights,
  (iii) introducing a porous surface,
  (iv) changing the dune profile from a simple triangle to more complex shapes,
  (v) introducing sediment in the system so as to allow flow and bed forms to interact more freely.

APPENDIX A : Sand Details

PARTICLE SIZE DISTRIBUTION

Silica Sand #1

Type 0.3-0.65 mm   Initial Mass = 323.5 g

SIEVE SIZE (mm)	MASS RETAINED (g)	PERCENTAGE RETAINED	PERCENTAGE FINER BY MASS
0.85	0.6	0.2	99.8
0.6	62.6	19.3	80.5
0.425	163.3	50.5	30.0
0.3	74.2	22.9	7.1
0.212	18.4	5.7	1.4
0.15	2.8	0.9	0.5
PAN	1.6	0.5	0.0
TOTAL	323.5	100	-

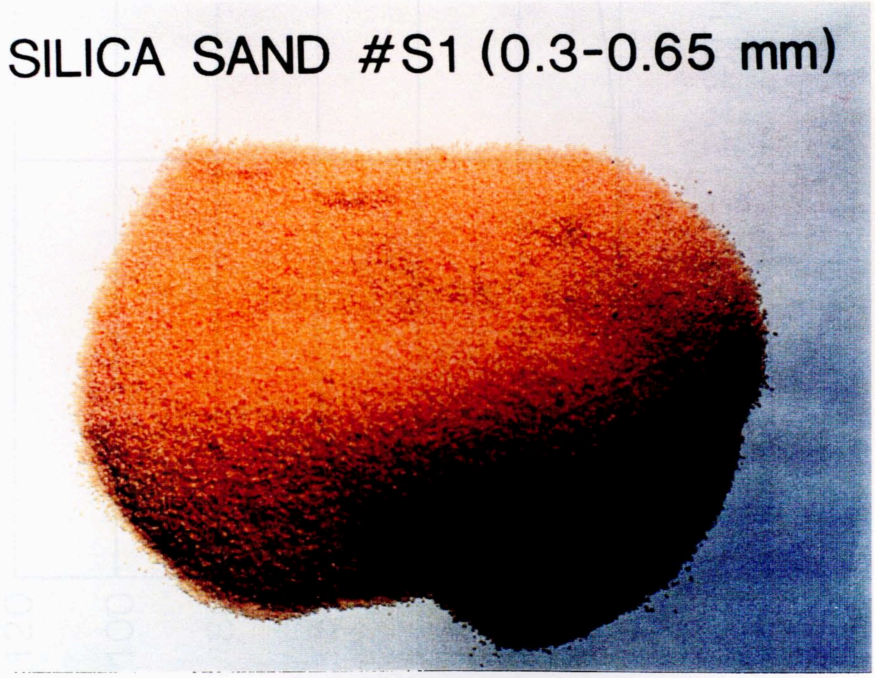

Particle Size Distribution

Silica Sand S1

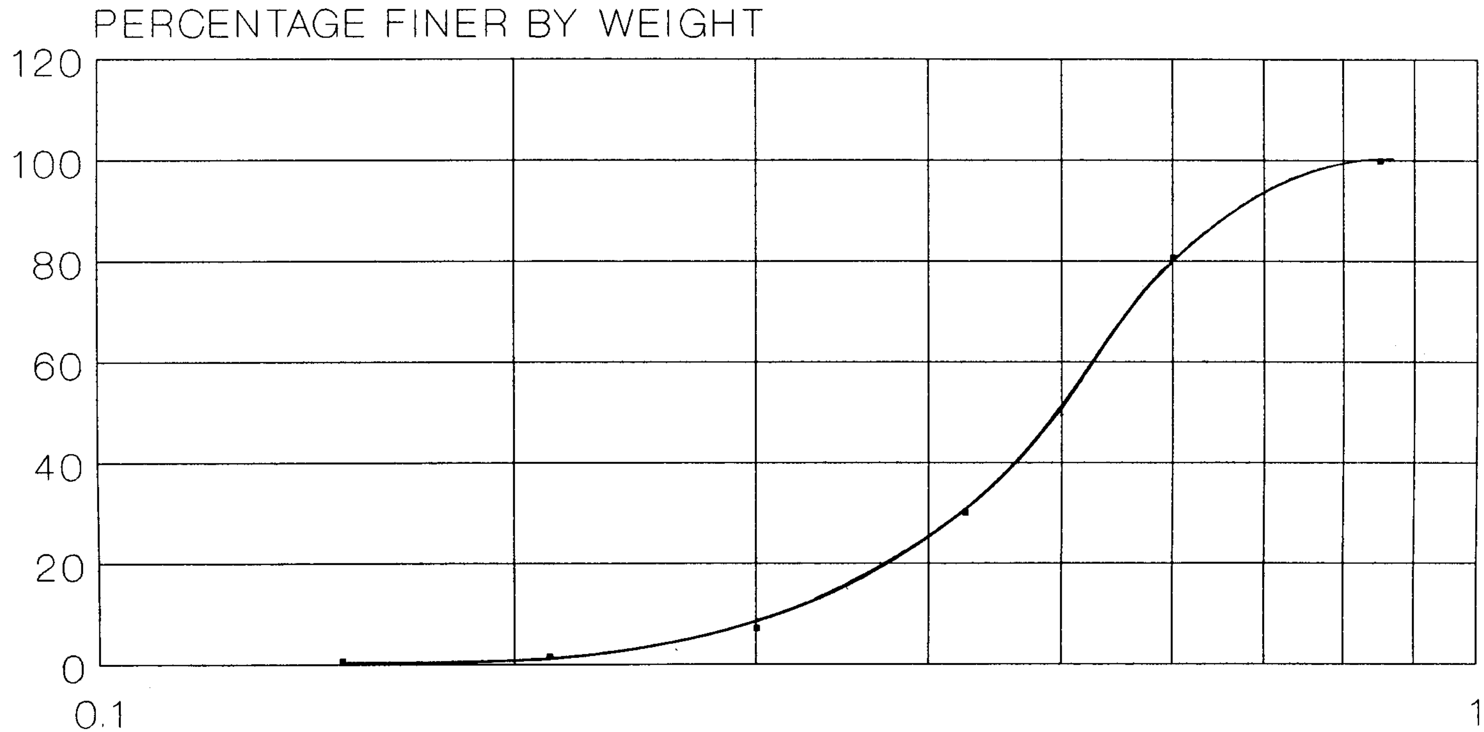

Range 0.3-0.65 mm

PARTICLE SIZE DISTRIBUTION

Silica Sand #2

Type 0.6-1.2 mm   Initial Mass = 301.3 g

SIEVE SIZE (mm)	MASS RETAINED (g)	PERCENTAGE RETAINED	PERCENTAGE FINER BY MASS
1.7	0.1	0.03	99.97
1.18	35.7	11.85	88.12
0.85	160.7	53.34	34.78
0.6	86.2	28.61	6.17
0.425	17.5	5.81	0.36
0.3	0.9	0.3	0.06
0.212	0.1	0.03	0.03
PAN	0.1	0.03	-
TOTAL	301.3	-	-

SILICA SAND #S2 (0.6-1.2 mm)

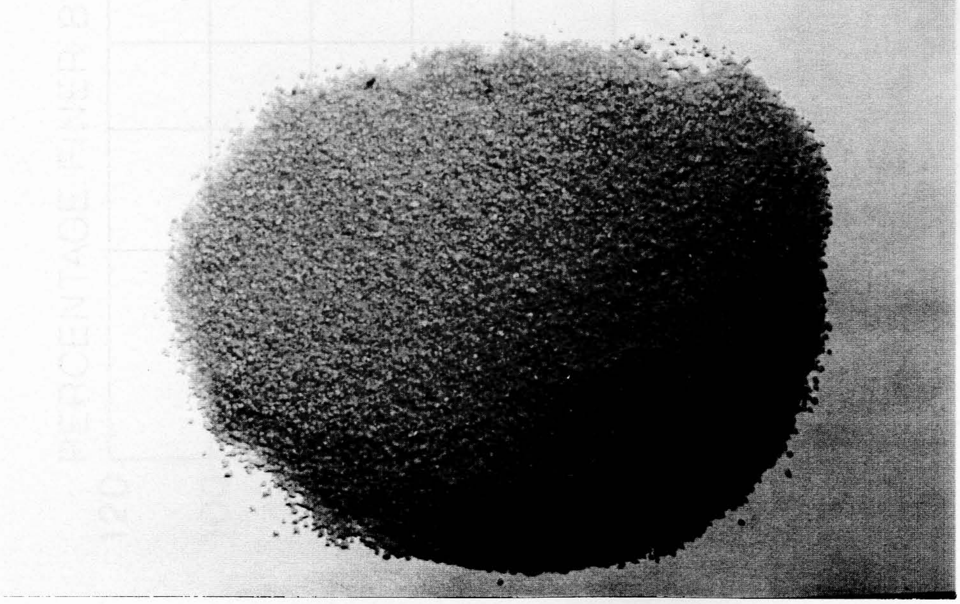

PARTICLE SIZE DISTRIBUTION

Silica Sand #2

Type 0.6-1.2 mm   Initial Mass = 301.3 g

SIEVE SIZE (mm)	MASS RETAINED (g)	PERCENTAGE RETAINED	PERCENTAGE FINER BY MASS
1.7	0.1	0.03	99.97
1.18	35.7	11.85	88.12
0.85	160.7	53.34	34.78
0.6	86.2	28.61	6.17
0.425	17.5	5.81	0.36
0.3	0.9	0.3	0.06
0.212	0.1	0.03	0.03
PAN	0.1	0.03	-
TOTAL	301.3	-	-

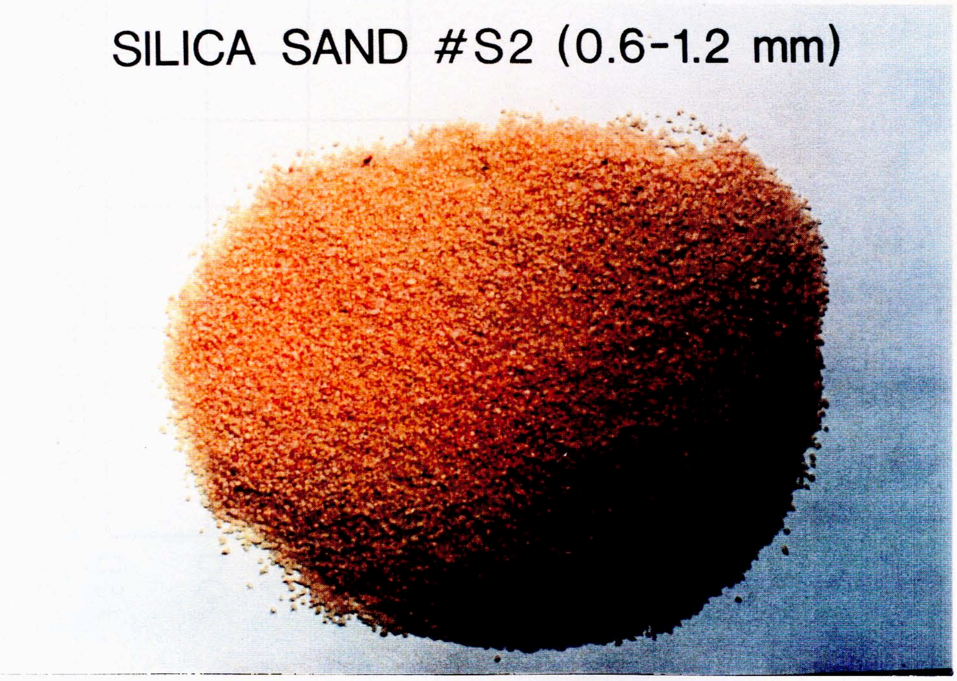

Particle Size Distribution
Silica Sand S2

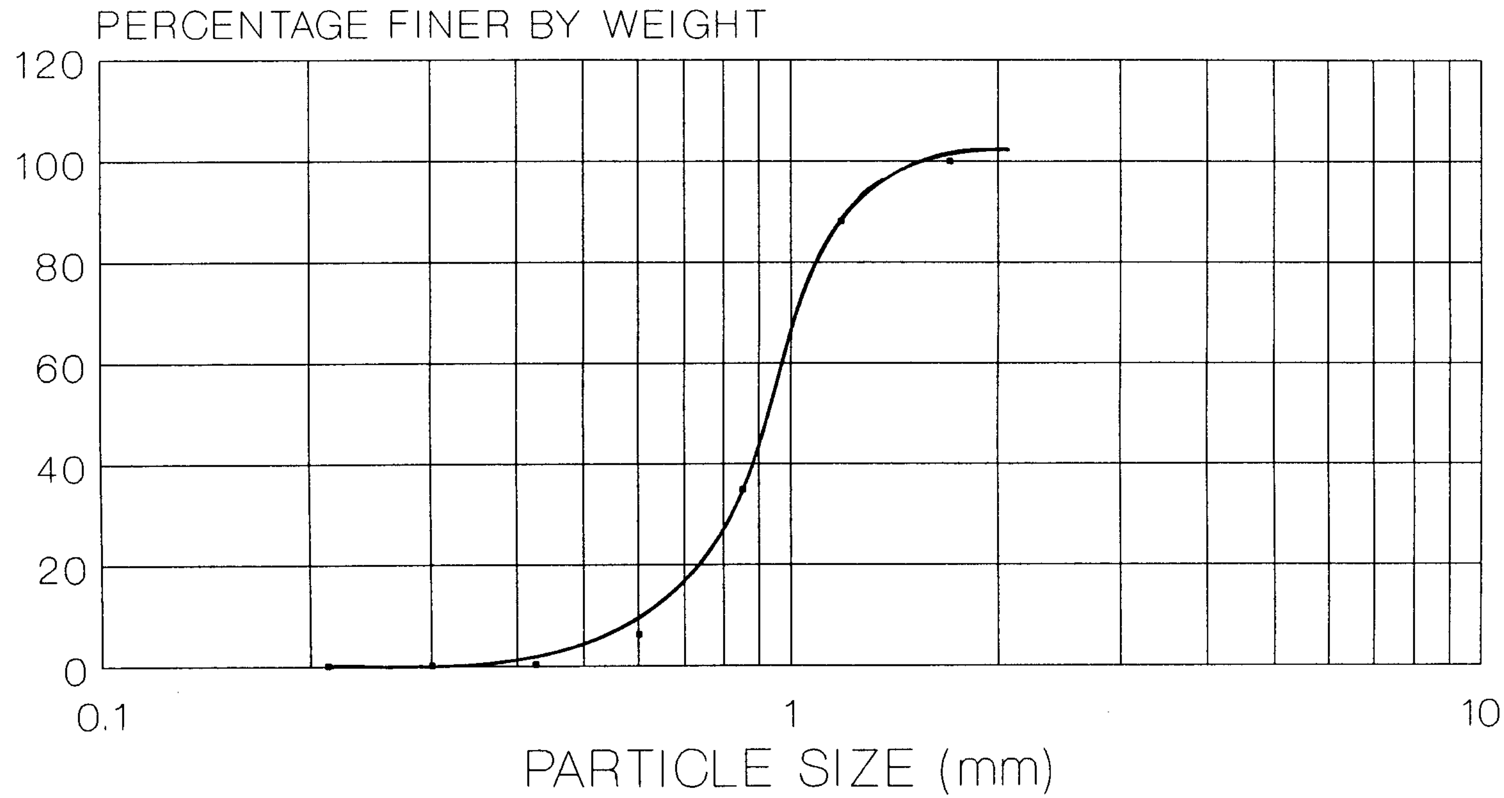

Range 0.6-1.2

PARTICLE SIZE DISTRIBUTION

Silica Sand #3

Type 0.8-1.8 mm   Initial Mass = 281.4 g

SIEVE SIZE (mm)	MASS RETAINED (g)	PERCENTAGE RETAINED	PERCENTAGE FINER BY MASS
2.36	1.9	0.7	99.3
1.70	60.6	21.5	77.5
1.18	181.2	64.4	13.4
0.85	36.0	12.8	0.6
0.6	1.4	0.5	0.1
0.425	0.2	0.1	0.0
PAN	0.1	0.0	0.0
TOTAL	281.4	100	-

SILICA SAND #S3 (0.8-1.8 mm)

Particle Size Distribution

Silica Sand S3

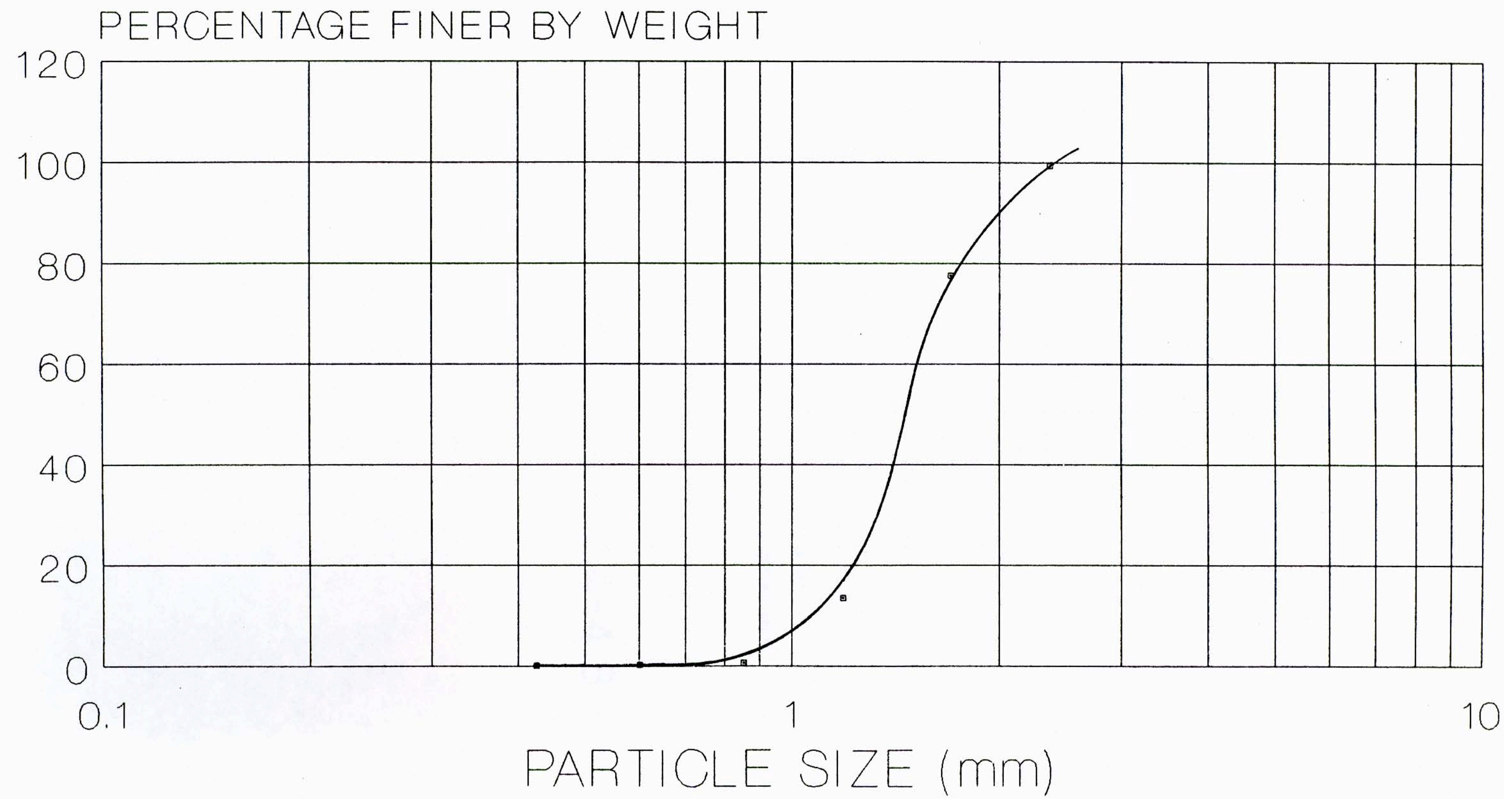

Range 0.8-1.8 mm

PARTICLE SIZE DISTRIBUTION

Silica Sand #4

Type 2.4-4.8 mm   Initial Mass = 310.3 g

SIEVE SIZE (mm)	MASS RETAINED (g)	PERCENTAGE RETAINED	PERCENTAGE FINER BY MASS
4.75	12.1	3.9	96.1
3.35	91.8	29.6	66.5
2.36	149.5	48.2	18.3
1.70	41.0	13.2	5.1
1.18	9.7	3.1	2.0
0.85	3.8	1.2	0.8
PAN	2.4	0.8	0.0
TOTAL	310.3	100	-

SILICA SAND #S4 (2.4-4.8 mm)

Particle Size Distribution

Silica Sand S4

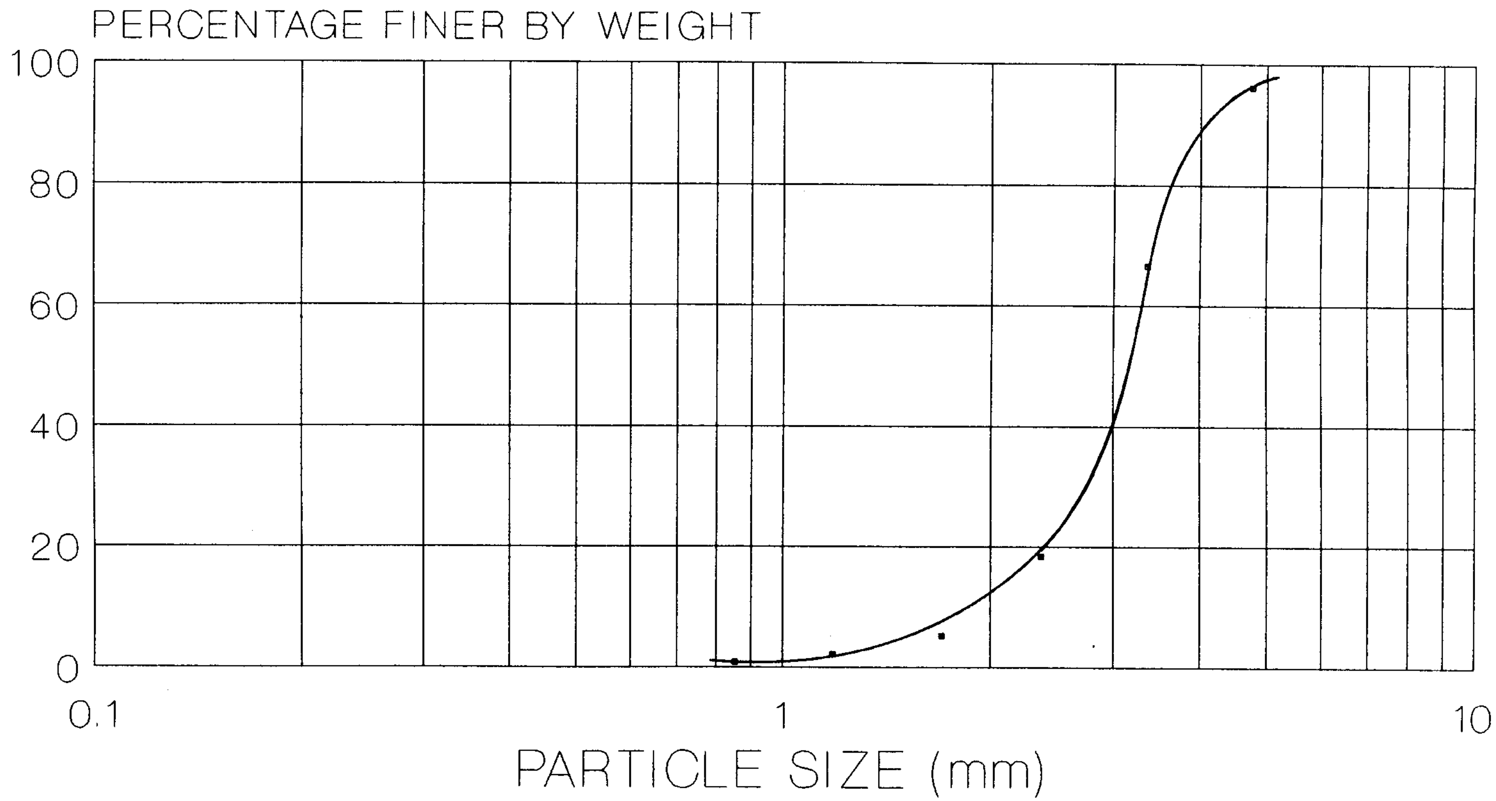

Range 2.4-4.8 mm

APPENDIX B : Preston Tube Calibration

PRESTON CALIBRATION EXPERIMENTAL DATA SUMMARY

$$\Delta P = 500\ (u_{b,ave}) \qquad T_0'' = 1000\ \left(\frac{slope}{5.75}\right)^2$$

RUN	$u_{b,ave}$ (m/s)	ΔP (N/m^2)	T_o'' (N/m^2)
C8	0.12	7.2	0.13
C9	0.15	11.25	0.19
C10	0.19	18.05	0.3
C11	0.25	31.25	0.51
C12	0.3	45.0	0.87
C13	0.35	61.25	1.27
C14	0.4	80.0	1.74
C15	0.5	125.0	2.37
C16	0.12	7.2	0.13
C17	0.15	11.25	0.19
C18	0.2	20.0	0.44
C19	0.25	31.25	0.64
C20	0.297	44.1	1.15
C21	0.35	61.25	1.6
C22	0.4	80.0	1.89
C23	0.53	140.5	3.1
C1	0.2	20.0	0.47
C2	0.21	22.05	0.51
C3	0.307	47.12	1.46

RUN	$u_{b,ave}$ (m/s)	ΔP (N/m^2)	τ_o'' (N/m^2)
C4	0.353	62.3	1.74
C5	0.413	85.28	2.29
C6	0.443	98.12	2.91
C7	0.547	149.6	4.25
C24	0.12	7.2	0.37
C25	0.157	12.33	0.64
C26	0.197	19.41	0.87
C27	0.25	31.25	1.33
C28	0.3	45.0	1.89
C29	0.35	61.25	2.91
C30	0.41	84.05	3.92

PRESTON TUBE CALIBRATION EQUATIONS

ROUGHNESS	EQUATION
S1	$\tau_o'' = - 0.02609 + 0.02006 * \Delta P$
S2	$\tau_o'' = 0.01517 + 0.0228 * \Delta P$
S3	$\tau_o'' = - 0.06934 + 0.02914 * \Delta P$
S4	$\tau_o'' = - 0.01751 + 0.04628 * \Delta P$

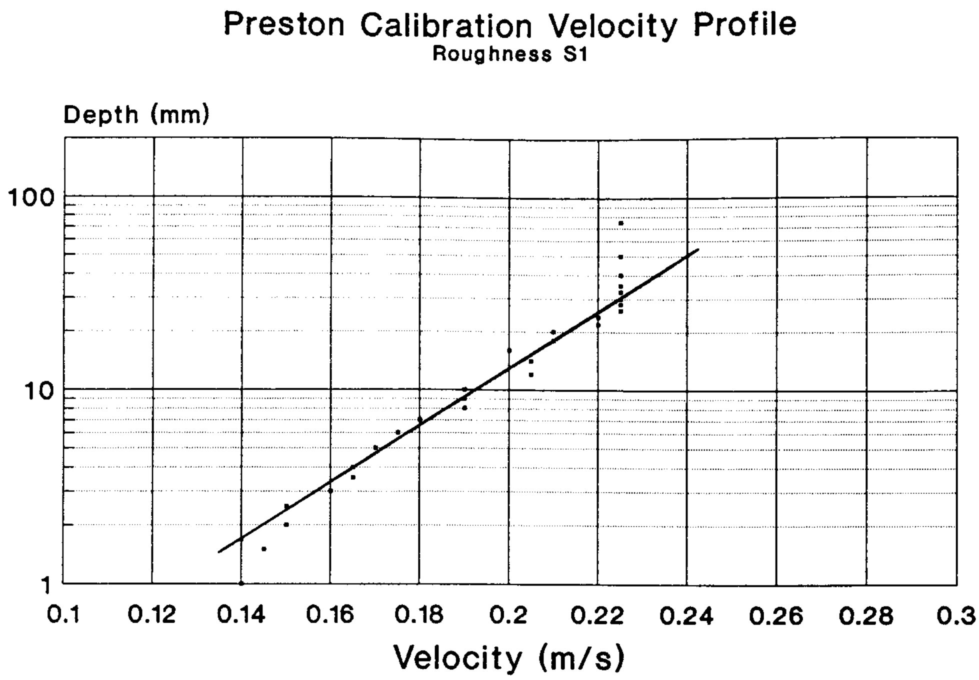

Bed Reading • 12 %

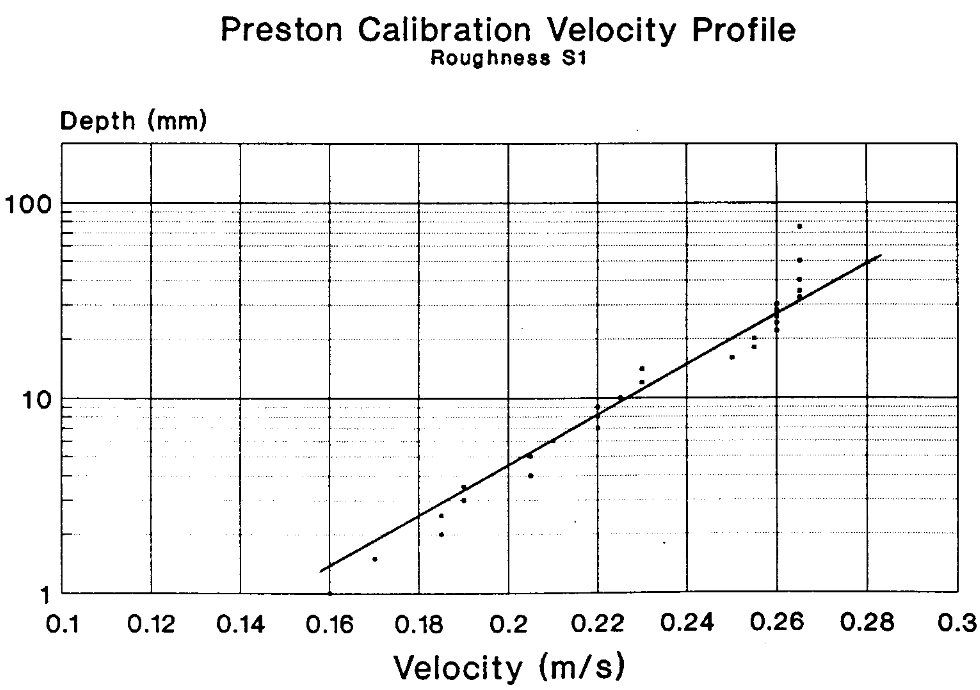

Bed Reading • 15 %

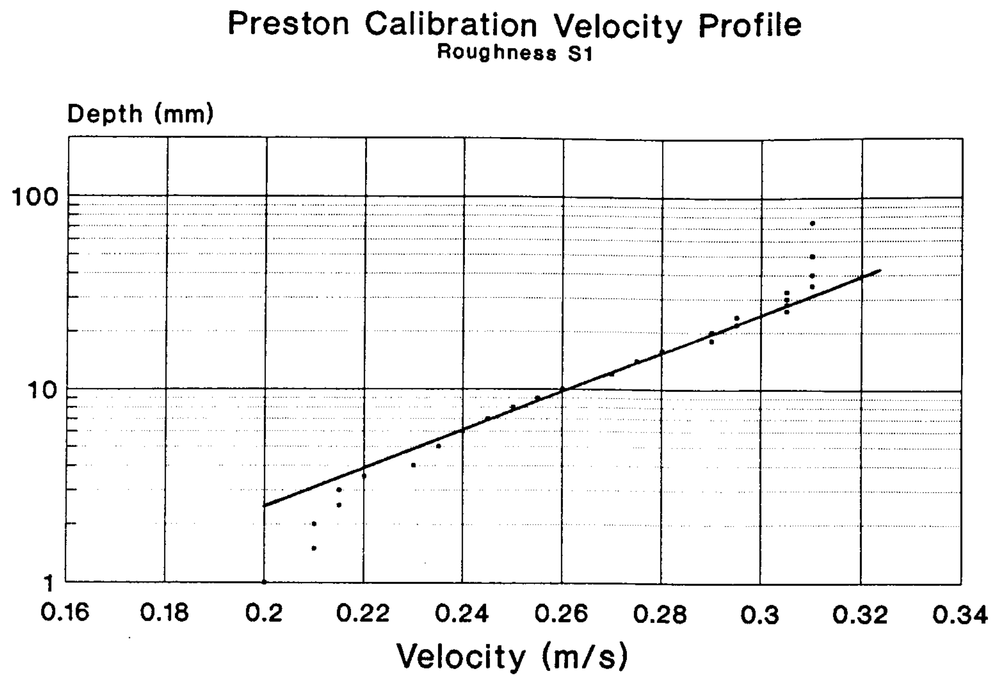

Bed Reading = 19 %

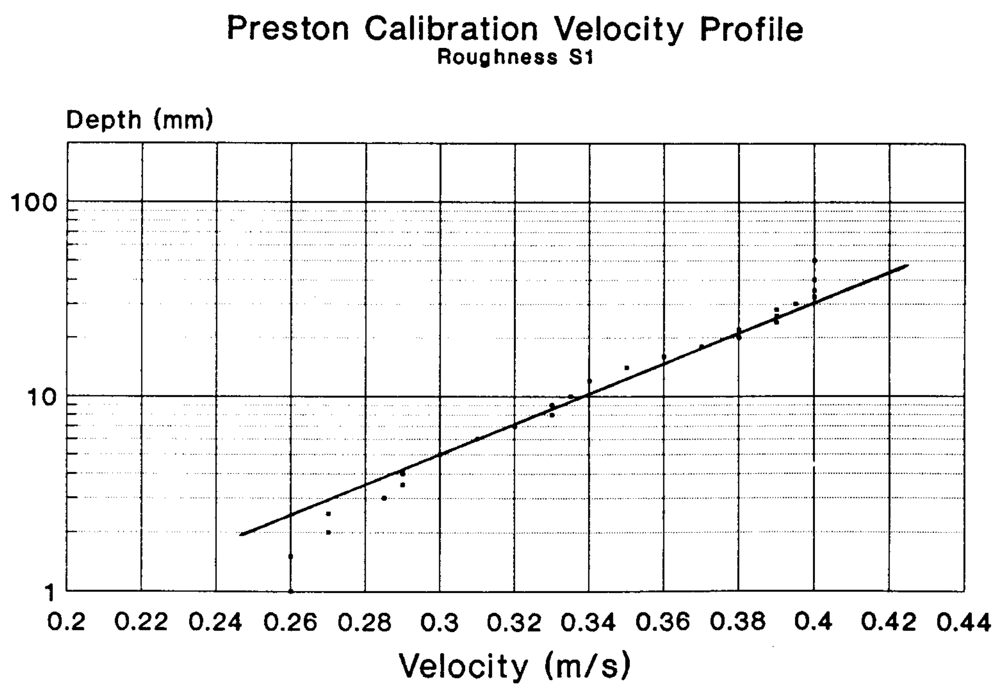

Bed Reading = 25 %

Preston Calibration Velocity Profile
Roughness S1

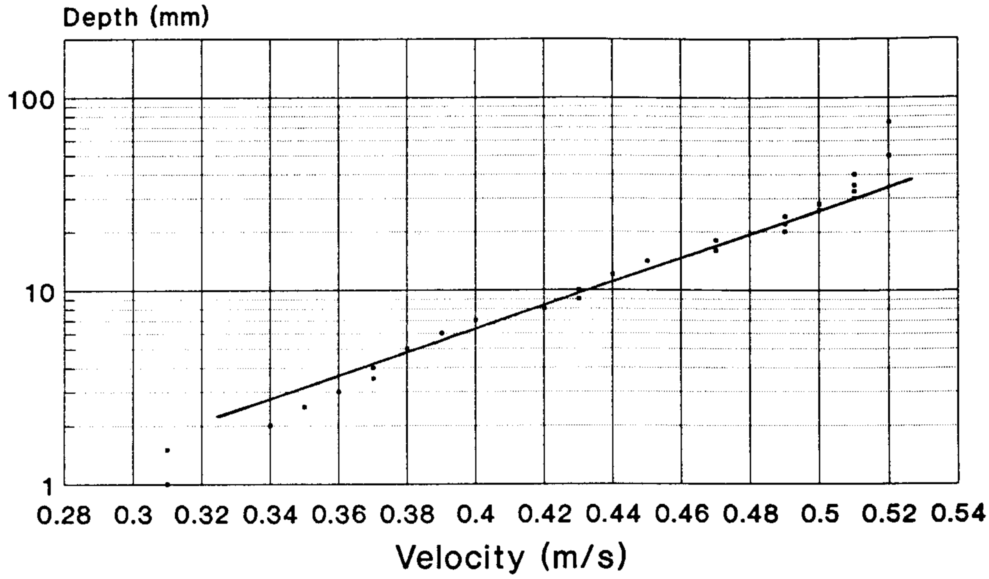

Bed Reading = 30 %

Preston Calibration Velocity Profile
Roughness S1

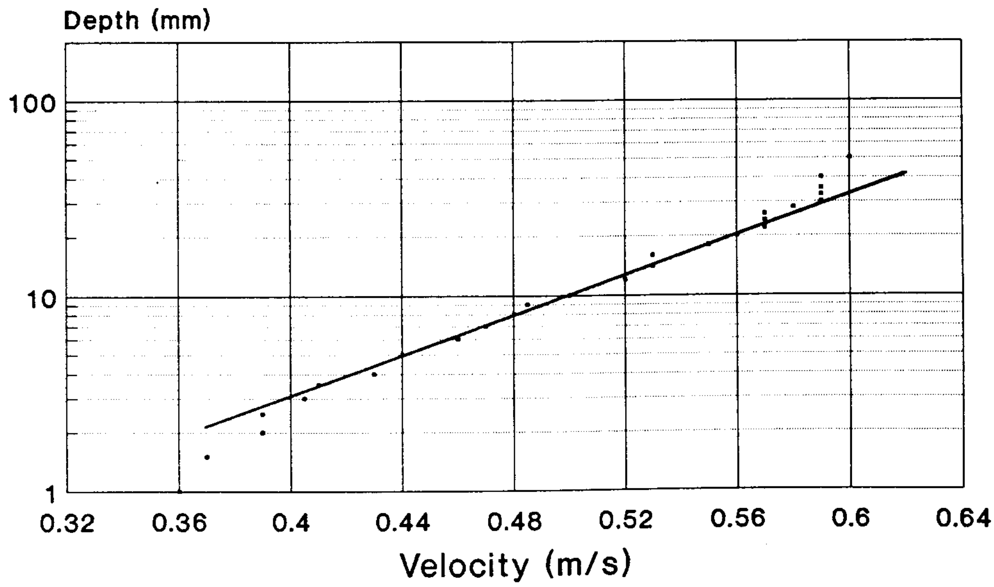

Bed Reading = 35 %

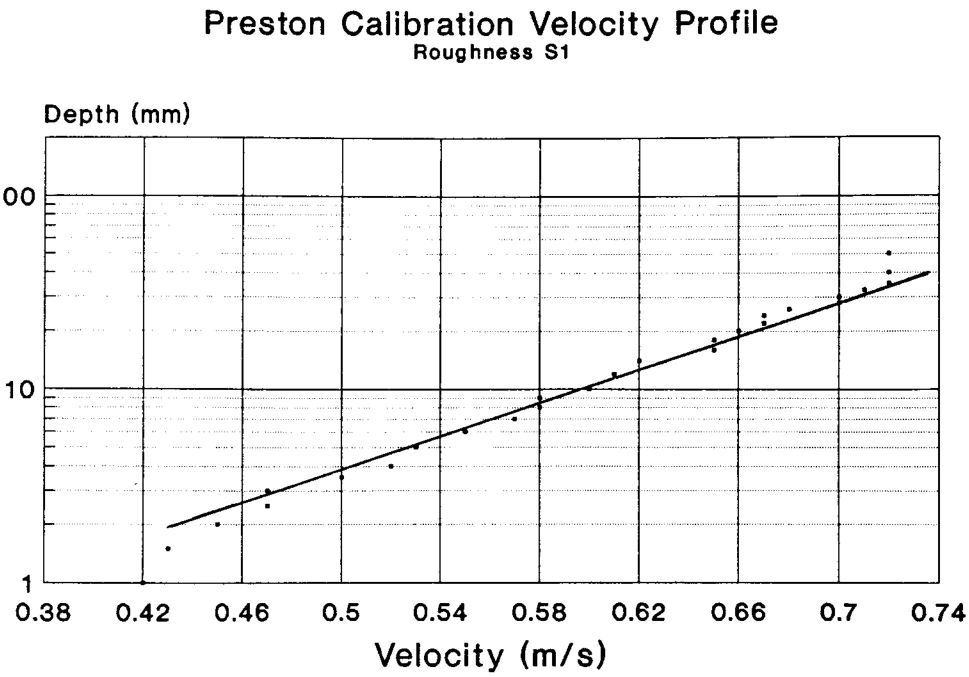

Bed Reading = 40 %

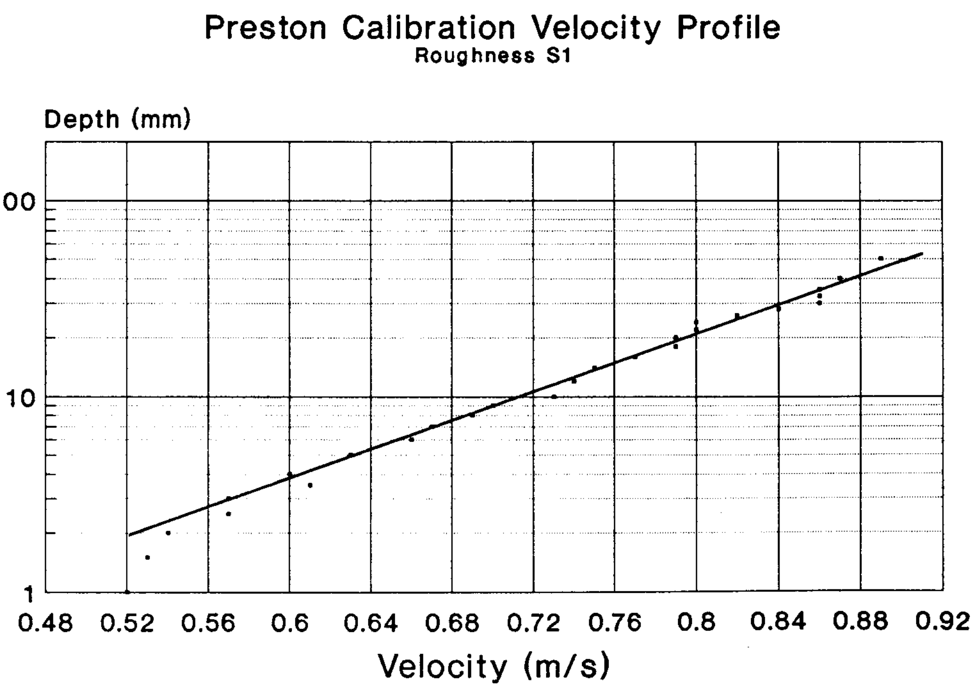

Bed Reading = 50 %

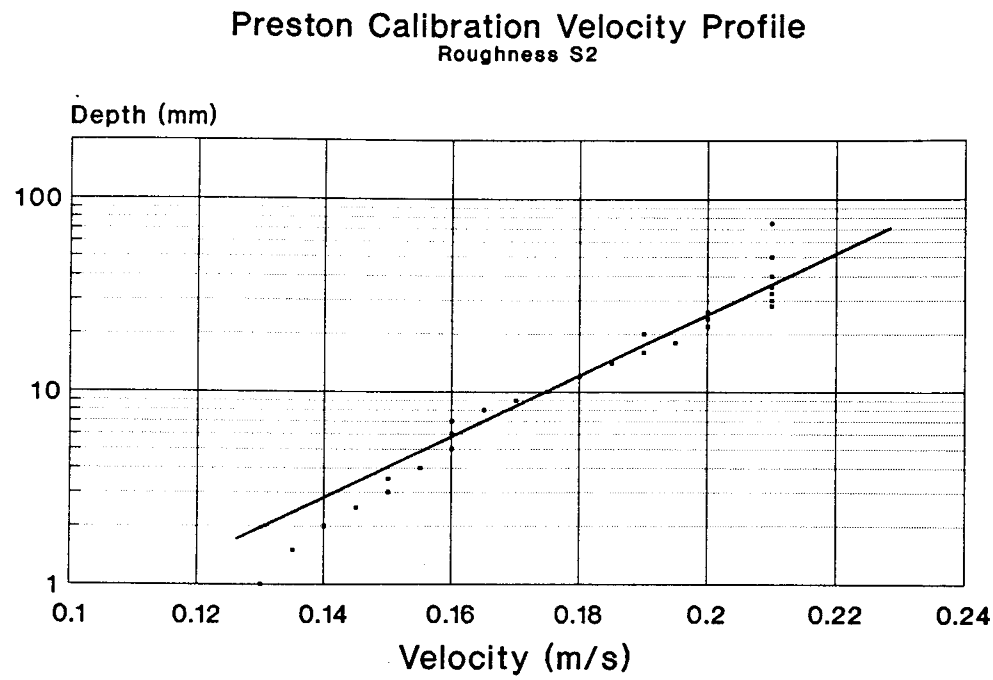

Bed Reading = 12 %

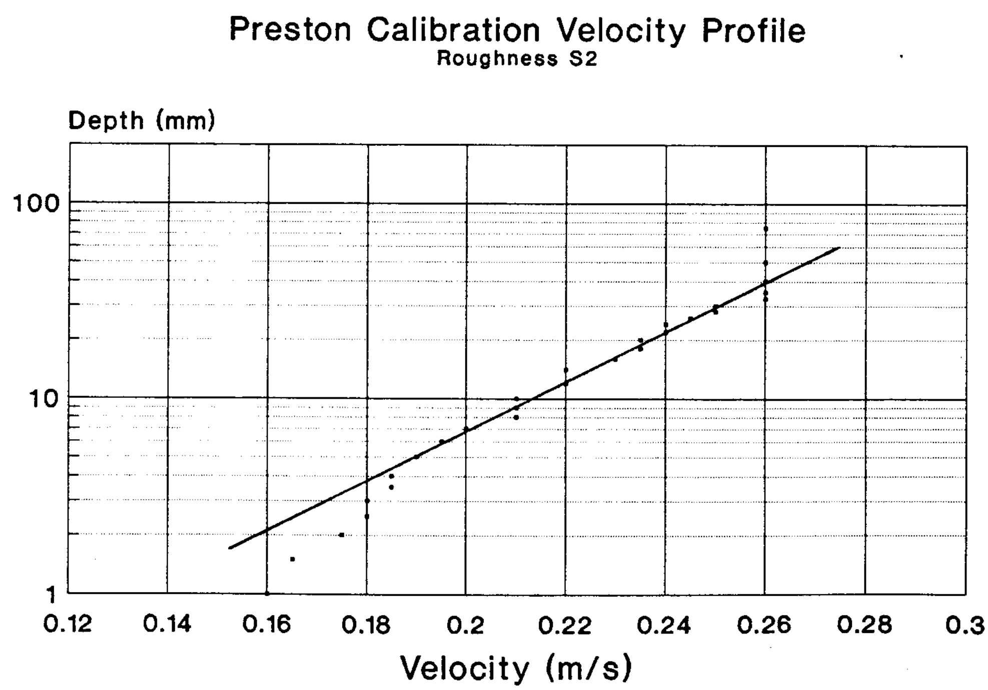

Bed Reading = 15 %

Preston Calibration Velocity Profile
Roughness S2

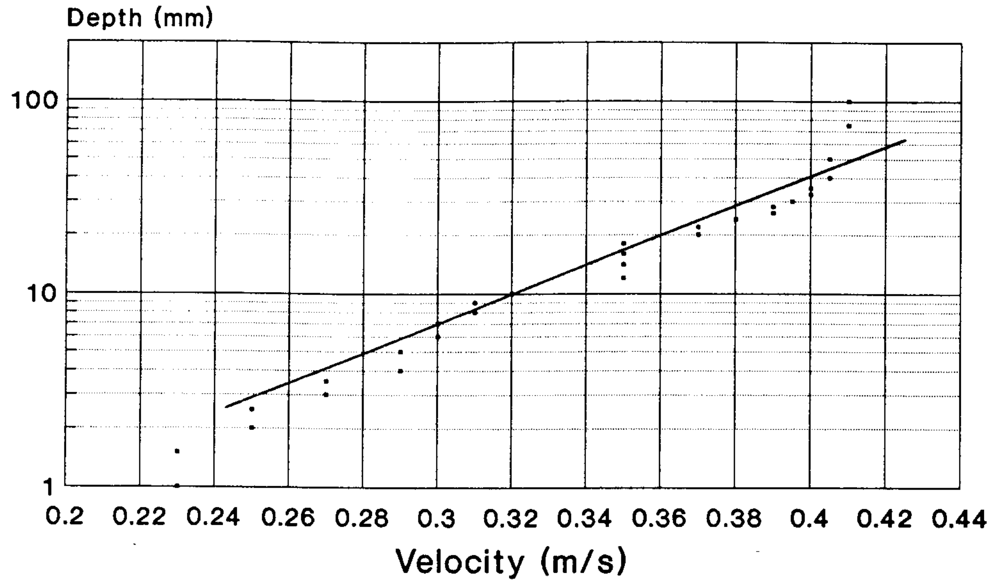

Bed Reading = 20 %

Preston Calibration Velocity Profile
Roughness S2

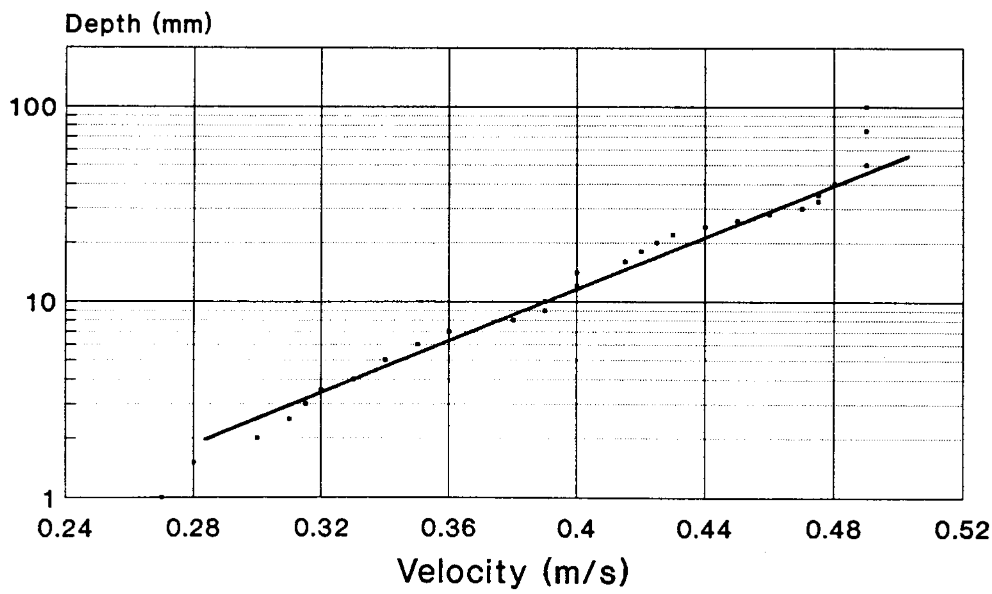

Bed Reading = 25 %

Preston Calibration Velocity Profile
Roughness S2

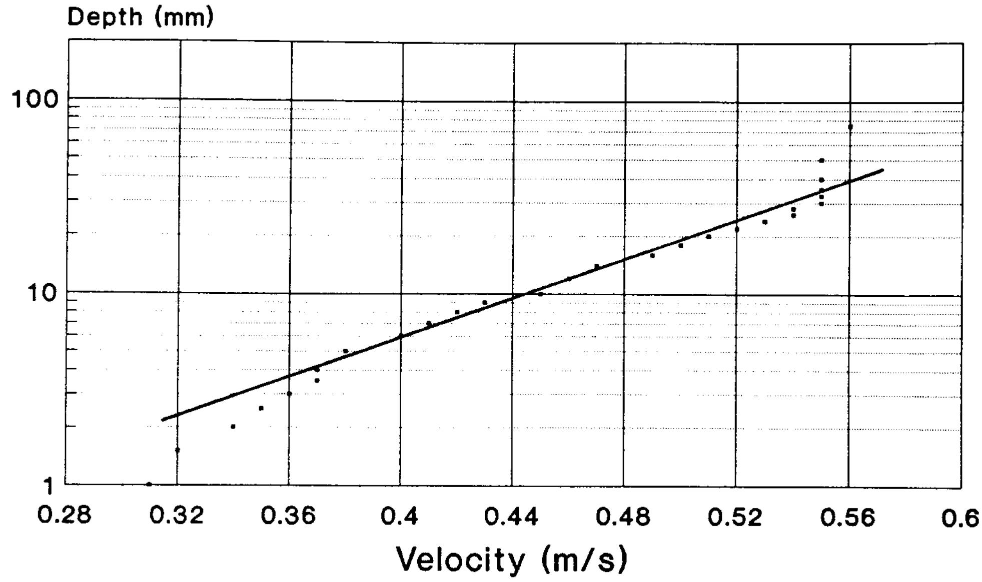

Bed Reading = 29.7 %

Preston Calibration Velocity Profile
Roughness S2

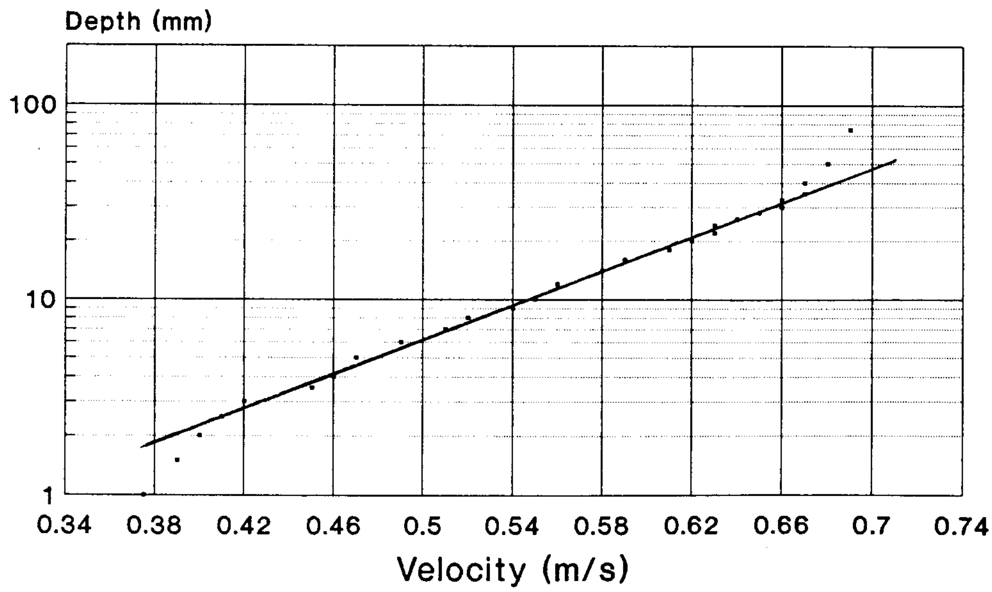

Bed Reading = 35 %

Preston Calibration Velocity Profile
Roughness S2

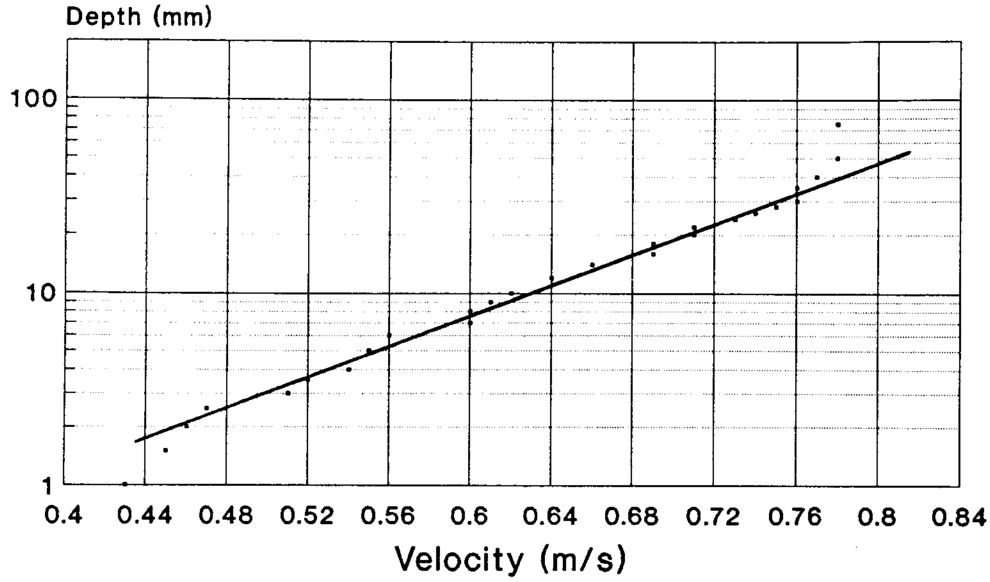

Bed Reading = 40 %

Preston Calibration Velocity Profile
Roughness S2

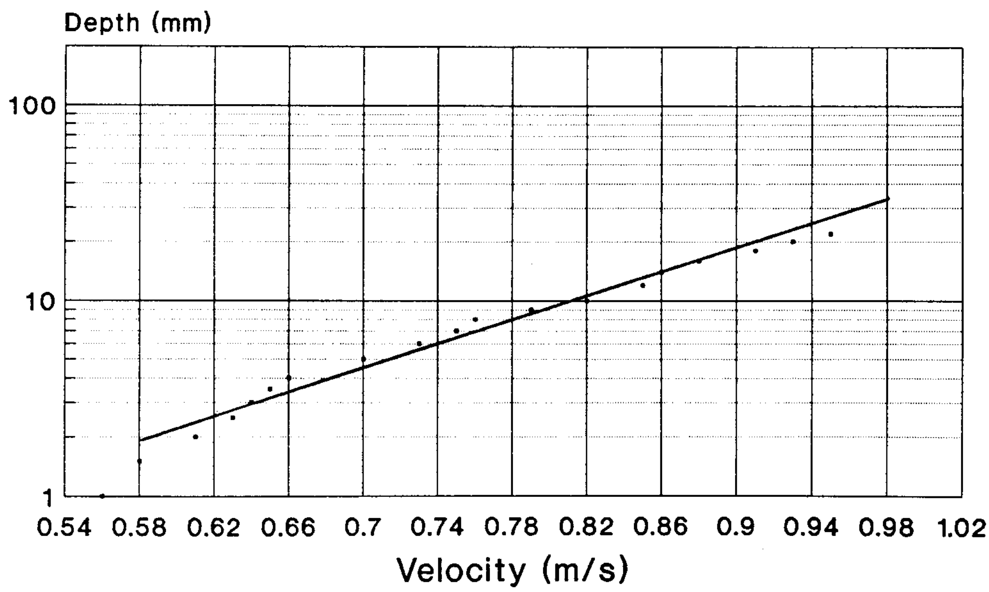

Bed Reading = 53 %

Preston Calibration Velocity Profile

Roughness S3

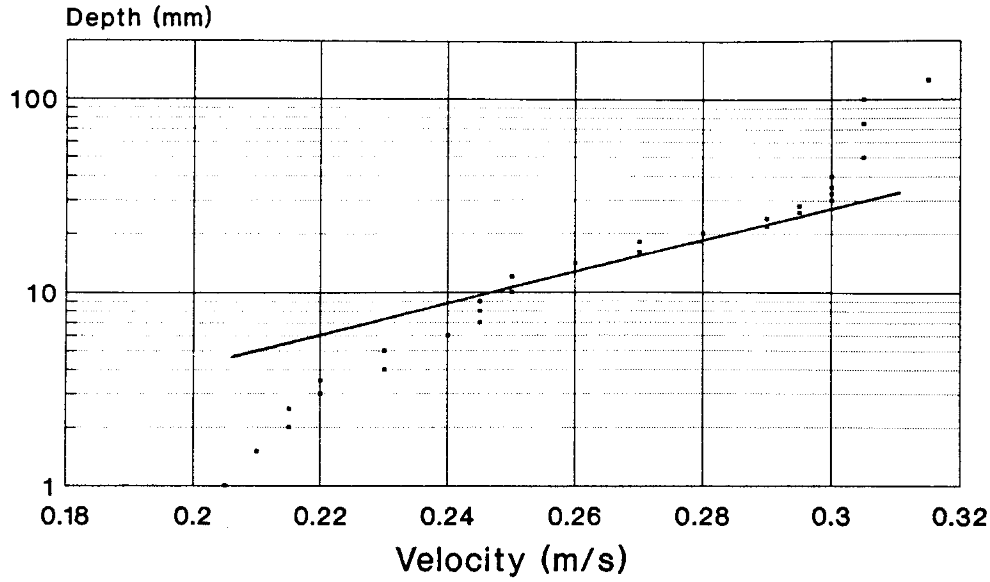

Bed Reading = 20.0 %

Preston Calibration Velocity Profile

Roughness S3

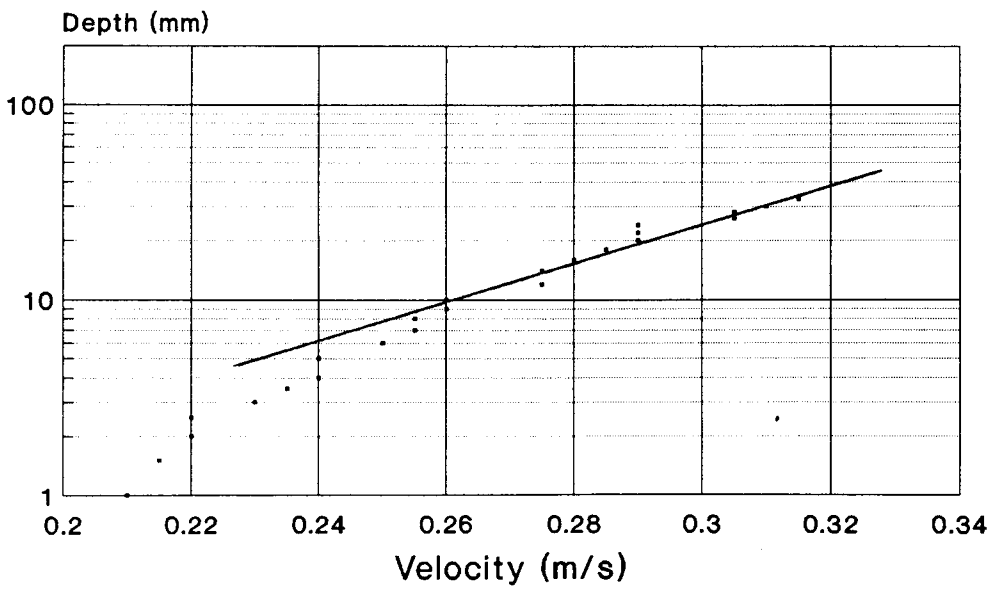

Bed Reading = 21.0 %

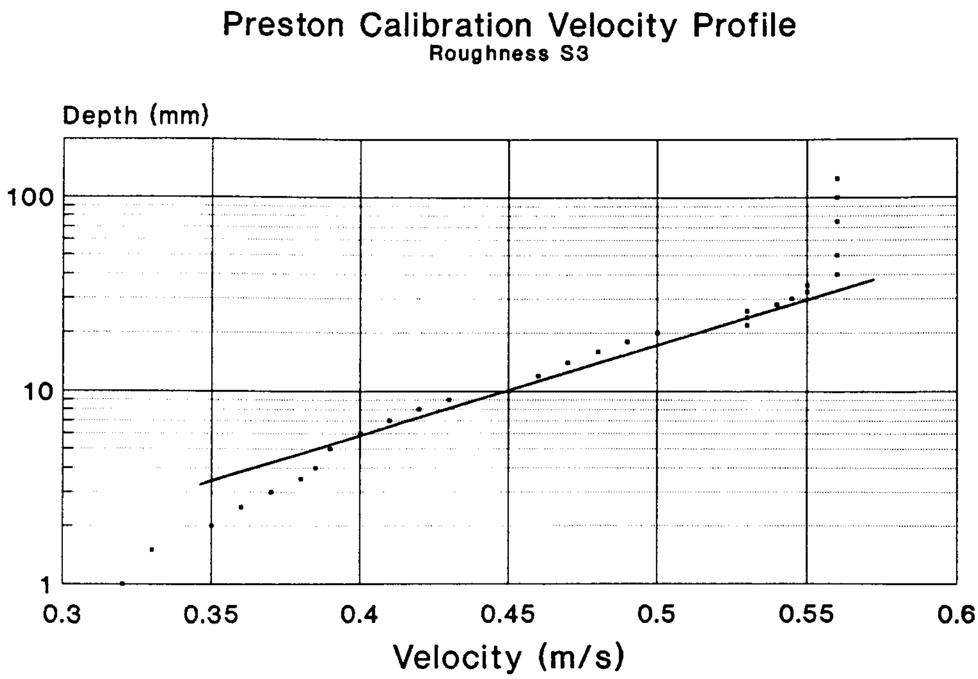

Bed Reading = 30.7 %

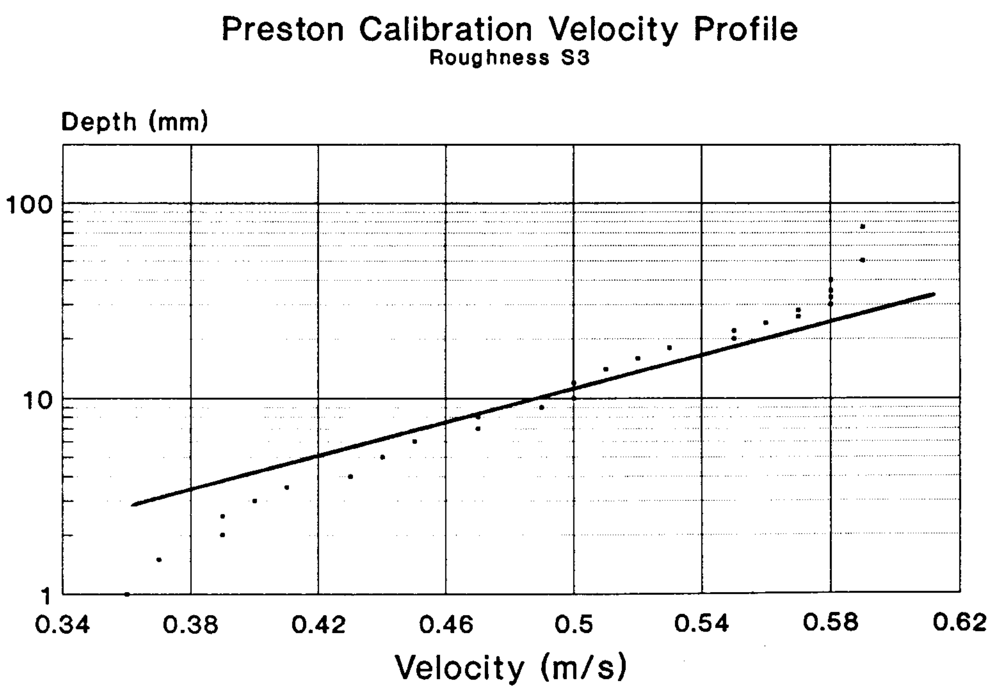

Bed Reading = 35.3 %

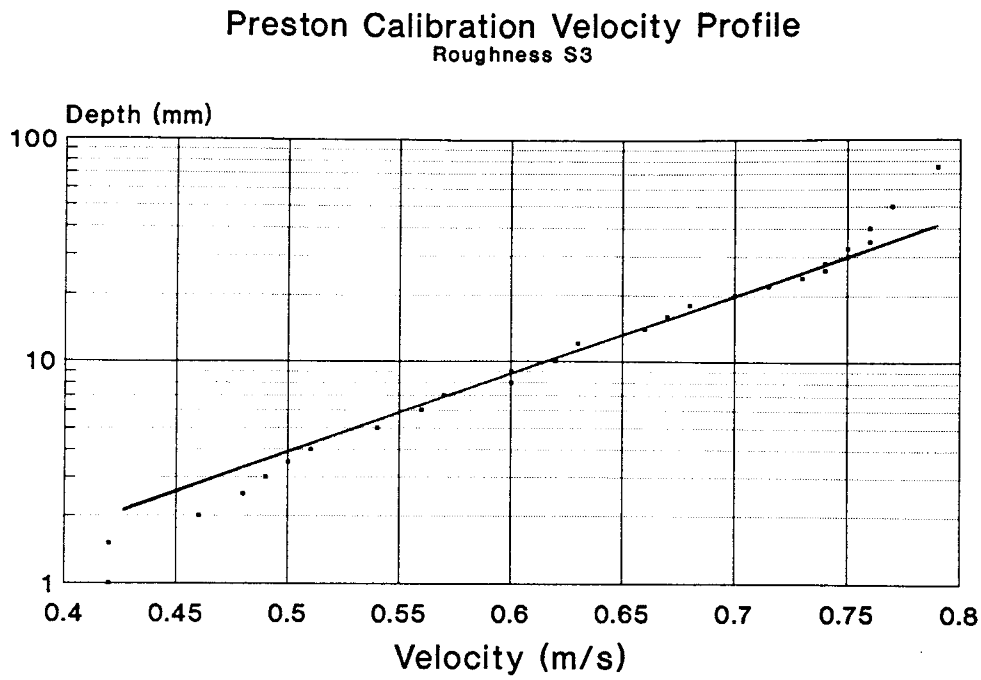

Bed Reading = 41.3 %

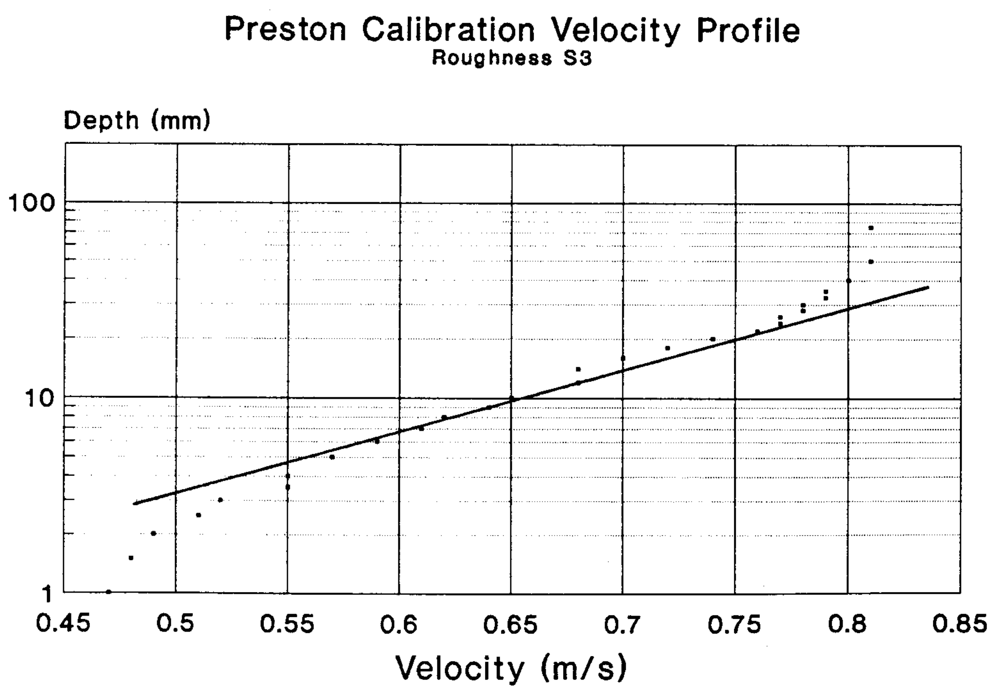

Bed Reading = 44.3 %

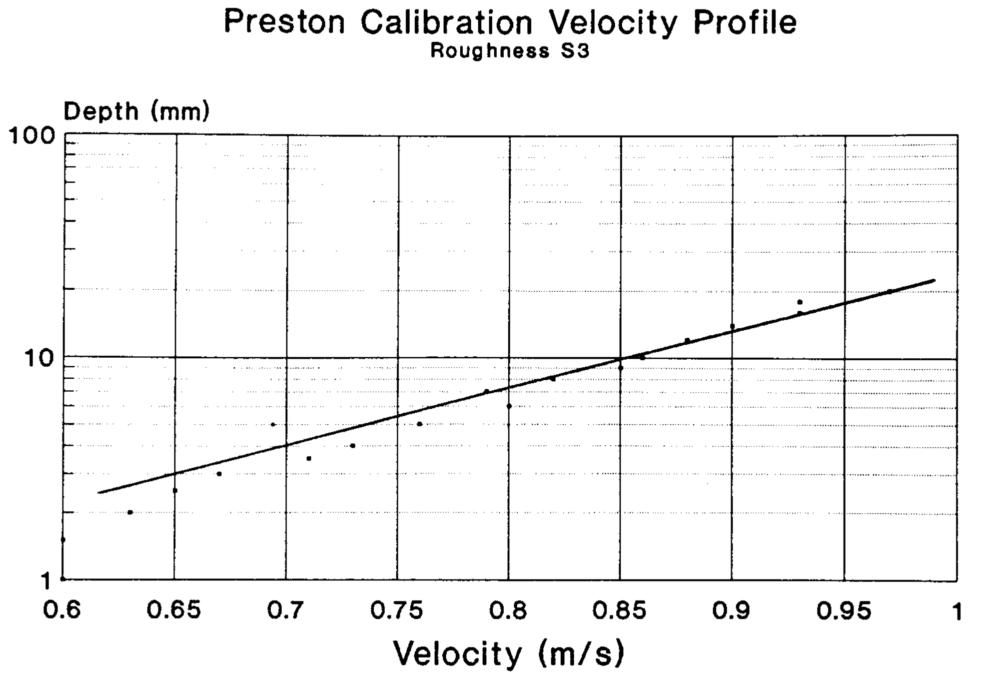

Bed Reading = 54.7 %

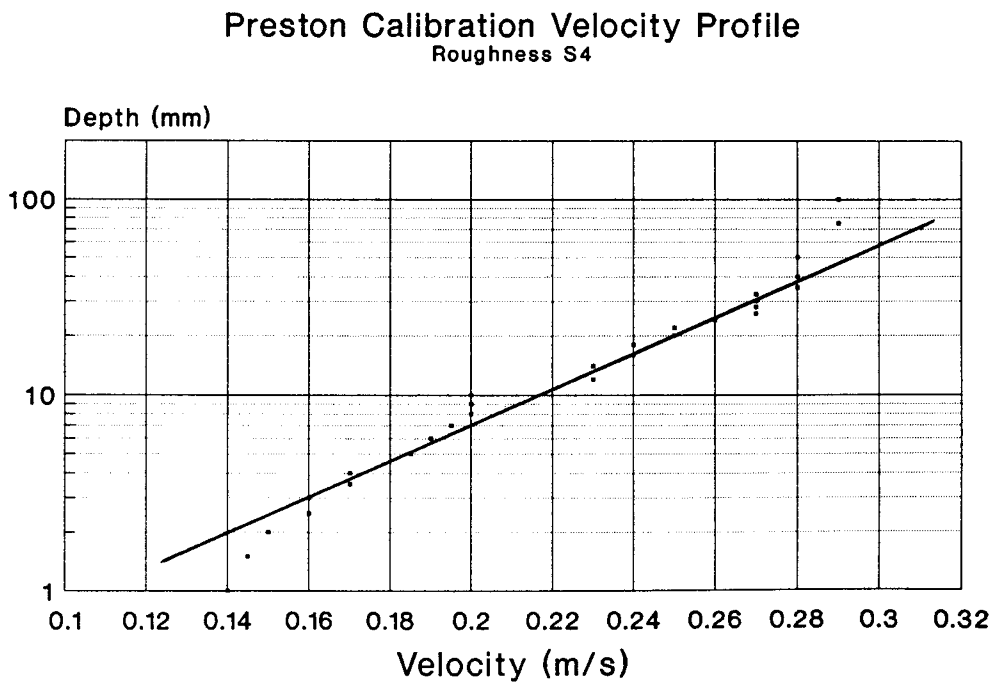

Bed Reading = 12 %

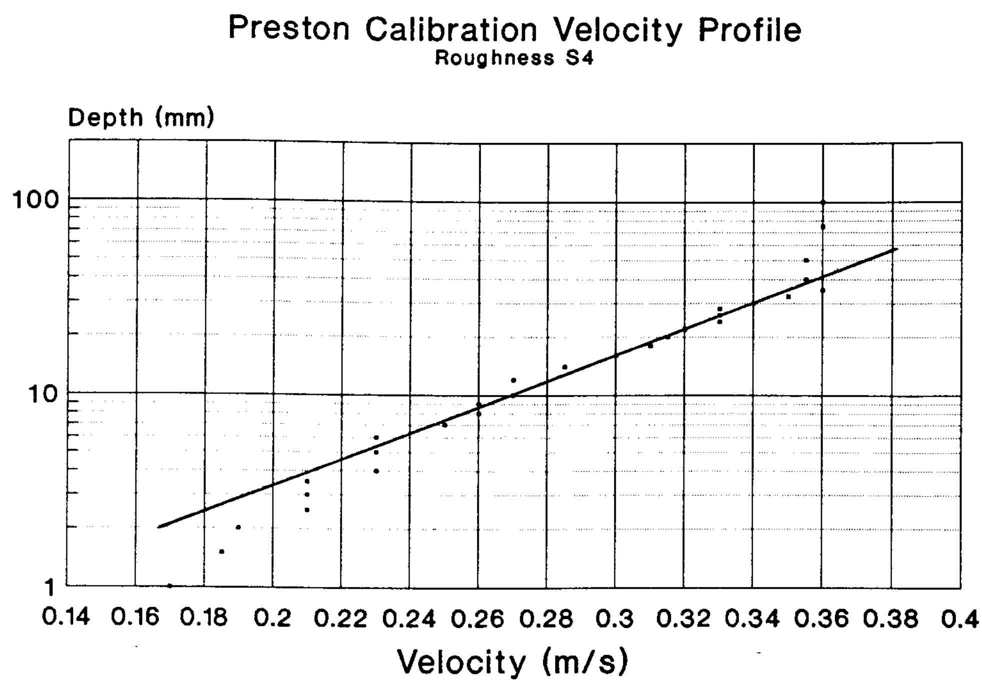

Bed Reading = 15.7 %

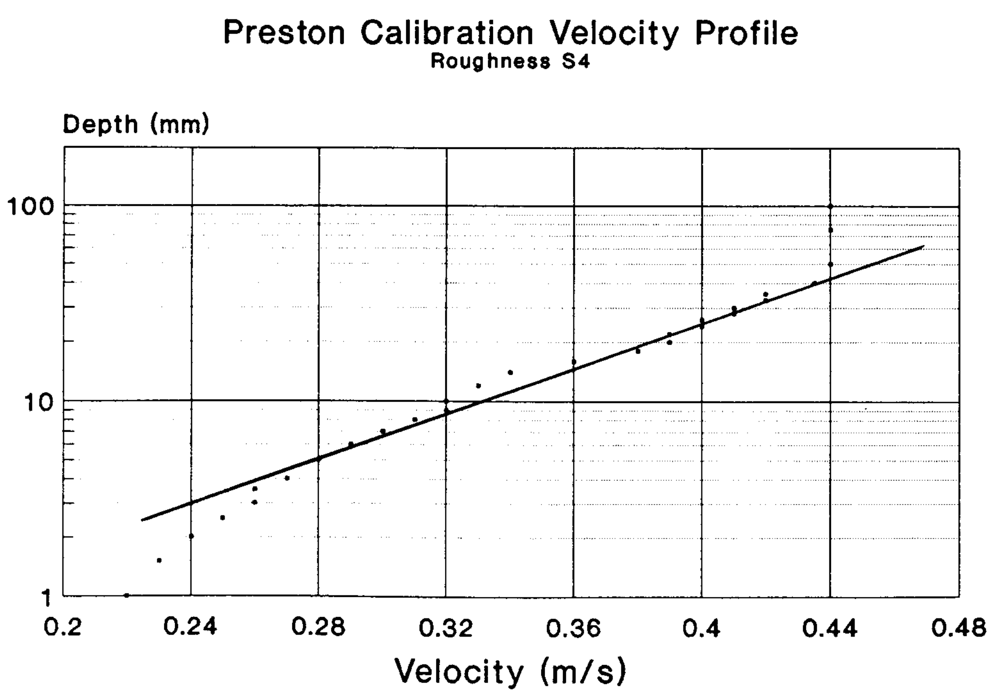

Bed Reading = 19.7 %

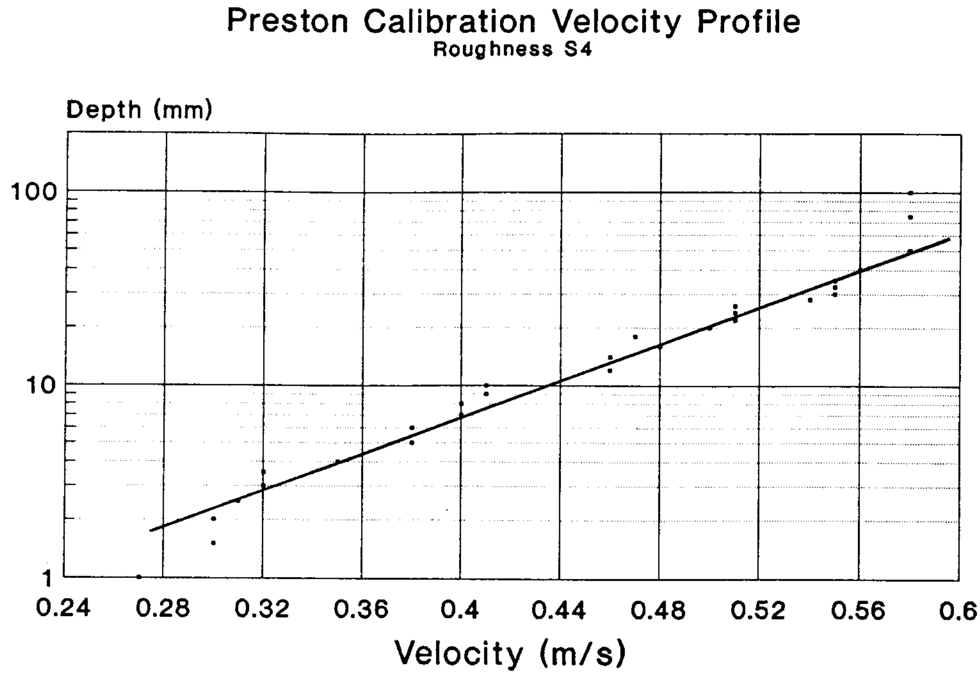

Bed Reading = 25 %

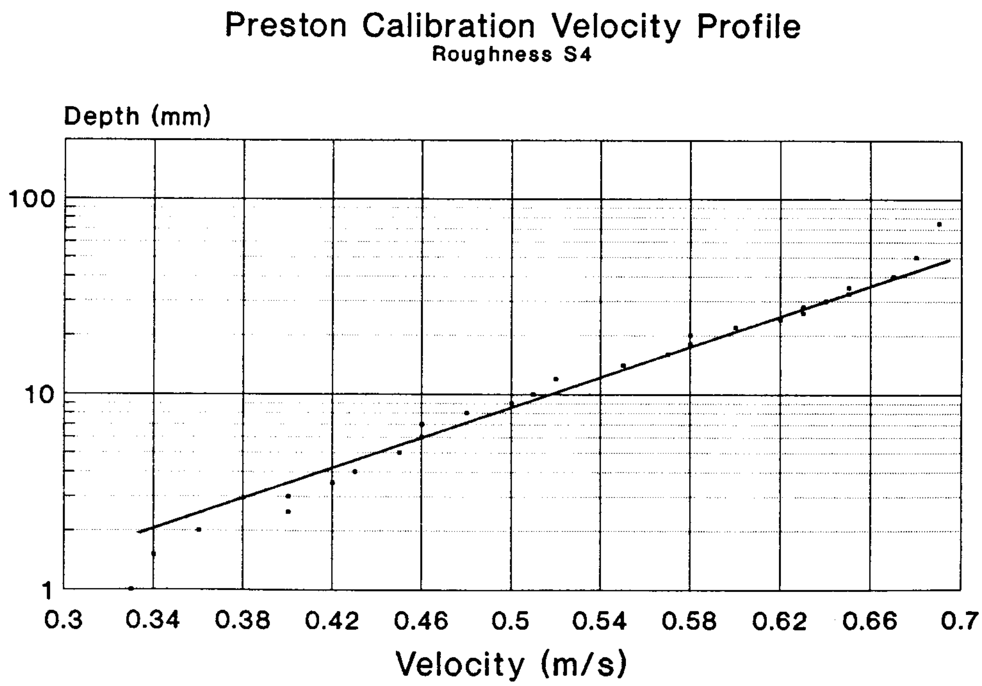

Bed Reading = 30 %

Preston Calibration Velocity Profile
Roughness S4

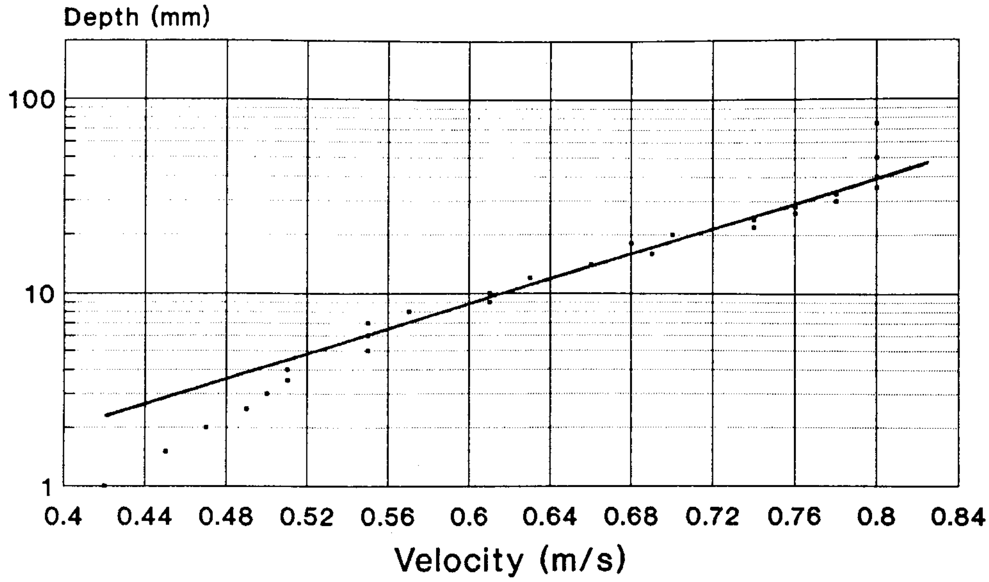

Bed Reading - 35 %

Preston Calibration Velocity Profile
Roughness S4

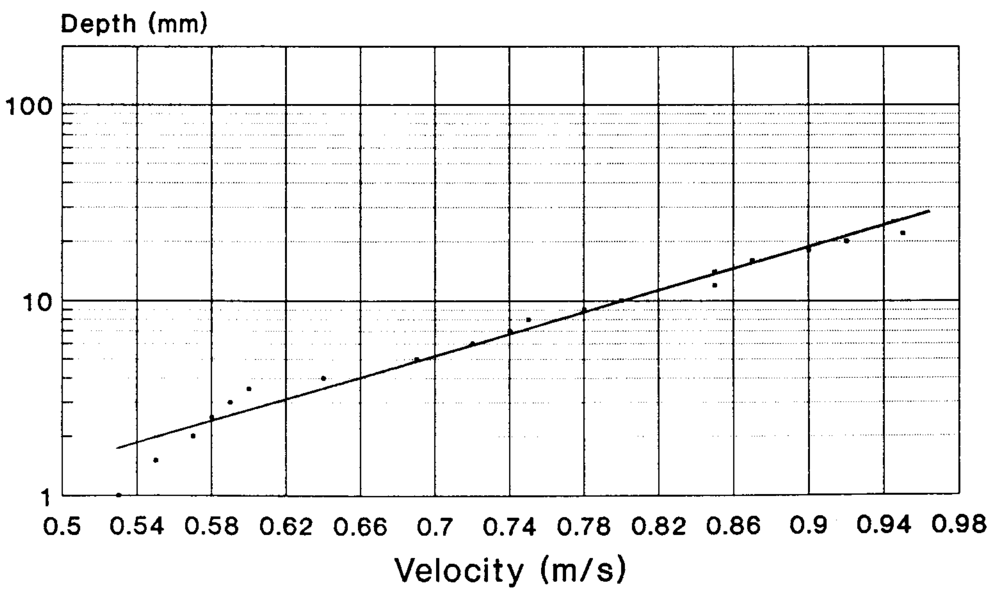

Bed Reading - 41 %

PRESTON CALIBRATION EXPERIMENTAL DATA SUMMARY

ROUGHNESS	D_{50} (mm)	RUN No.
S1	0.5	C8 to C15
S2	0.93	C16 to C23
S3	1.6	C1 to C7
S4	3.05	C24 to C30

LIST OF VELOCITY PROFILE SLOPES

RUN	SLOPE	RUN	SLOPE
C8	0.065	C22	0.32
C9	0.08	C23	0.125
C10	0.10	C1	0.13
C11	0.13	C2	0.22
C12	0.17	C3	0.24
C13	0.205	C4	0.275
C14	0.24	C5	0.31
C15	0.28	C6	0.375
C16	0.065	C7	0.11
C17	0.08	C24	0.145
C18	0.12	C25	0.17
C19	0.145	C26	0.21
C20	0.195	C27	0.25
C21	0.23	C29	0.31
C22	0.25	C30	0.36

PRESTON CALIBRATION CHART

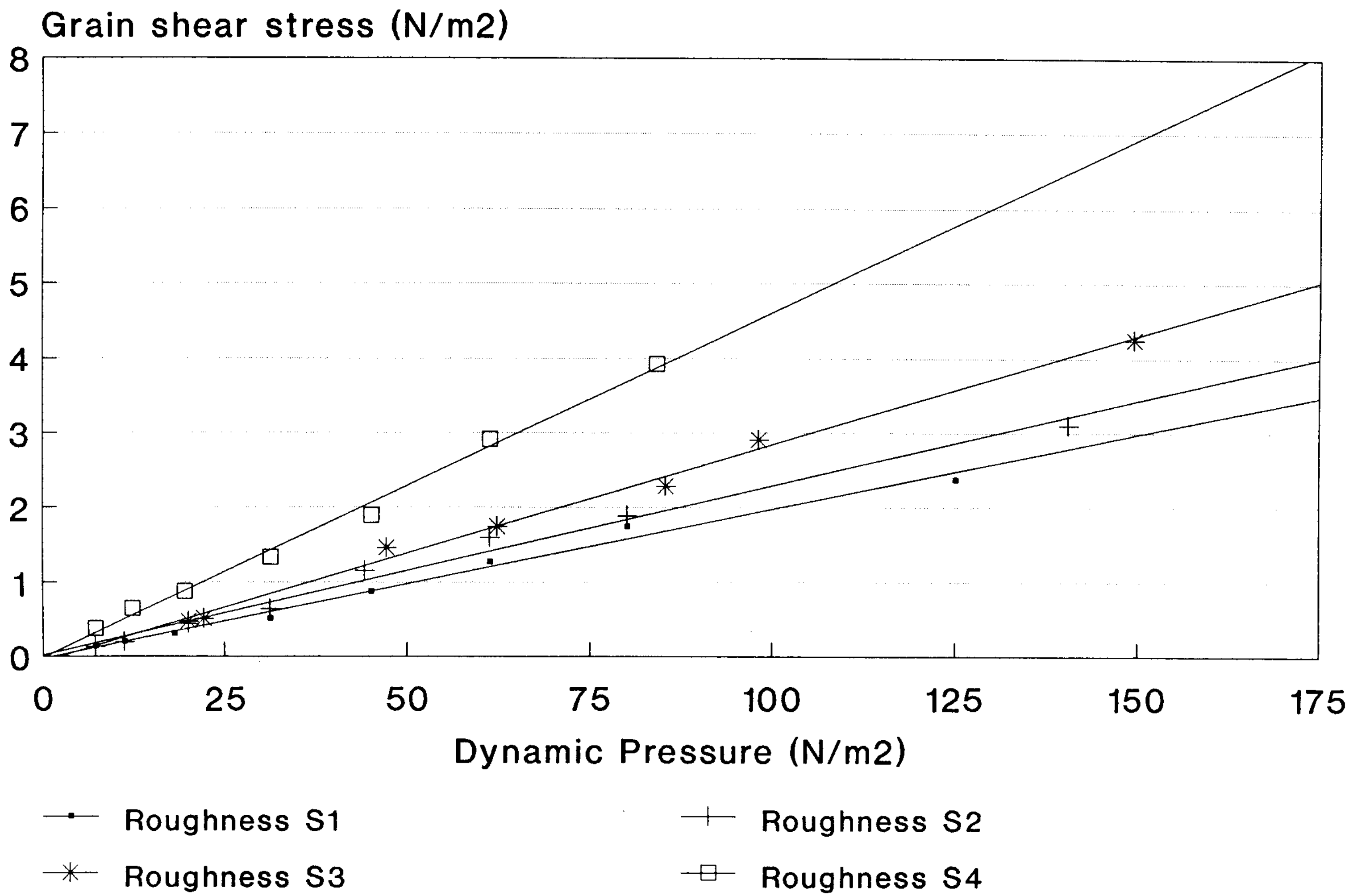

APPENDIX C : Water Profiles and Average Depth

AVERAGE DEPTH, AVERAGE VELOCITY AND FROUDE NUMBERS.

RUN	Q (l/s)	H (mm)	V (m/s)	Fr
1	10	78.5	0.34	0.39
2	15	94.5	0.42	0.44
3	20	109.5	0.48	0.46
4	25	119.5	0.55	0.51
5	30	128.5	0.61	0.54
6	35	136.5	0.67	0.58
7	10	80.5	0.33	0.37
8	15	97.5	0.40	0.41
9	20	112.5	0.47	0.45
10	25	124.5	0.53	0.48
11	30	136.5	0.58	0.50
12	35	140.9	0.65	0.55
14	10	79.5	0.33	0.37
15	15	96.5	0.41	0.42
16	20	108.5	0.49	0.47
17	25	122.5	0.54	0.49
18	30	130.5	0.60	0.53
19	35	147.5	0.62	0.52
20	40	158.5	0.66	0.53
21	45	157.5	0.75	0.60
22	10	82.5	0.32	0.36
23	15	100.5	0.39	0.39
24	20	114.5	0.46	0.43
25	25	126.5	0.52	0.47

AVERAGE DEPTH, AVERAGE VELOCITY AND FROUDE NUMBERS.

RUN	Q (l/s)	H (mm)	V (m/s)	Fr
26	30	138.5	0.57	0.49
27	35	147.5	0.62	0.52
28	40	158.5	0.66	0.53
29	45	163.5	0.72	0.57
30	10	81.5	0.32	0.36
31	15	97.5	0.40	0.41
32	20	112.5	0.47	0.45
33	25	122.5	0.54	0.49
34	30	139.5	0.57	0.49
35	35	148.5	0.62	0.51
36	40	151.5	0.69	0.57
37	45	160.5	0.74	0.59
38	10	84.5	0.31	0.34
39	15	100.5	0.39	0.39
40	20	113.5	0.46	0.44
41	25	124.5	0.53	0.49
42	30	136.5	0.58	0.50
43	35	143.5	0.64	0.54
44	40	155.5	0.68	0.55
45	45	161.5	0.73	0.58
46	10	84.5	0.31	0.34
47	15	99.5	0.40	0.40
48	20	113.5	0.46	0.44

AVERAGE DEPTH, AVERAGE VELOCITY AND FROUDE NUMBERS.

RUN	Q (l/s)	H (mm)	V (m/s)	Fr
49	25	125.5	0.52	0.47
50	30	139.5	0.57	0.49
51	35	143.5	0.64	0.54
52	40	156.5	0.67	0.54
53	45	163.5	0.72	0.57

COMPARISON OF AVERAGE AND EFFECTIVE FLOW DEPTH

RUN	H (mm)	H' (mm)	(H'-H) (mm)	(H'-H) (%)
1	78.5	79.0	0.50	0.64
2	94.5	95.7	1.20	1.27
3	109.5	111.7	2.20	2.01
4	119.5	123.4	3.90	3.26
5	128.5	133.4	4.90	3.81
6	136.5	142.1	5.60	4.10
7	80.5	82.1	1.60	1.99
8	97.5	99.7	2.20	2.26
9	112.5	115.7	3.20	2.84
10	124.5	127.1	2.60	2.09
11	136.5	139.6	3.10	2.27
12	140.9	147.6	6.70	4.76
14	79.5	82.3	2.80	3.52
15	96.5	100.4	3.90	4.04
16	108.5	114.0	5.50	5.07
17	122.5	126.4	3.90	3.18
18	130.5	137.1	6.60	5.06
19	147.5	148.3	0.80	0.54
20	158.5	156.7	-1.80	-1.14
21	157.5	156.7	-0.80	-0.51
22	82.5	85.9	3.40	4.12
23	100.5	104.6	4.10	4.08
24	114.5	119.1	4.60	4.02
25	126.5	132.0	5.50	4.35
26	138.5	143.7	5.20	3.75

COMPARISON OF AVERAGE AND EFFECTIVE FLOW DEPTH

RUN	H (mm)	H' (mm)	(H'-H) (mm)	(H'-H) (%)
27	147.5	153.9	6.40	4.34
28	158.5	164.4	5.90	3.72
29	163.5	174.0	10.50	6.42
30	81.5	83.0	1.50	1.84
31	97.5	100.1	2.60	2.67
32	112.5	114.6	2.10	1.87
33	122.5	126.0	3.50	2.86
34	139.5	138.9	-0.60	-0.43
35	148.5	150.1	1.60	1.08
36	151.5	157.9	6.40	4.22
37	160.5	169.0	8.50	5.30
38	84.5	85.7	1.20	1.42
39	100.5	102.6	2.10	2.09
40	113.5	115.9	2.40	2.11
41	124.5	127.4	2.90	2.33
42	136.5	138.4	1.90	1.39
43	143.5	150.0	6.50	4.53
44	155.5	159.6	4.10	2.64
45	161.5	168.1	6.60	4.09
46	84.5	85.7	1.20	1.42
47	99.5	101.7	2.20	2.21
48	113.5	116.0	2.50	2.20
49	125.5	127.9	2.40	1.91
50	139.5	139.7	0.20	0.14
51	143.5	149.6	6.10	4.25
52	156.5	161.1	4.60	2.94
53	163.5	171.6	8.10	4.95

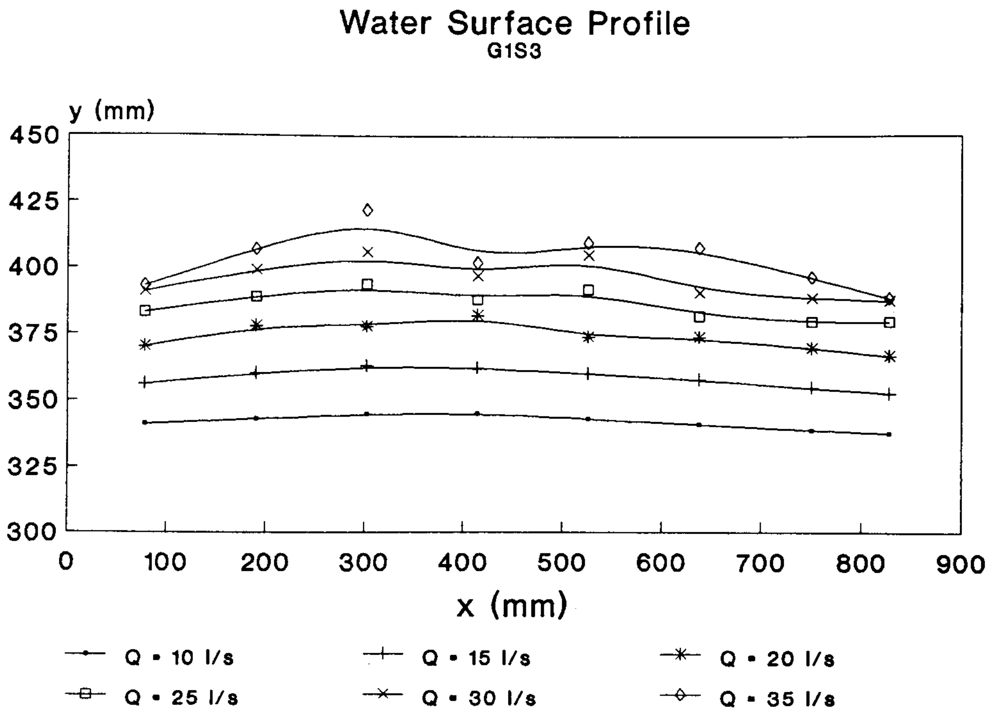

Water Surface Profile
G1S3
y (mm)
450
425
400
375
350
325
300
0
100
200
300
400
500
600
700
800
900
x (mm)
Q = 10 l/s
Q = 15 l/s
Q = 20 l/s
Q = 25 l/s
Q = 30 l/s
Q = 35 l/s

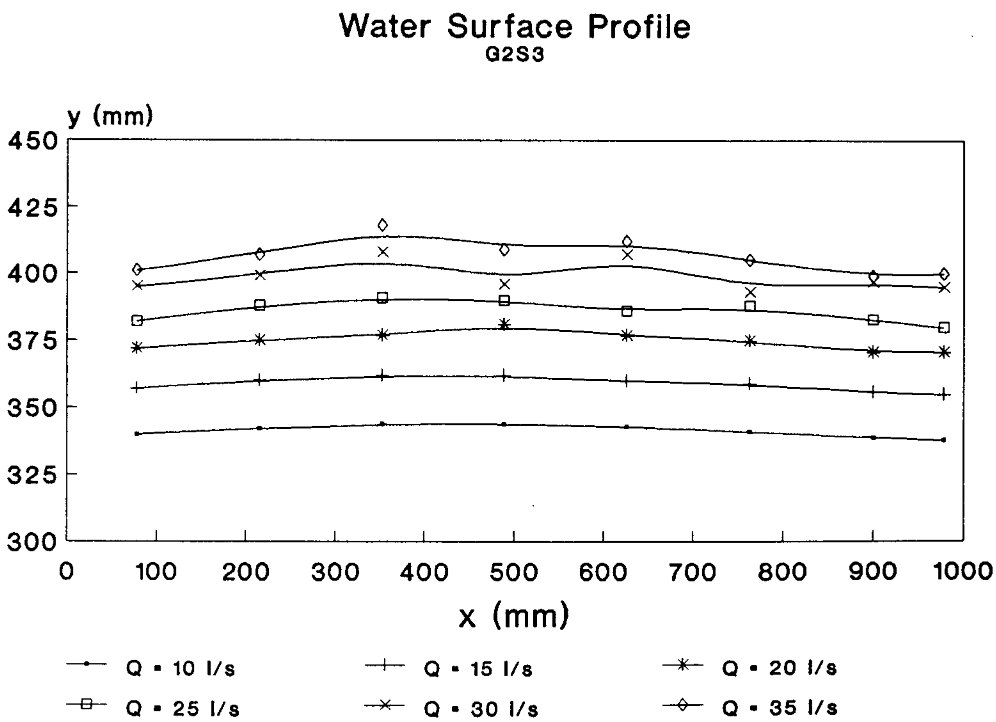

Water Surface Profile
G2S3
y (mm)
450
425
400
375
350
325
300
0
100
200
300
400
500
600
700
800
900
1000
x (mm)
Q = 10 l/s
Q = 15 l/s
Q = 20 l/s
Q = 25 l/s
Q = 30 l/s
Q = 35 l/s

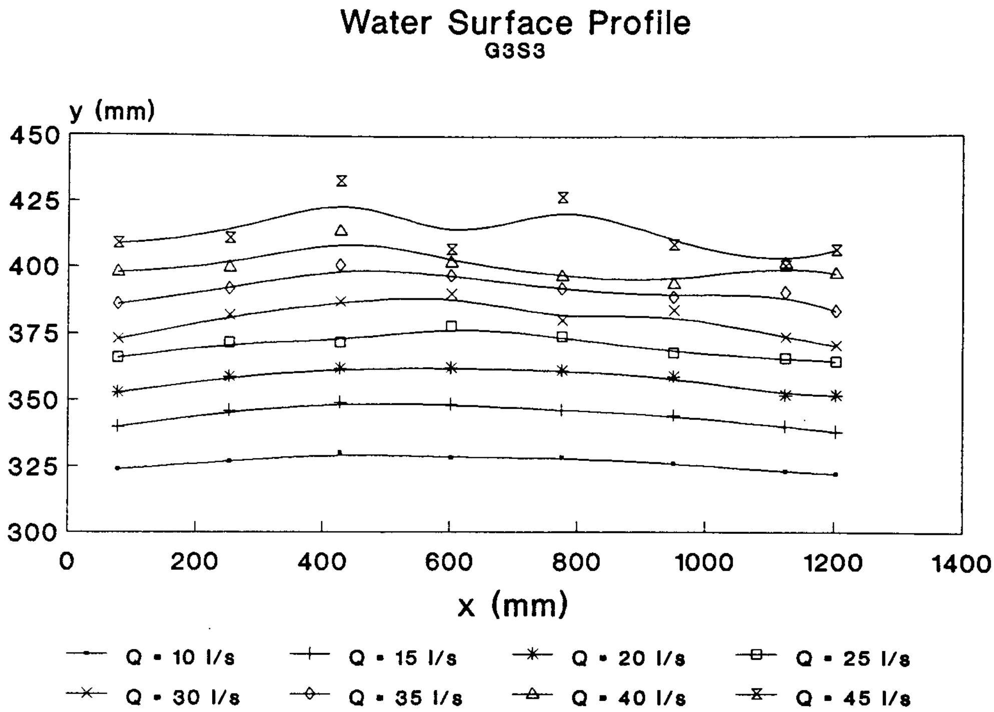
Water Surface Profile
G3S3
y (mm)
450
425
400
375
350
325
300
0
200
400
600
800
1000
1200
1400
x (mm)
Q = 10 l/s
Q = 15 l/s
Q = 20 l/s
Q = 25 l/s
Q = 30 l/s
Q = 35 l/s
Q = 40 l/s
Q = 45 l/s

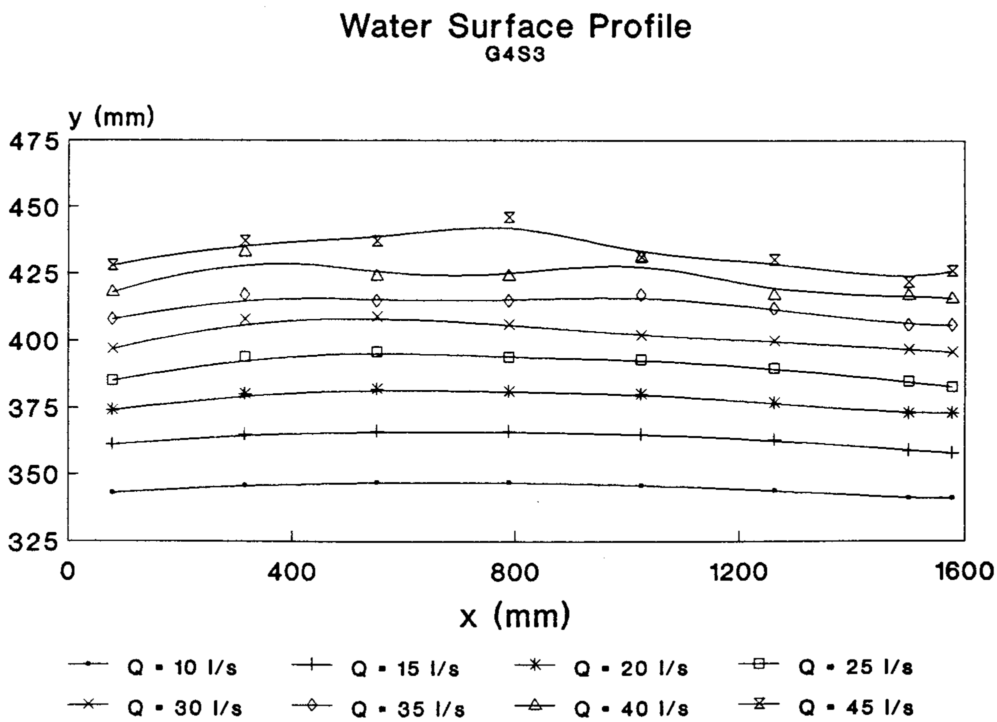
Water Surface Profile
G4S3
y (mm)
475
450
425
400
375
350
325
0
400
800
1200
1600
x (mm)
Q = 10 l/s
Q = 15 l/s
Q = 20 l/s
Q = 25 l/s
Q = 30 l/s
Q = 35 l/s
Q = 40 l/s
Q = 45 l/s

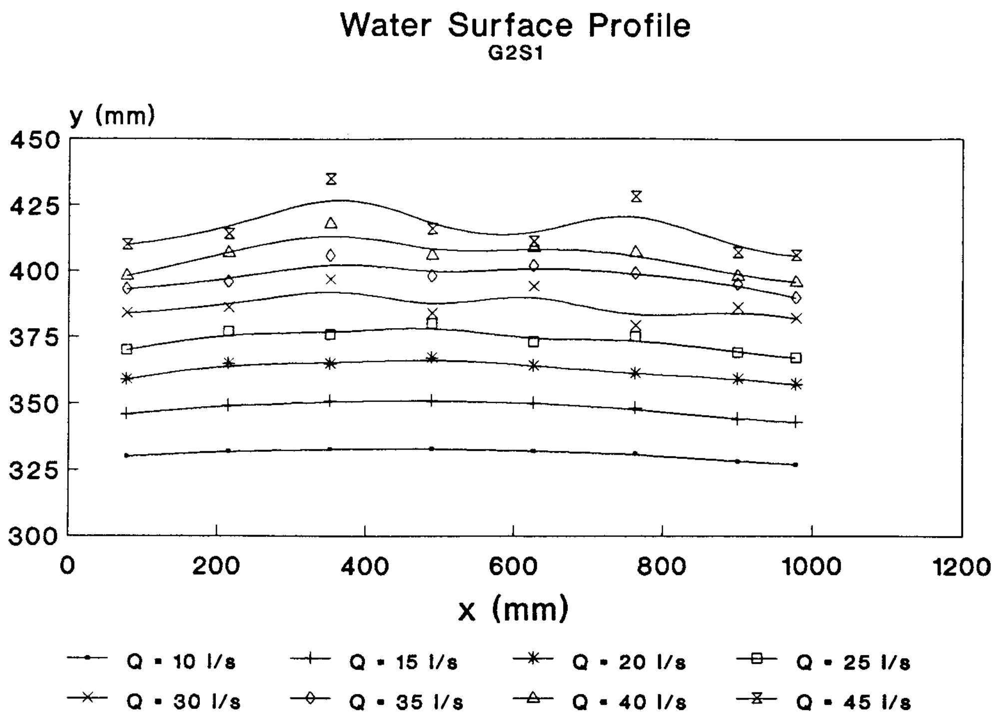
Water Surface Profile
G2S1
y (mm)
450
425
400
375
350
325
300
0
200
400
600
800
1000
1200
x (mm)
Q = 10 l/s
Q = 15 l/s
Q = 20 l/s
Q = 25 l/s
Q = 30 l/s
Q = 35 l/s
Q = 40 l/s
Q = 45 l/s

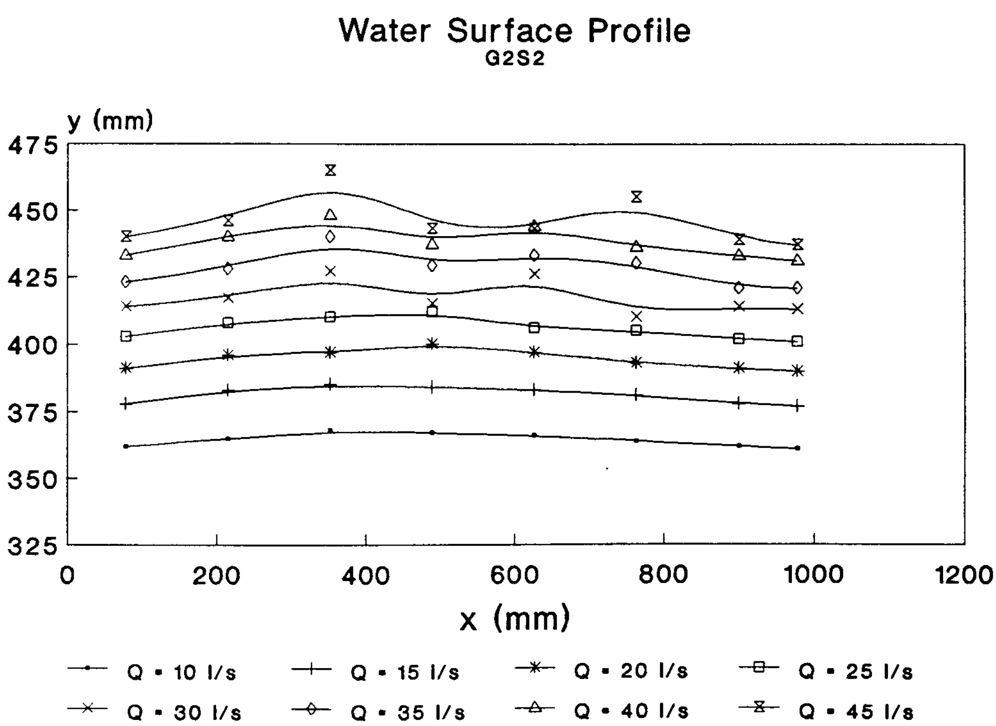
Water Surface Profile
G2S2
y (mm)
475
450
425
400
375
350
325
0
200
400
600
800
1000
1200
x (mm)
Q = 10 l/s
Q = 15 l/s
Q = 20 l/s
Q = 25 l/s
Q = 30 l/s
Q = 35 l/s
Q = 40 l/s
Q = 45 l/s

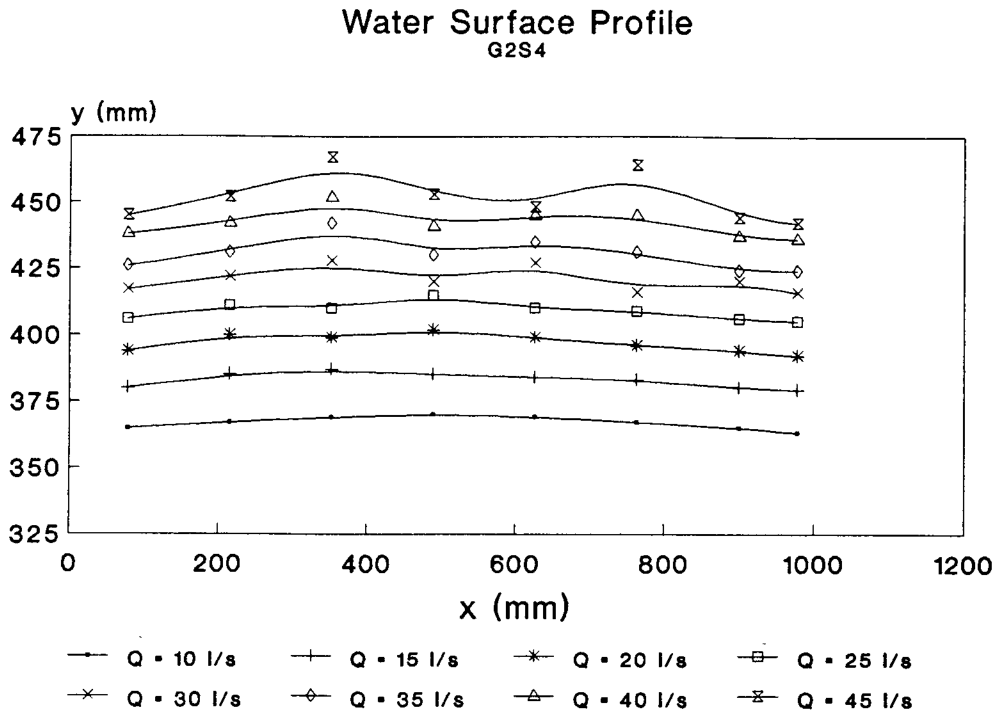
Water Surface Profile
G2S4
y (mm)
475
450
425
400
375
350
325
0
200
400
600
800
1000
1200
x (mm)
Q = 10 l/s
Q = 15 l/s
Q = 20 l/s
Q = 25 l/s
Q = 30 l/s
Q = 35 l/s
Q = 40 l/s
Q = 45 l/s

APPENDIX D : Length of Separation

LENGTH OF SEPARATION AND REATTACHMENT POINT

RUN	L	L/Δ	L/λ
1	284	6.31	0.38
2	276	6.13	0.37
3	270	6.00	0.36
4	262	5.82	0.35
5	268	5.96	0.36
6	275	6.11	0.37
6A	281	6.24	0.37
6B	284	6.31	0.38
7	311	6.91	0.35
8	303	6.73	0.34
9	290	6.44	0.32
10	283	6.29	0.31
11	273	6.07	0.30
12	285	6.33	0.32
13	297	6.60	0.33
14	379	8.42	0.34
15	365	8.11	0.32
16	346	7.69	0.31
17	338	7.51	0.30
18	324	7.20	0.29
19	338	7.51	0.30
20	343	7.62	0.30
21	349	7.76	0.31
22	441	9.80	0.29
23	426	9.47	0.28

LENGTH OF SEPARATION AND REATTACHMENT POINT

RUN	L	L/Δ	L/λ
24	407	9.04	0.27
25	400	8.89	0.27
26	386	8.58	0.26
27	402	8.93	0.27
28	407	9.04	0.27
29	420	9.33	0.28
30	344	7.64	0.38
31	332	7.38	0.37
32	320	7.11	0.36
33	309	6.87	0.34
34	302	6.71	0.34
35	293	6.51	0.33
36	304	6.76	0.34
37	309	6.87	0.34
38	327	7.27	0.36
39	317	7.04	0.35
40	307	6.82	0.34
41	299	6.64	0.33
42	290	6.44	0.32
43	287	6.38	0.32
44	300	6.67	0.33
45	305	6.78	0.34
46	302	6.71	0.34
47	293	6.51	0.33
48	284	6.31	0.32

LENGTH OF SEPARATION AND REATTACHMENT POINT

RUN	L	L/Δ	L/λ
49	279	6.20	0.31
50	271	6.02	0.30
51	282	6.27	0.31
52	292	6.49	0.32
53	301	6.69	0.33

Length of Separation (Results summary)

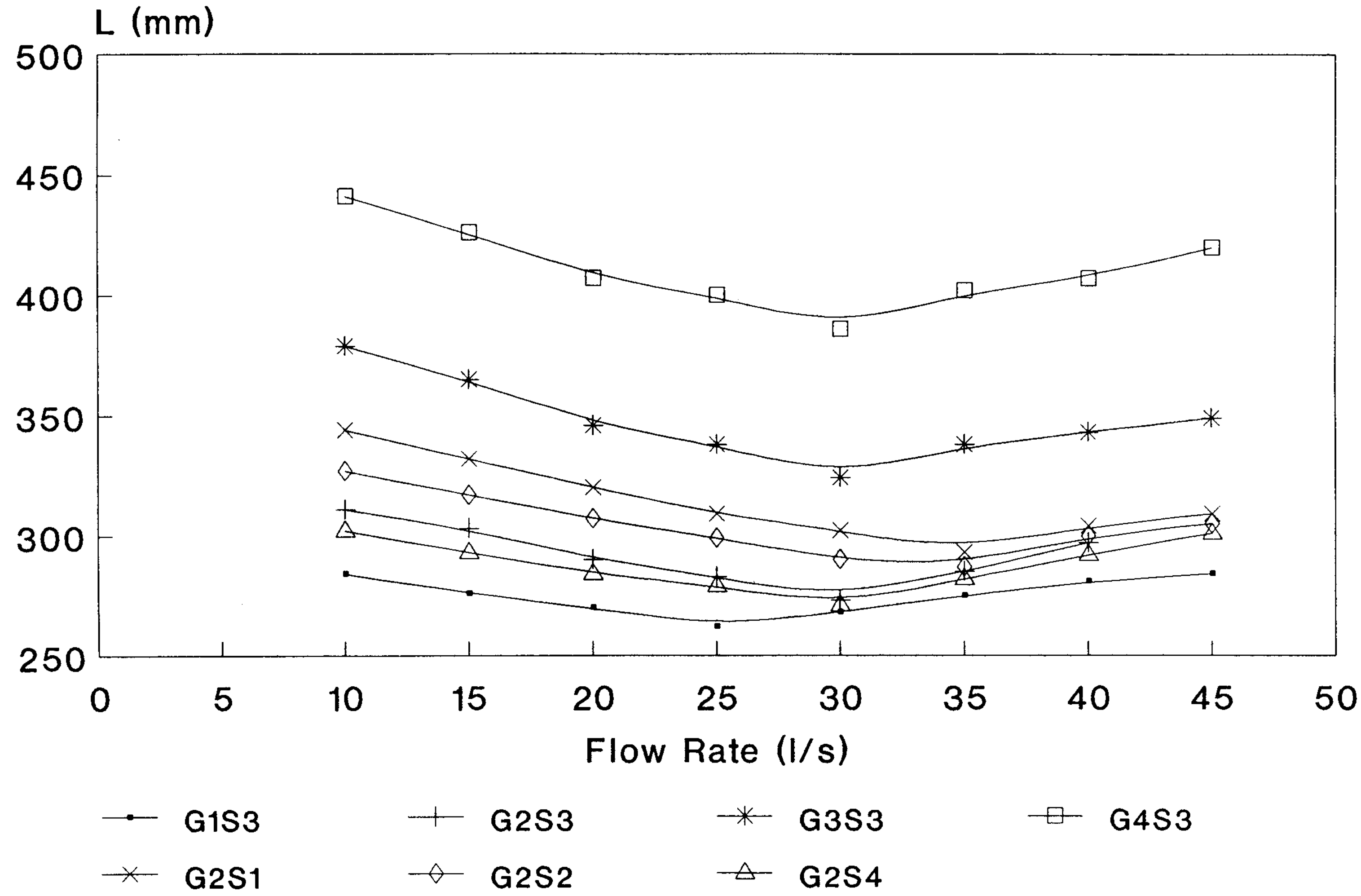

Dimensionless Length of Separation
varying roughness

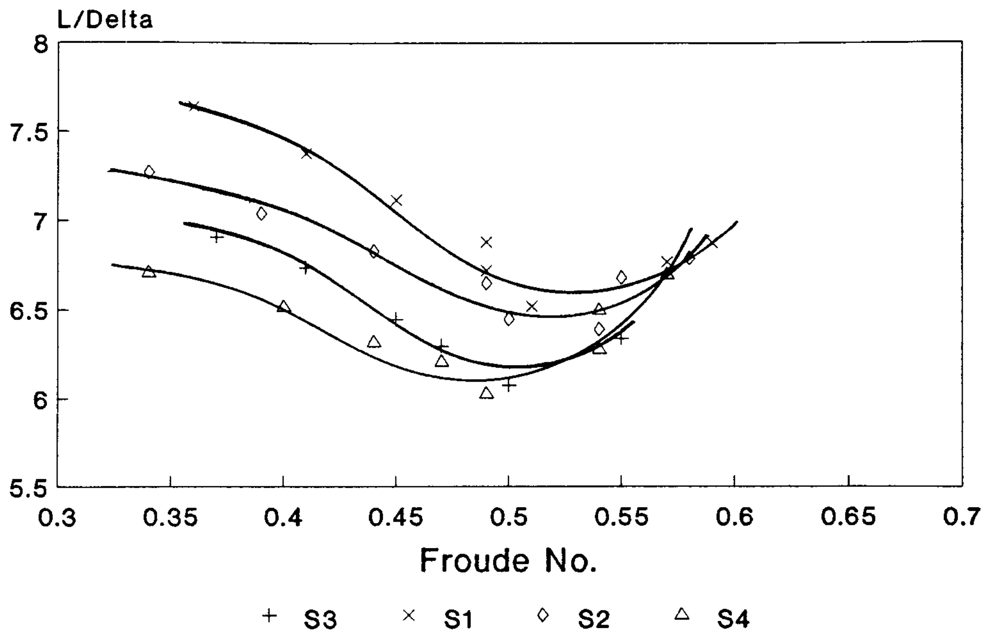

Dimensioless Length of Separation
varying roughness

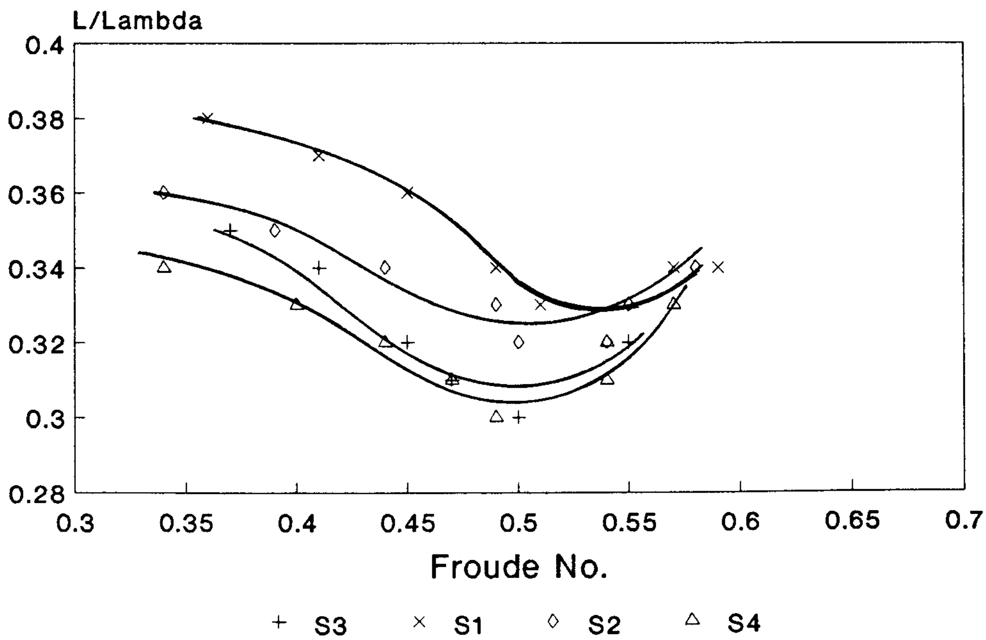

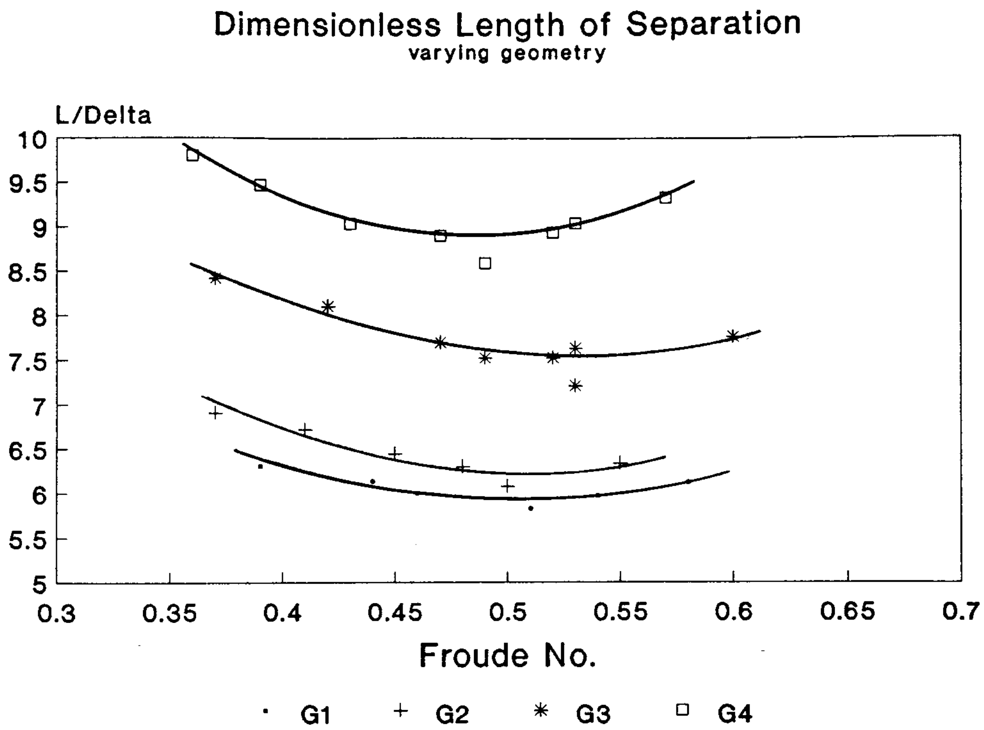
Dimensionless Length of Separation
varying geometry
L/Delta
10
9.5
9
8.5
8
7.5
7
6.5
6
5.5
5
0.3
0.35
0.4
0.45
0.5
0.55
0.6
0.65
0.7
Froude No.
G1
G2
G3
G4

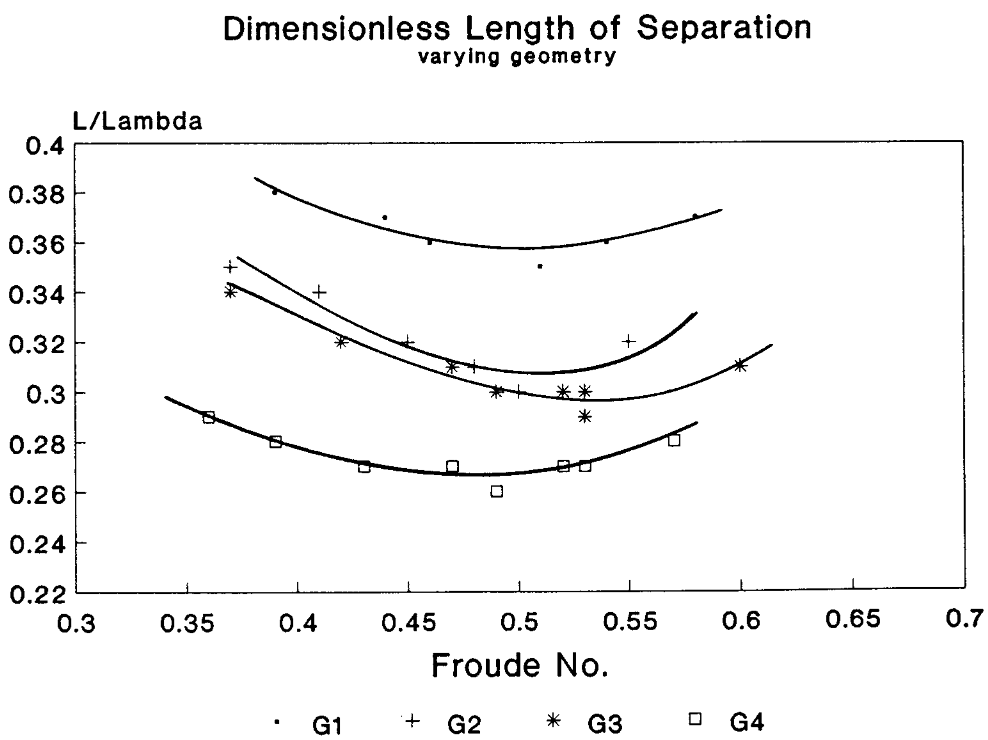
Dimensionless Length of Separation
varying geometry
L/Lambda
0.4
0.38
0.36
0.34
0.32
0.3
0.28
0.26
0.24
0.22
0.3
0.35
0.4
0.45
0.5
0.55
0.6
0.65
0.7
Froude No.
G1
G2
G3
G4

APPENDIX E : Bed Pressure

BED PRESSURE DISTRIBUTION SUMMARY

	RUN No.		P/γ (mm)		
POINT	**1**	**2**	**3**	**4**	**5**
1_a	193	206	223	234	245
1_b					
1_c					
2	194	207	224	236	247
RP	188	202	219	233	243
3	187	200	217	229	241
4	180	193	210	222	234
5	172	185	202	214	225
6	164	177	193	204	216
CR	154	165	181	192	202
CR_a					
CR_b					
	6	**7**	**8**	**9**	**10**
1_a	254	195	211	228	239
1_b		195	211	227	238
1_c		195	211	227	239
2	256	193	210	227	240
RP	252	188	205	224	237
3	251	187	205	222	234
4	243	179	196	213	225
5	234	170	186	203	216
6	225	160	177	193	205
CR	211	148	165	180	191
CR_a		169	186	201	210
CR_b		184	201	216	225

BED PRESSURE DISTRIBUTION SUMMARY

	RUN No.		P/γ (mm)		
POINT	**11**	**12**	**14**	**15**	**16**
1_a	249	260	193	211	225
1_b	249	259	193	211	225
1_c	250	261	193	211	225
2	251	262	193	211	225
RP	249	259	188	208	224
3	246	257	187	206	221
4	236	247	179	197	213
5	227	238	172	190	205
6	215	227	164	182	197
CR	202	211	154	172	186
CR_a	221	230	164	182	196
CR_b	236	245	182	200	214
	17	**18**	**19**	**22**	**23**
1_a	236	249	259	201	220
1_b	236	249	259	201	220
1_c	236	249	259	200	219
2	237	250	260	200	218
RP	236	250	259	197	215
3	232	246	256	193	211
4	224	238	247	184	203
5	216	229	238	176	194
6	207	220	228	167	184
CR	196	207	217	156	173
CR_a	206	217	227	174	190
CR_b	224	235	245	191	207

BED PRESSURE DISTRIBUTION SUMMARY

	RUN No.		P/γ (mm)		
POINT	**24**	**25**	**26**	**27**	**30**
1_a	233	246	257	268	196
1_b	233	246	257	269	195
1_c	233	246	258	269	195
2	234	246	258	270	194
RP	232	245	258	269	187
3	227	240	252	264	187
4	218	231	243	254	179
5	210	223	235	245	171
6	200	212	224	234	160
CR	188	200	212	221	149
CR_a	205	217	229	237	169
CR_b	222	234	246	254	184
	31	**32**	**33**	**34**	**35**
1_a	214	227	238	250	260
1_b	214	227	238	250	260
1_c	214	227	238	251	261
2	214	226	238	252	262
RP	208	222	235	249	261
3	207	220	232	246	256
4	198	211	223	236	247
5	190	202	215	227	238
6	179	191	203	214	225
CR	167	186	191	202	211
CR_a	187	199	209	220	229
CR_b	202	214	224	235	244

BED PRESSURE DISTRIBUTION SUMMARY

	RUN No.		P/γ (mm)		
POINT	**38**	**39**	**40**	**41**	**42**
1_a	198	212	227	239	250
1_b	197	212	227	239	251
1_c	197	212	227	239	252
2	197	212	227	239	252
RP	191	207	223	236	250
3	191	206	221	234	246
4	182	197	212	234	236
5	173	188	202	214	226
6	164	179	193	205	215
CR	153	166	180	192	204
CR_a	172	187	201	211	223
CR_b	186	201	215	225	237
	43	**46**	**47**	**48**	**49**
1_a	261	201	214	228	240
1_b	261	200	214	228	240
1_c	262	200	214	228	240
2	263	199	214	228	240
RP	261	196	212	227	239
3	257	192	207	221	233
4	247	184	199	213	225
5	237	174	189	203	214
6	227	165	180	194	204
CR	212	155	169	182	192
CR_a	231	175	189	202	210
CR_b	245	191	205	218	226

BED PRESSURE DISTRIBUTION SUMMARY

	RUN No.		P/γ (mm)		
POINT	**50**	**51**			
1_a	251	262			
1_b	251	262			
1_c	252	263			
2	252	264			
RP	251	261			
3	246	257			
4	238	249			
5	227	238			
6	216	227			
CR	205	213			
CR_a	223	231			
CR_b	239	247			

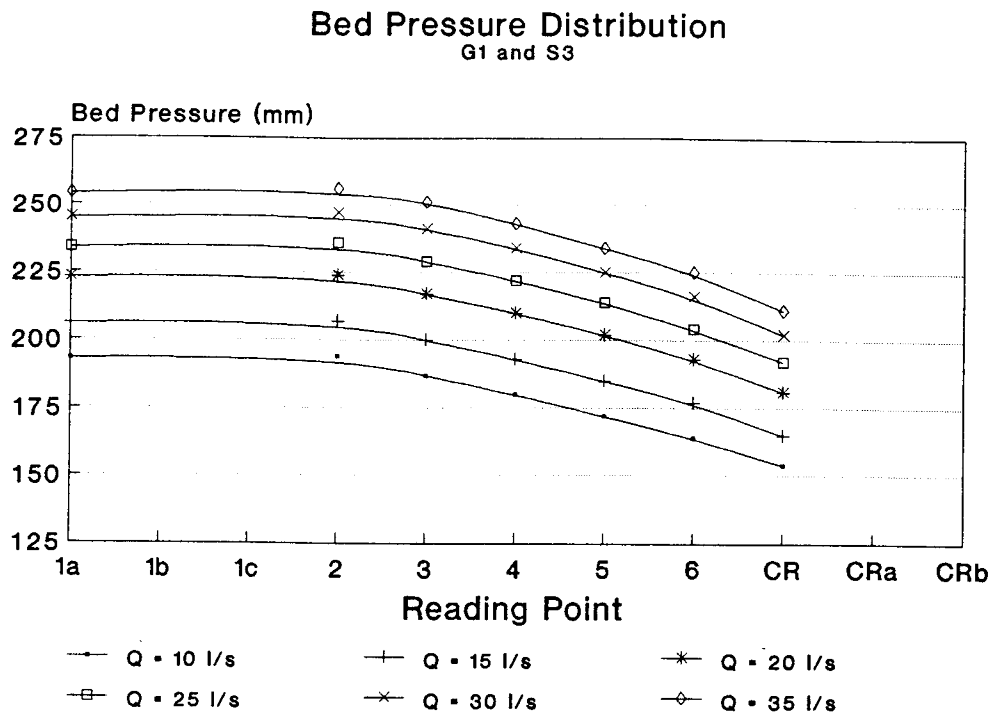

Bed Pressure Distribution
G1 and S3
Bed Pressure (mm)
275
250
225
200
175
150
125
1a
1b
1c
2
3
4
5
6
CR
CRa
CRb
Reading Point
Q = 10 l/s
Q = 15 l/s
Q = 20 l/s
Q = 25 l/s
Q = 30 l/s
Q = 35 l/s

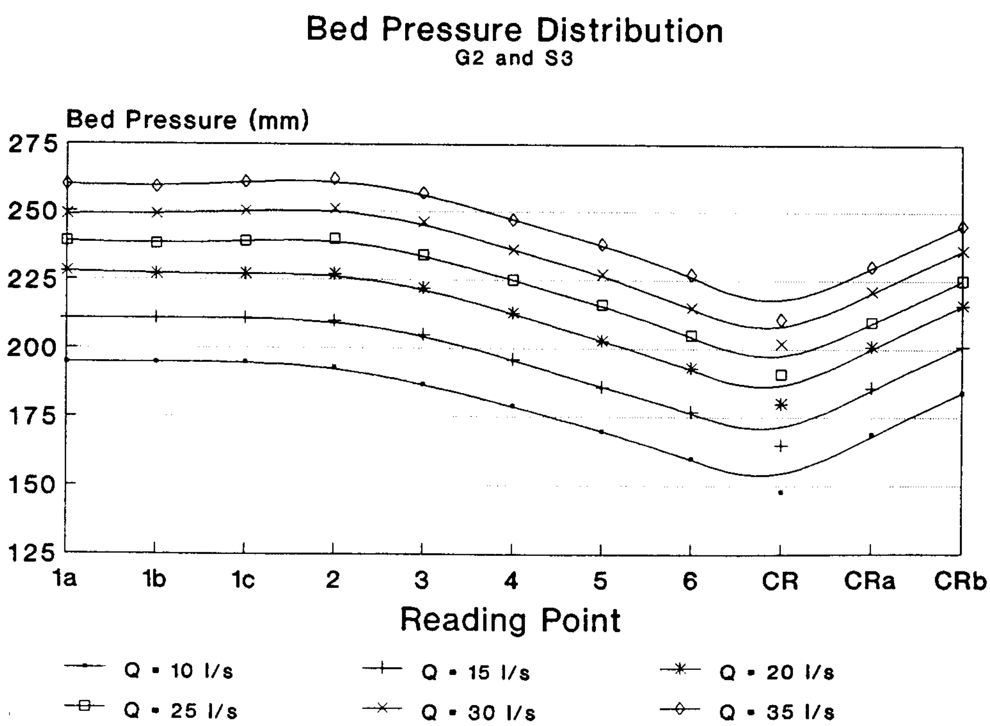

Bed Pressure Distribution
G2 and S3
Bed Pressure (mm)
275
250
225
200
175
150
125
1a
1b
1c
2
3
4
5
6
CR
CRa
CRb
Reading Point
Q = 10 l/s
Q = 15 l/s
Q = 20 l/s
Q = 25 l/s
Q = 30 l/s
Q = 35 l/s

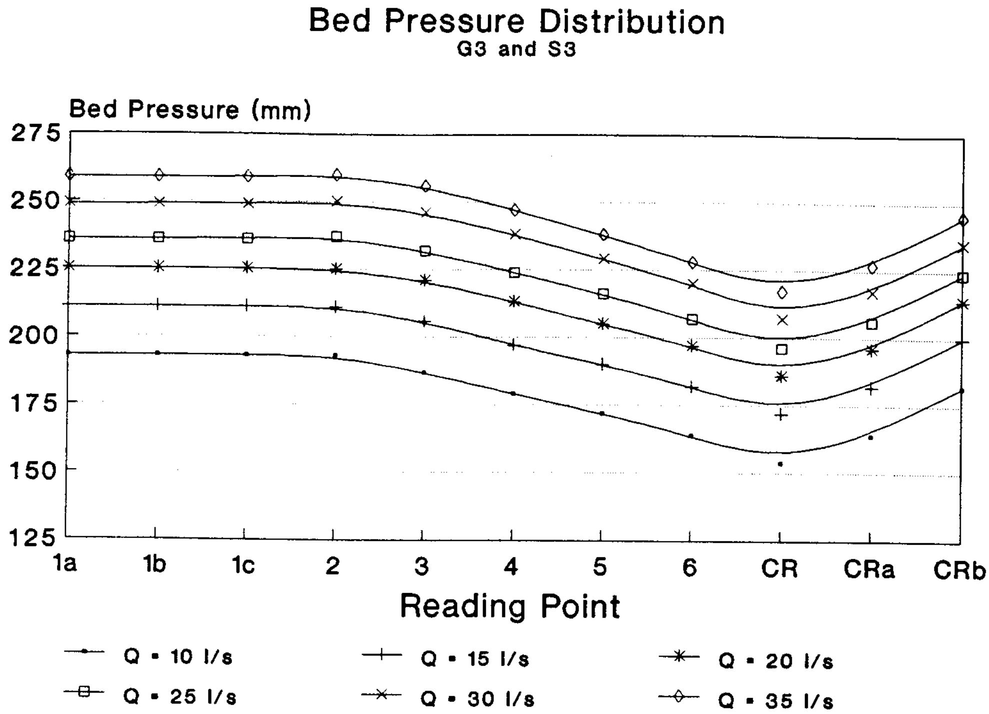
Bed Pressure Distribution
G3 and S3
Bed Pressure (mm)
275
250
225
200
175
150
125
1a
1b
1c
2
3
4
5
6
CR
CRa
CRb
Reading Point
Q = 10 l/s
Q = 15 l/s
Q = 20 l/s
Q = 25 l/s
Q = 30 l/s
Q = 35 l/s

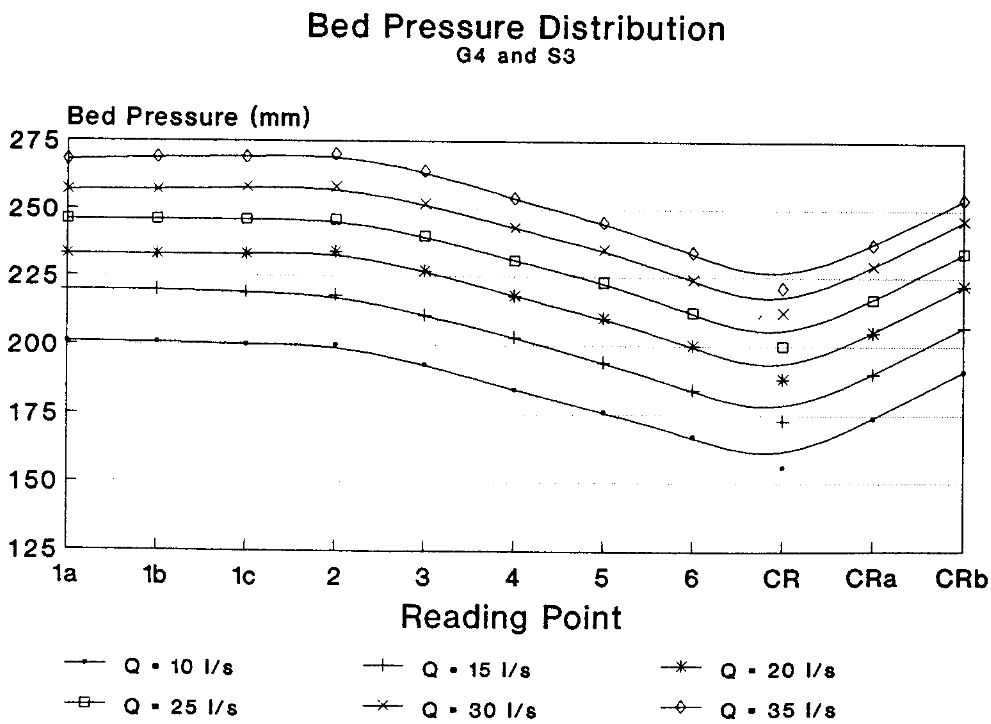
Bed Pressure Distribution
G4 and S3
Bed Pressure (mm)
275
250
225
200
175
150
125
1a
1b
1c
2
3
4
5
6
CR
CRa
CRb
Reading Point
Q = 10 l/s
Q = 15 l/s
Q = 20 l/s
Q = 25 l/s
Q = 30 l/s
Q = 35 l/s

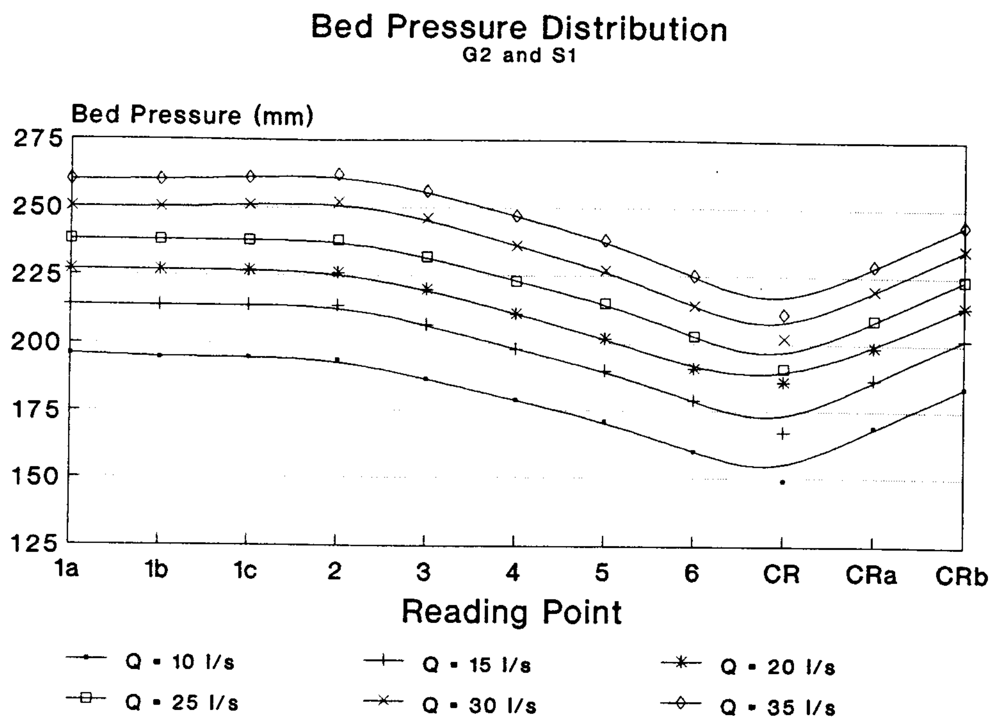
Bed Pressure Distribution
G2 and S1
Bed Pressure (mm)
275
250
225
200
175
150
125
1a
1b
1c
2
3
4
5
6
CR
CRa
CRb
Reading Point
Q = 10 l/s
Q = 15 l/s
Q = 20 l/s
Q = 25 l/s
Q = 30 l/s
Q = 35 l/s

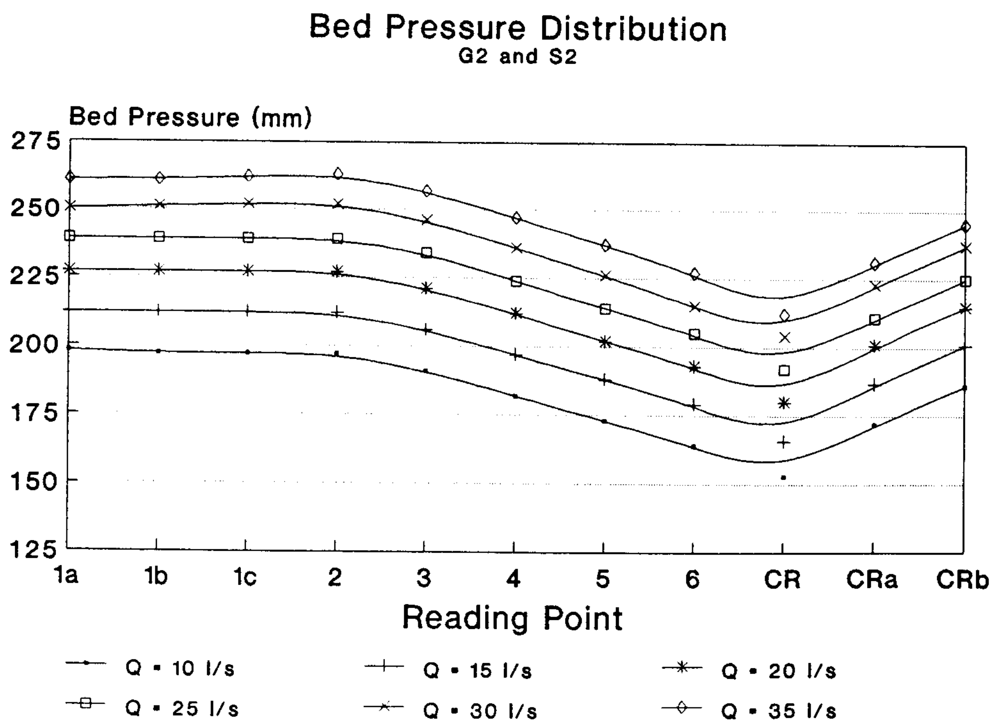
Bed Pressure Distribution
G2 and S2
Bed Pressure (mm)
275
250
225
200
175
150
125
1a
1b
1c
2
3
4
5
6
CR
CRa
CRb
Reading Point
Q = 10 l/s
Q = 15 l/s
Q = 20 l/s
Q = 25 l/s
Q = 30 l/s
Q = 35 l/s

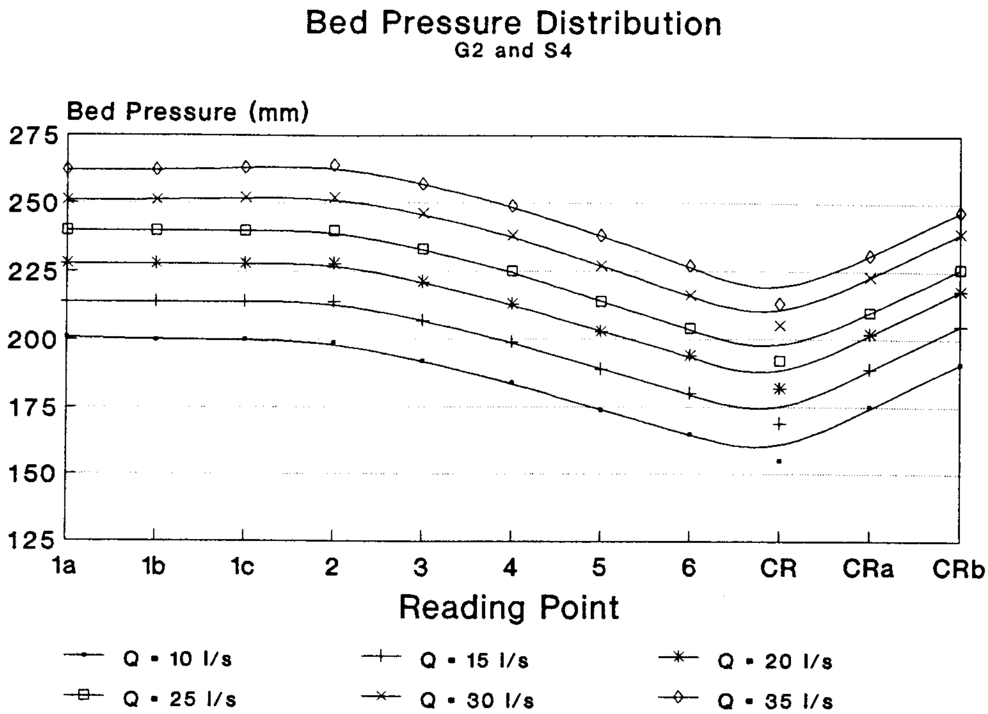
Bed Pressure Distribution
G2 and S4
Bed Pressure (mm)
275
250
225
200
175
150
125
1a
1b
1c
2
3
4
5
6
CR
CRa
CRb
Reading Point
Q = 10 l/s
Q = 15 l/s
Q = 20 l/s
Q = 25 l/s
Q = 30 l/s
Q = 35 l/s

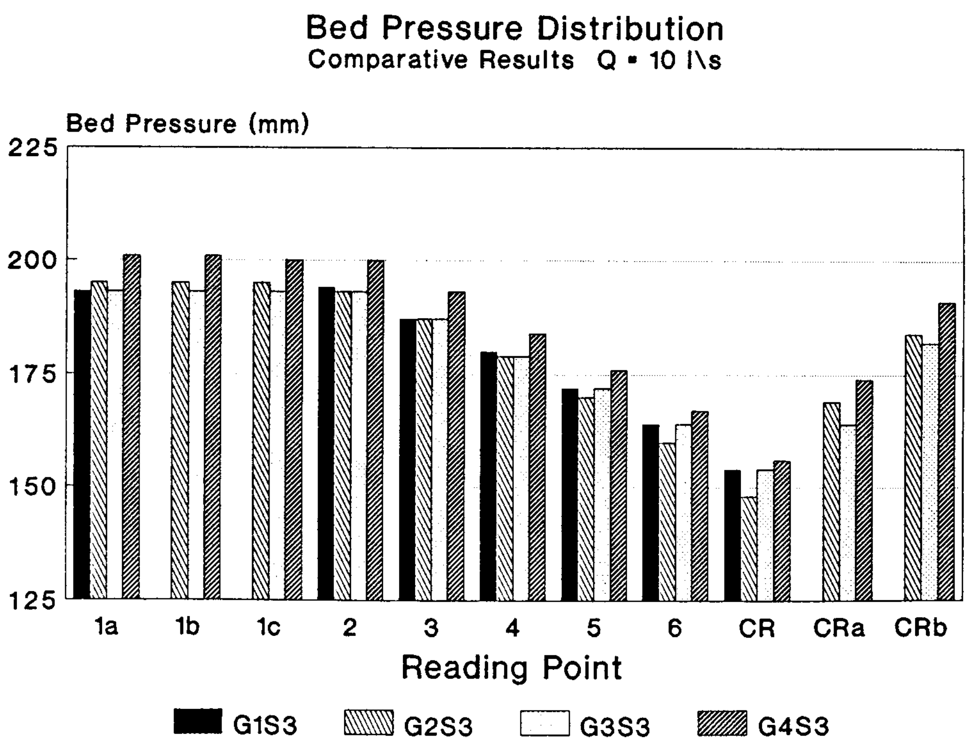
Bed Pressure Distribution
Comparative Results Q = 10 l\s
Bed Pressure (mm)
225
200
175
150
125
1a
1b
1c
2
3
4
5
6
CR
CRa
CRb
Reading Point
G1S3
G2S3
G3S3
G4S3

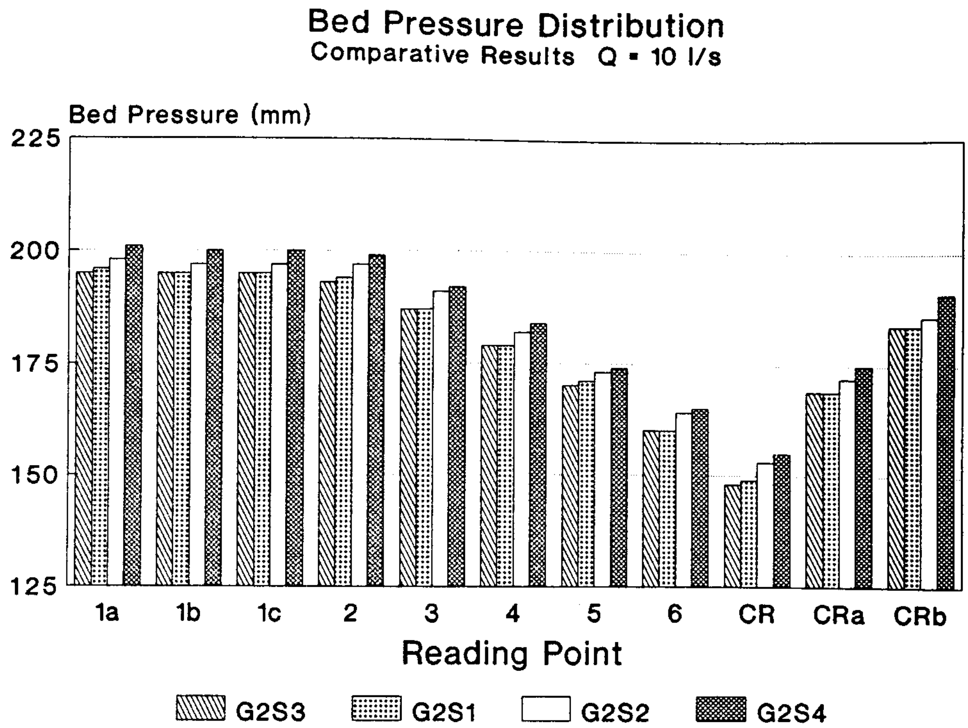
Bed Pressure Distribution
Comparative Results Q = 10 l/s
Bed Pressure (mm)
225
200
175
150
125
1a
1b
1c
2
3
4
5
6
CR
CRa
CRb
Reading Point
G2S3
G2S1
G2S2
G2S4

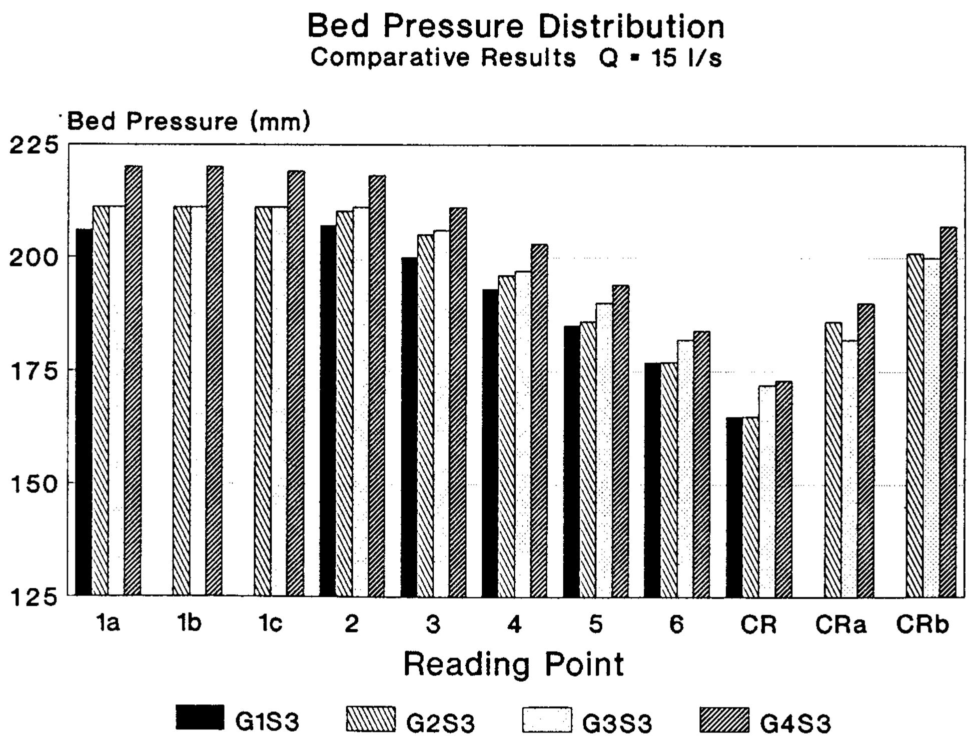
Bed Pressure Distribution
Comparative Results Q = 15 l/s
Bed Pressure (mm)
225
200
175
150
125
1a
1b
1c
2
3
4
5
6
CR
CRa
CRb
Reading Point
G1S3
G2S3
G3S3
G4S3

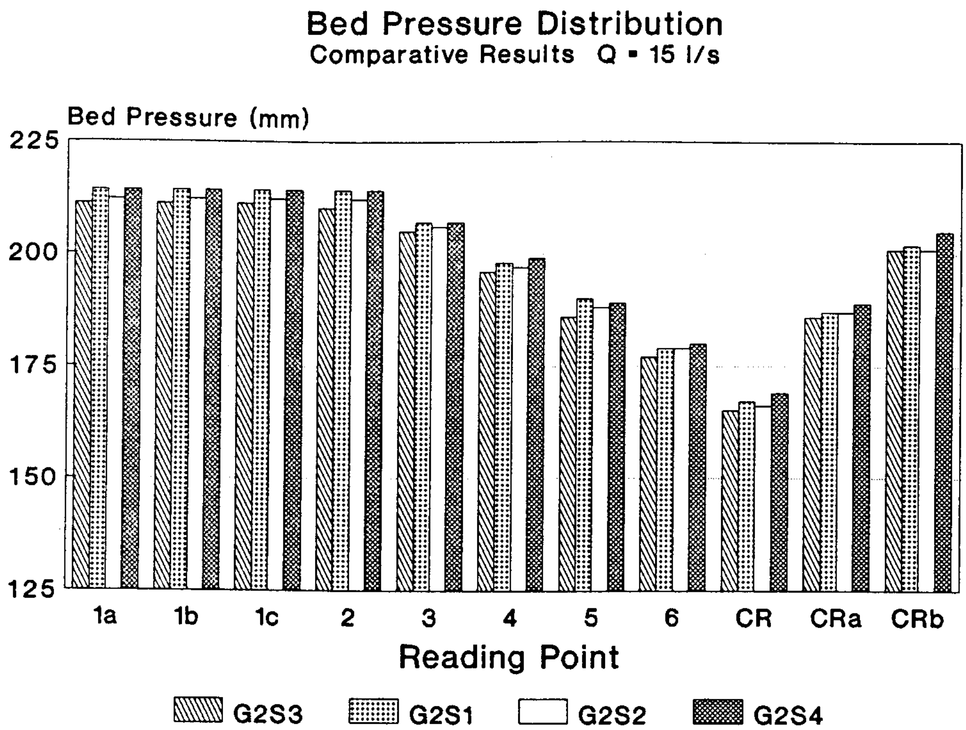
Bed Pressure Distribution
Comparative Results Q = 15 l/s
Bed Pressure (mm)
225
200
175
150
125
1a
1b
1c
2
3
4
5
6
CR
CRa
CRb
Reading Point
G2S3
G2S1
G2S2
G2S4

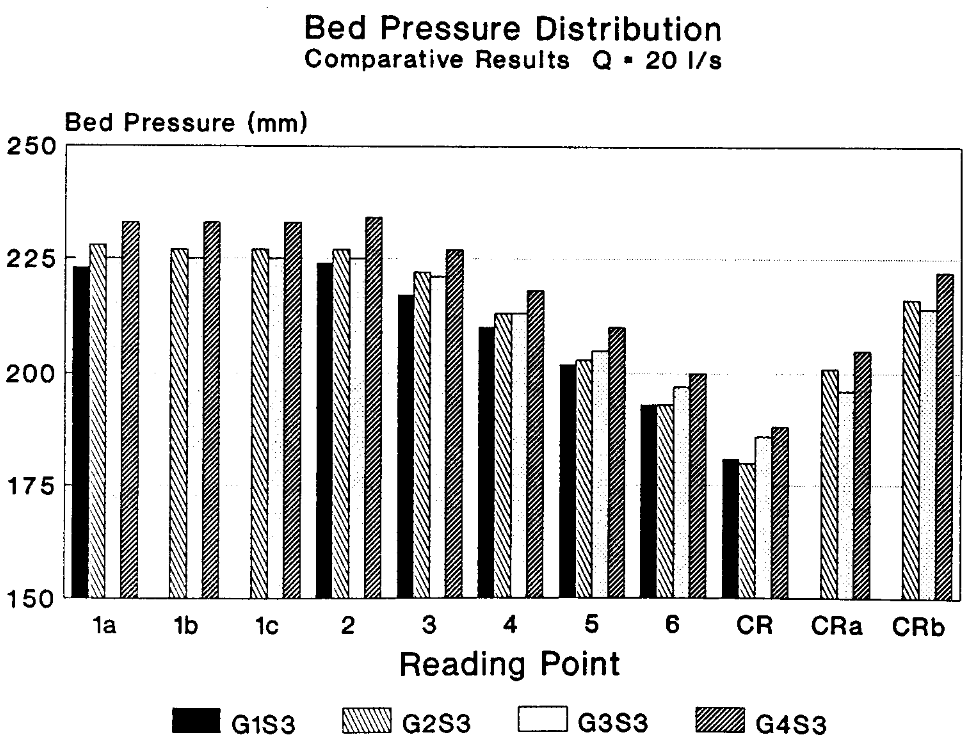
Bed Pressure Distribution
Comparative Results Q = 20 l/s
Bed Pressure (mm)
250
225
200
175
150
1a
1b
1c
2
3
4
5
6
CR
CRa
CRb
Reading Point
G1S3
G2S3
G3S3
G4S3

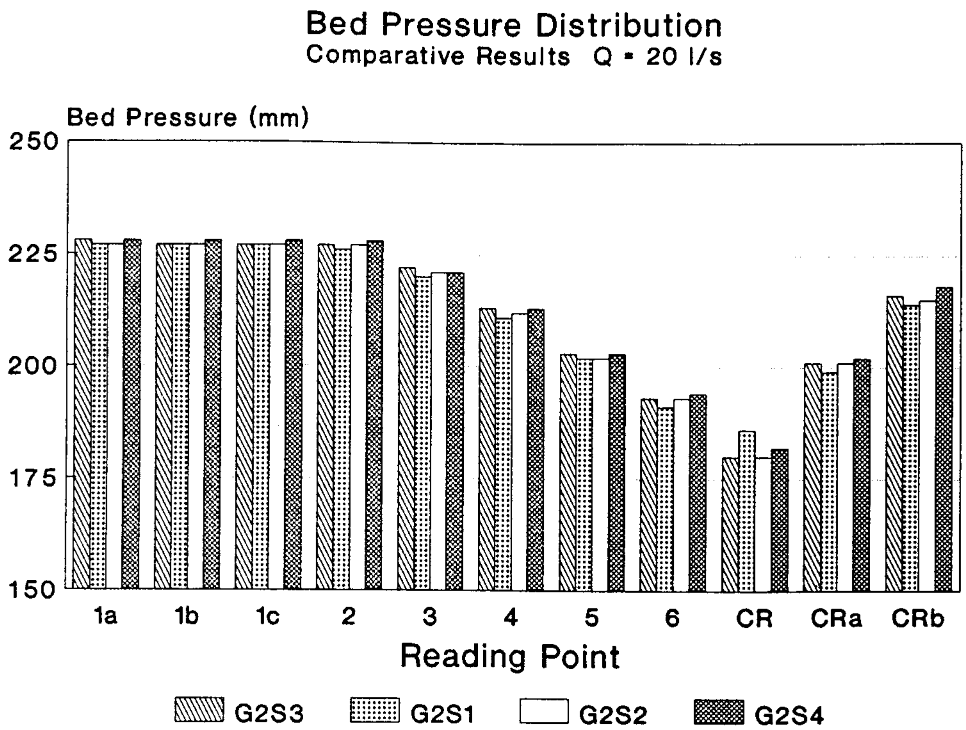
Bed Pressure Distribution
Comparative Results Q = 20 l/s
Bed Pressure (mm)
250
225
200
175
150
1a
1b
1c
2
3
4
5
6
CR
CRa
CRb
Reading Point
G2S3
G2S1
G2S2
G2S4

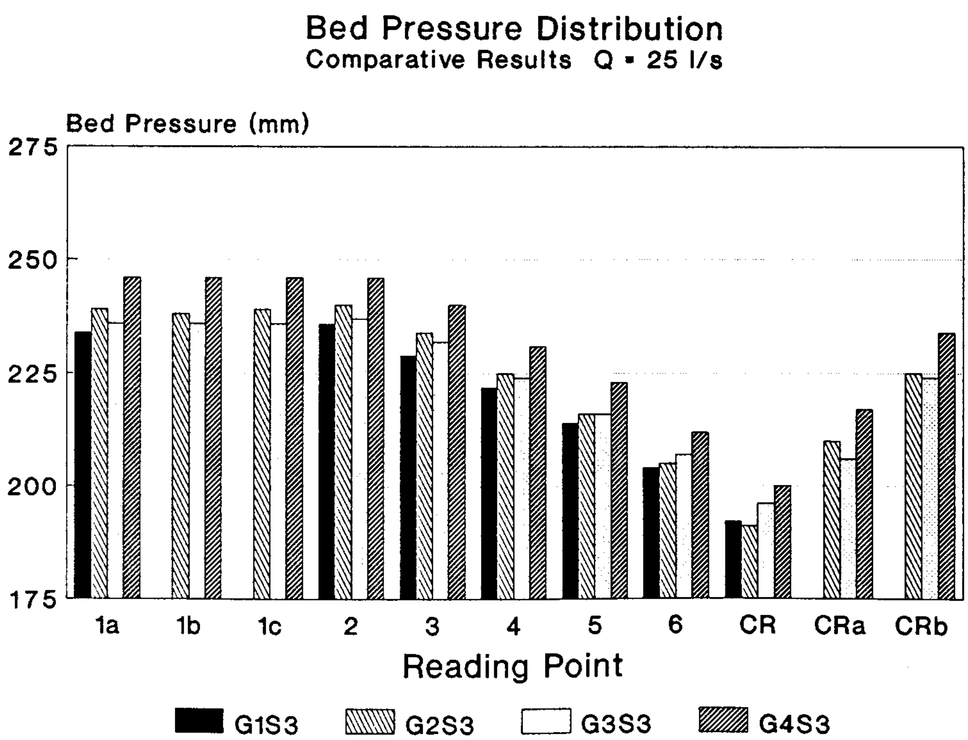
Bed Pressure Distribution
Comparative Results Q = 25 l/s
Bed Pressure (mm)
275
250
225
200
175
1a
1b
1c
2
3
4
5
6
CR
CRa
CRb
Reading Point
G1S3
G2S3
G3S3
G4S3

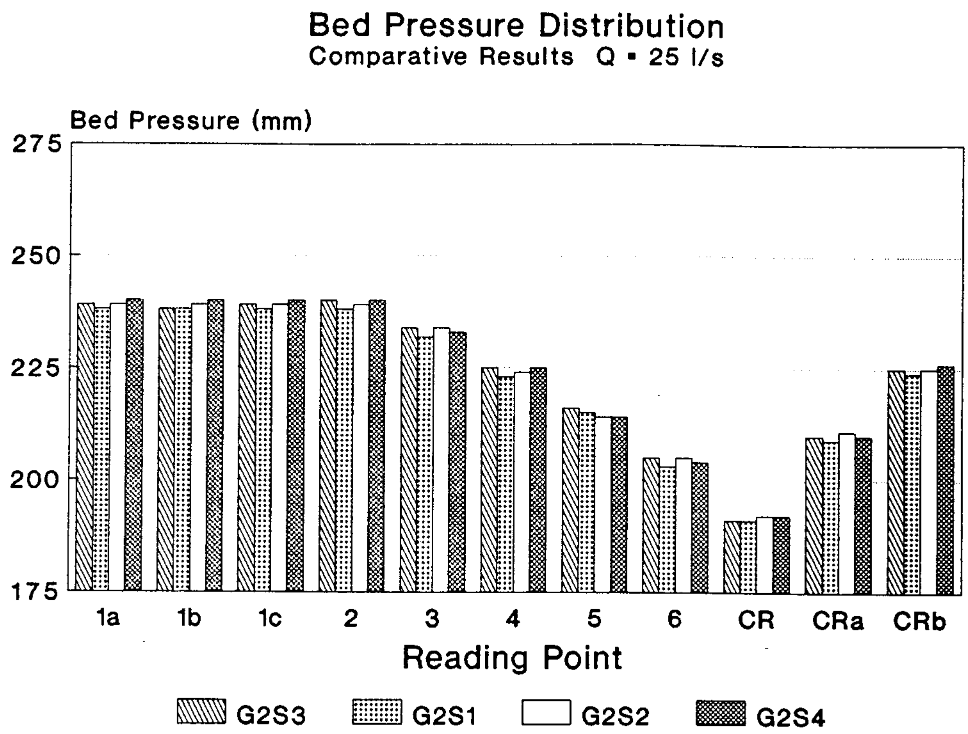
Bed Pressure Distribution
Comparative Results Q = 25 l/s
Bed Pressure (mm)
275
250
225
200
175
1a
1b
1c
2
3
4
5
6
CR
CRa
CRb
Reading Point
G2S3
G2S1
G2S2
G2S4

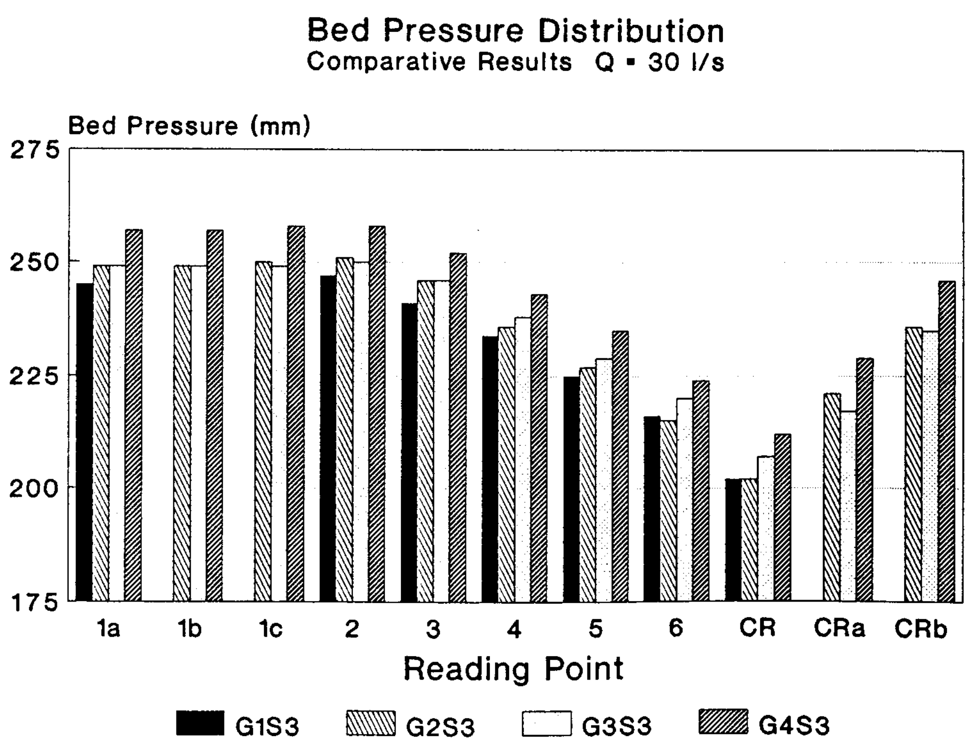
Bed Pressure Distribution
Comparative Results Q = 30 l/s
Bed Pressure (mm)
275
250
225
200
175
1a
1b
1c
2
3
4
5
6
CR
CRa
CRb
Reading Point
G1S3
G2S3
G3S3
G4S3

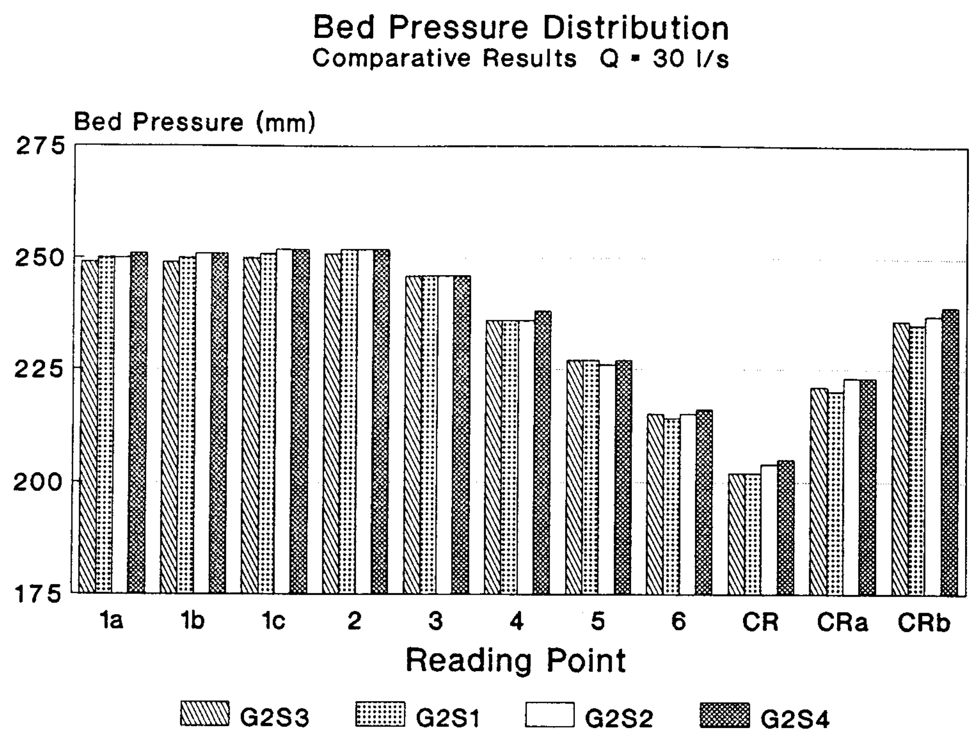
Bed Pressure Distribution
Comparative Results Q = 30 l/s
Bed Pressure (mm)
275
250
225
200
175
1a
1b
1c
2
3
4
5
6
CR
CRa
CRb
Reading Point
G2S3
G2S1
G2S2
G2S4

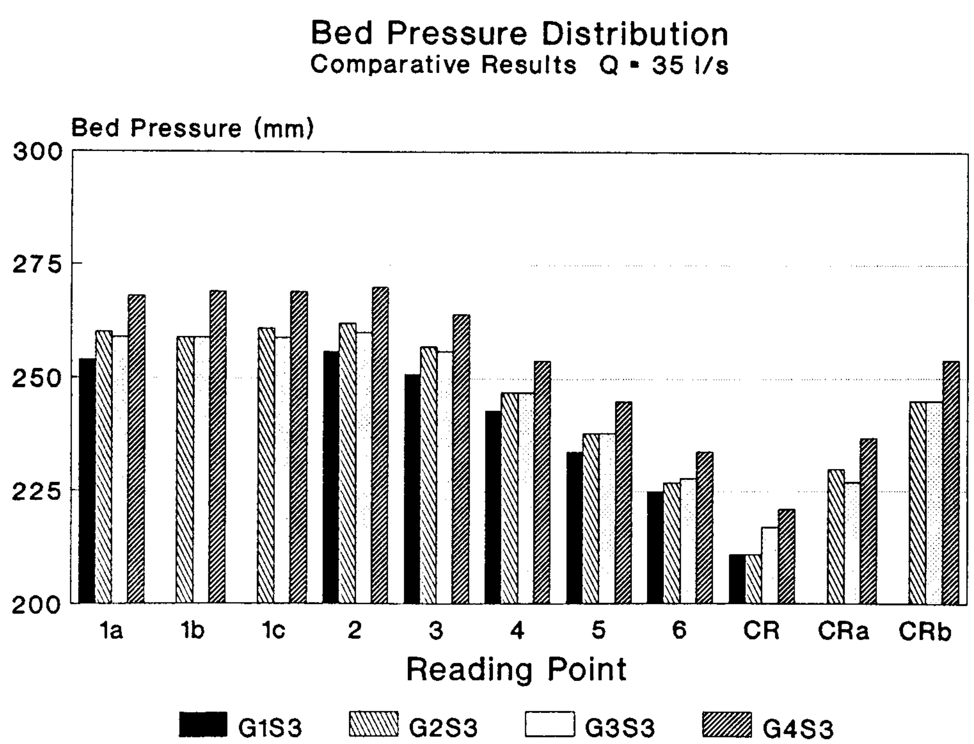
Bed Pressure Distribution
Comparative Results Q = 35 l/s
Bed Pressure (mm)
300
275
250
225
200
1a
1b
1c
2
3
4
5
6
CR
CRa
CRb
Reading Point
G1S3
G2S3
G3S3
G4S3

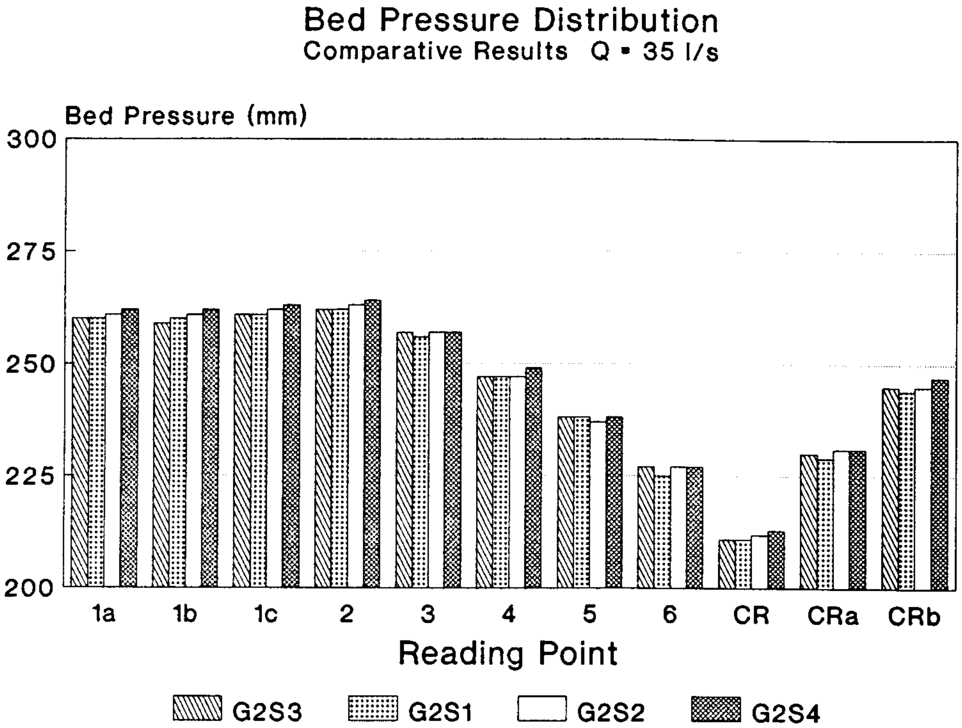

Bed Pressure Distribution
Comparative Results Q = 35 l/s
Bed Pressure (mm)
300
275
250
225
200
1a
1b
1c
2
3
4
5
6
CR
CRa
CRb
Reading Point
G2S3
G2S1
G2S2
G2S4

APPENDIX F : Grain Shear Stress

CONVERTING POINT VELOCITY TO GRAIN SHEAR STRESS VALUES.

The following equations will be used for roughness S3 :

$\Delta P = 500\ (u_b)^2$ $\qquad T''_o = -\ 0.06934 + 0.02914\ \Delta P$

RUN	POINT	u_b (m/s)	ΔP (N/m^2)	T_o'' (N/m^2)
1	3_c	0.135	9.10	0.20
	4	0.18	16.20	0.40
	5	0.25	31.25	0.84
	6	0.307	47.10	1.30
	CR	0.354	62.65	1.75
2	3_a	0.124	7.70	0.15
	3_d	0.179	16.00	0.40
	4	0.214	22.90	0.60
	5	0.274	37.55	1.02
	6	0.340	57.80	1.61
	CR	0.395	78.00	2.20
3	3	0.133	8.85	0.19
	3_c	0.219	24.00	0.63
	4	0.251	31.50	0.85
	5	0.322	51.85	1.44
	6	0.388	75.25	2.12
	CR	0.472	111.40	3.17
4	RP_a	0.136	9.25	0.20
	3	0.174	15.15	0.37
	3_c	0.265	35.10	0.95
	4	0.304	46.20	1.28
	5	0.35	61.25	1.71

$\Delta P = 500\ (u_b)^2$ $T''_o = -0.06934 + 0.02914\ \Delta P$

RUN	POINT	u_b (m/s)	ΔP (N/m^2)	T_o'' (N/m^2)
4	6	0.435	94.60	2.68
	CR	0.49	120.05	3.42
5	3	0.167	13.95	0.34
	3_c	0.267	35.65	0.97
	4	0.320	51.20	1.42
	5	0.376	70.70	1.99
	6	0.450	101.25	2.88
	CR	0.525	137.80	3.94
6	3_b	0.271	36.70	1.00
	3_e	0.325	52.80	1.47
	4	0.362	65.50	1.84
	5	0.418	87.35	2.47
	6	0.449	100.80	2.86
	CR	0.541	146.35	4.19
7	3_b	0.102	5.20	0.08
	3_c	0.121	7.30	0.14
	4	0.150	11.25	0.26
	5	0.186	17.30	0.43
	6	0.244	29.75	0.80
	CR	0.301	45.30	1.25
8	3_a	0.113	6.40	0.12
	3_c	0.166	13.80	0.33

$\Delta P = 500\ (u_b)^2$ $\quad T''_o = -0.06934 + 0.02914\ \Delta P$

RUN	POINT	u_b (m/s)	ΔP (N/m^2)	T_o'' (N/m^2)
8	4	0.203	20.60	0.53
	5	0.240	28.80	0.77
	6	0.276	38.10	1.04
	CR	0.330	54.45	1.52
9	3	0.134	9.00	0.19
	3_b	0.201	20.20	0.52
	4	0.240	28.80	0.77
	5	0.272	37.00	1.01
	6	0.328	53.80	1.50
	CR	0.388	75.25	2.12
10	RP_b	0.126	7.95	0.16
	3	0.174	15.15	0.37
	3_b	0.232	26.90	0.71
	4	0.281	39.50	1.08
	5	0.311	48.35	1.34
	6	0.361	65.15	1.83
	6_b	0.396	78.40	2.21
	CR	0.438	95.90	2.72
11	RP_b	0.129	8.30	0.17
	3	0.195	19.00	0.48
	3_b	0.279	38.90	1.06
	4	0.316	49.95	1.38
	5	0.348	60.55	1.69

$\Delta P = 500\,(u_b)^2$ $\qquad$ $T''_o = -\,0.06934 + 0.02914\,\Delta P$

RUN	POINT	u_b (m/s)	ΔP (N/m^2)	T_o'' (N/m^2)
11	6	0.393	77.20	2.18
	CR	0.459	105.35	3.00
12	RP_b	0.139	9.65	0.21
	3	0.207	21.40	0.55
	4	0.338	57.10	1.59
	5	0.367	67.35	1.89
	6	0.403	81.20	2.29
	6_b	0.462	106.70	3.04
	CR	0.502	126.00	3.60
14	3_b	0.108	5.85	0.10
	4	0.168	14.10	0.34
	5	0.199	19.80	0.51
	5_b	0.220	24.20	0.63
	6	0.258	33.30	0.90
	CR	0.279	38.90	1.06
15	3_a	0.166	13.80	0.33
	3_c	0.189	17.85	0.45
	4	0.227	25.75	0.68
	5	0.268	35.90	0.98
	6	0.309	47.75	1.32
	CR	0.335	56.10	1.56
16	3	0.145	10.50	0.24

$\Delta P = 500 (u)^2$ $T_o = - 0.1326 + 0.02475 \Delta P$

RUN	POINT	u_b (m/s)	ΔP (N/m^2)	T_o'' (N/m^2)
16	3_b	0.205	21.00	0.54
	4	0.262	34.30	0.93
	5	0.315	49.60	1.37
	6	0.344	59.15	1.65
	CR	0.385	74.10	2.09
17	3	0.197	19.40	0.50
	3_b	0.264	34.85	0.94
	4	0.314	49.30	1.37
	5	0.350	61.25	1.71
	6	0.390	76.05	2.14
	CR	0.408	83.25	2.35
18	RP_b	0.158	12.50	0.29
	3	0.238	28.30	0.75
	4	0.316	49.95	1.38
	5	0.365	66.60	1.87
	6	0.397	78.80	2.22
	6_b	0.424	89.90	2.55
	CR	0.454	103.05	2.93
19	RP_b	0.174	15.15	0.37
	3	0.253	32.00	0.86
	4	0.343	58.80	1.64
	5	0.381	72.60	2.04

$\Delta P = 500\ (u_b)^2$ $\tau''_o = -\ 0.06934 + 0.02914\ \Delta P$

RUN	POINT	u_b (m/s)	ΔP (N/m^2)	τ_o'' (N/m^2)
19	6	0.432	93.30	2.65
	CR	0.510	130.05	3.72
22	3	0.113	6.40	0.12
	4	0.173	14.95	0.37
	5	0.200	20.00	0.51
	6	0.233	27.15	0.72
	CR	0.266	35.40	0.96
23	RP_b	0.118	6.95	0.13
	3	0.174	15.15	0.37
	4	0.217	23.55	0.62
	5	0.239	28.55	0.76
	6	0.297	44.10	1.21
	CR	0.334	55.80	1.55
24	RP_b	0.148	10.95	0.25
	3	0.202	20.40	0.52
	4	0.244	29.75	0.80
	5	0.274	37.55	1.02
	6	0.306	46.80	1.29
	6_b	0.335	56.10	1.56
	CR	0.378	71.45	2.01
25	RP_b	0.176	15.50	0.38
	3	0.226	25.55	0.67

$\Delta P = 500\ (u_b)^2$ $\quad T_o'' = -0.06934 + 0.02914\ \Delta P$

RUN	POINT	u_b (m/s)	ΔP (N/m^2)	T_o'' (N/m^2)
25	4	0.270	36.45	0.99
	5	0.300	45.00	1.24
	6	0.333	55.45	1.54
	6_b	0.354	62.65	1.75
	CR	0.397	78.80	2.22
26	RP_b	0.206	21.20	0.55
	3	0.256	32.75	0.88
	4	0.280	39.20	1.07
	5	0.324	52.50	1.46
	6	0.365	66.60	1.87
	6_b	0.381	72.60	2.04
	CR	0.441	97.25	2.76
27	RP_b	0.230	26.45	0.70
	3	0.276	38.10	1.04
	4	0.305	46.50	1.28
	5	0.342	58.50	1.63
	6	0.373	69.55	1.95
	6_b	0.399	79.60	2.25
	CR	0.462	106.70	3.04

CONVERTING POINT VELOCITY TO GRAIN SHEAR STRESS VALUES.

The following equations will be used for roughness S1 :

$\Delta P = 500\ (u_b)^2 \qquad T''_o = -\ 0.02609 + 0.02006\ \Delta P$

RUN	POINT	u_b (m/s)	ΔP (N/m^2)	T_o'' (N/m^2)
30	3_b	0.115	6.60	0.11
	4	0.175	15.30	0.28
	4_b	0.196	19.20	0.36
	5	0.238	28.30	0.54
	6	0.298	44.40	0.86
	CR	0.335	56.10	1.10
31	3	0.114	6.50	0.10
	3_b	0.190	18.05	0.34
	4	0.244	29.75	0.57
	5	0.300	45.00	0.87
	6	0.335	56.10	1.10
	CR	0.383	73.35	1.44
32	3	0.151	11.40	0.20
	3_b	0.242	29.30	0.56
	4	0.285	40.60	0.79
	5	0.342	58.50	1.14
	6	0.401	80.40	1.58
	CR	0.472	111.40	2.20
33	3	0.176	15.50	0.28
	3_b	0.266	35.40	0.68
	4	0.303	45.90	0.89
	5	0.368	67.70	1.33

$\Delta P = 500 (u_b)^2$ $\quad\quad$ $T''_o = -0.02609 + 0.02006\,\Delta P$

RUN	POINT	u_b (m/s)	ΔP (N/m^2)	T_0'' (N/m^2)
33	6	0.408	83.25	1.64
	6_b	0.445	99.00	1.95
	CR	0.496	123.00	2.43
34	RP_b	0.173	14.95	0.27
	3	0.233	27.15	0.52
	3_b	0.301	45.30	0.88
	4	0.342	58.50	1.14
	5	0.393	77.20	1.52
	6	0.446	99.45	1.96
	6_b	0.483	116.65	2.31
	CR	0.520	135.20	2.68
35	RP_b	0.203	20.60	0.39
	3	0.272	37.00	0.71
	4	0.370	68.45	1.34
	5	0.420	88.20	1.74
	6	0.466	108.60	2.15
	6_b	0.509	129.55	2.57
	CR	0.549	150.70	2.99

CONVERTING POINT VELOCITY TO GRAIN SHEAR STRESS VALUES.

The following equations will be used for roughness S2 :

$$\Delta P = 500\,(u_b)^2 \qquad T_o'' = 0.01517 + 0.0228\,\Delta P$$

RUN	POINT	u_b (m/s)	ΔP (N/m^2)	T_o'' (N/m^2)
38	3_b	0.120	7.20	0.18
	4	0.190	18.05	0.43
	5	0.223	24.85	0.58
	6	0.266	35.40	0.82
	CR	0.296	43.80	1.01
39	3_b	0.148	10.95	0.26
	4	0.232	26.90	0.63
	5	0.283	40.05	0.93
	6	0.320	51.20	1.18
	CR	0.356	63.35	1.46
40	3	0.121	7.30	0.18
	3_b	0.196	19.20	0.45
	4	0.268	35.90	0.83
	5	0.314	49.30	1.14
	6	0.370	68.45	1.58
	CR	0.390	76.05	1.75
41	3	0.166	13.80	0.33
	3_b	0.244	29.75	0.69
	4	0.305	46.50	1.08
	5	0.359	64.45	1.48
	6	0.385	74.10	1.70
	6_b	0.399	79.60	1.83

$\Delta P = 500\,(u_b)^2$ $\qquad T''_o = 0.01517 + 0.0228\,\Delta P$

RUN	POINT	u_b (m/s)	ΔP (N/m^2)	T_0'' (N/m^2)
41	CR	0.440	96.80	2.22
42	RP_b	0.144	10.35	0.25
	3	0.207	21.40	0.50
	3_b	0.287	41.20	0.95
	4	0.335	56.10	1.29
	5	0.355	63.00	1.45
	6	0.394	77.60	1.78
	6_b	0.412	84.85	1.95
	CR	0.431	92.90	2.13
43	RP_b	0.170	14.45	0.34
	3	0.235	27.60	0.64
	3_b	0.297	44.10	1.02
	4	0.369	68.10	1.57
	5	0.379	71.80	1.65
	6	0.436	95.05	2.18
	6_b	0.473	111.85	2.57
	CR	0.494	122.00	2.80

CONVERTING POINT VELOCITY TO GRAIN SHEAR STRESS VALUES.

The following equations will be used for roughness S4 :

$\Delta P = 500\,(u_b)^2$ $\qquad T''_o = -\,0.01751 + 0.04628\,\Delta P$

RUN	POINT	u_b (m/s)	ΔP (N/m^2)	T_o'' (N/m^2)
46	4	0.125	7.80	0.34
	5	0.201	20.20	0.92
	6	0.246	30.25	1.38
	CR	0.302	45.60	2.09
47	3_b	0.117	6.85	0.30
	4	0.166	13.80	0.62
	5	0.213	22.70	1.03
	6	0.271	36.70	1.68
	CR	0.340	57.80	2.65
48	3_b	0.145	10.50	0.47
	4	0.202	20.40	0.93
	5	0.240	28.80	1.31
	6	0.321	51.50	2.36
	CR	0.385	74.10	3.41
49	3	0.127	8.05	0.35
	3_b	0.169	14.30	0.64
	4	0.223	24.85	1.13
	5	0.282	39.75	1.82
	6	0.348	60.55	2.78
	6_b	0.383	73.35	3.37
	CR	0.417	86.95	4.00
50	RP_b	0.116	6.75	0.29

$\Delta P = 500\ (u_b)^2$ $\quad T_o'' = -\ 0.01751 + 0.04628\ \Delta P$

RUN	POINT	u_b (m/s)	ΔP (N/m^2)	T_o'' (N/m^2)
50	3	0.148	10.95	0.49
	3_b	0.200	20.00	0.91
	4	0.252	31.75	1.45
	5	0.313	49.00	2.25
	6	0.381	72.60	3.34
	6_b	0.414	85.70	3.94
	CR	0.451	101.70	4.68
51	RP_b	0.129	8.30	0.37
	3	0.172	14.80	0.67
	3_b	0.236	27.85	1.27
	4	0.298	44.40	2.03
	5	0.348	60.55	2.78
	6	0.418	87.35	4.02
	6_b	0.445	99.00	4.56
	CR	0.481	115.70	5.33

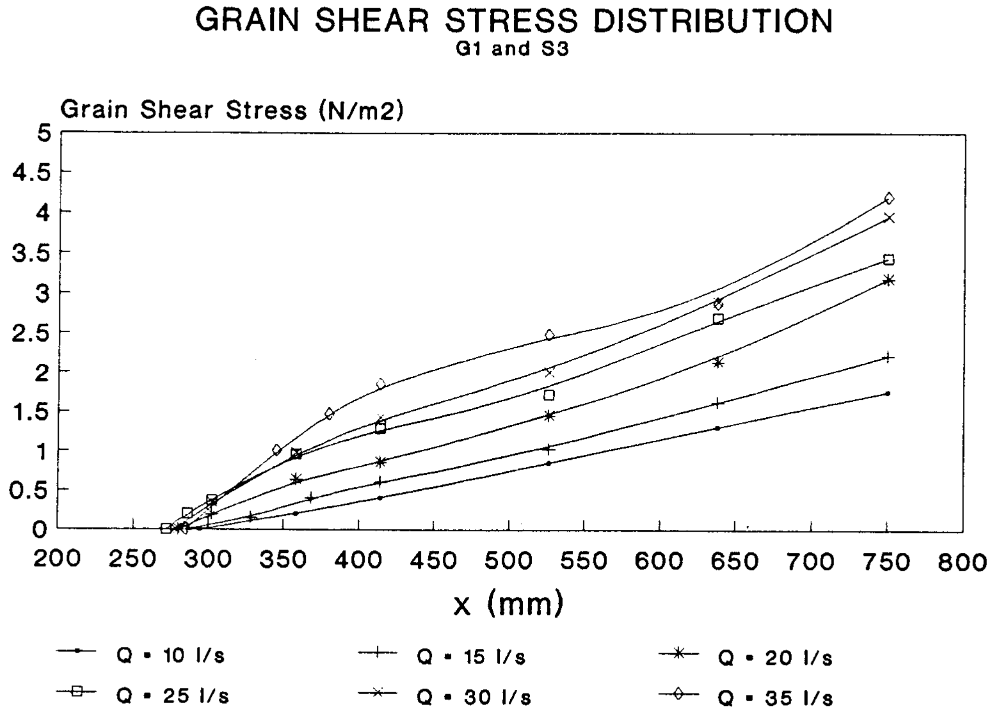
GRAIN SHEAR STRESS DISTRIBUTION
G1 and S3
Grain Shear Stress (N/m2)
5
4.5
4
3.5
3
2.5
2
1.5
1
0.5
0
200
250
300
350
400
450
500
550
600
650
700
750
800
x (mm)
Q = 10 l/s
Q = 15 l/s
Q = 20 l/s
Q = 25 l/s
Q = 30 l/s
Q = 35 l/s

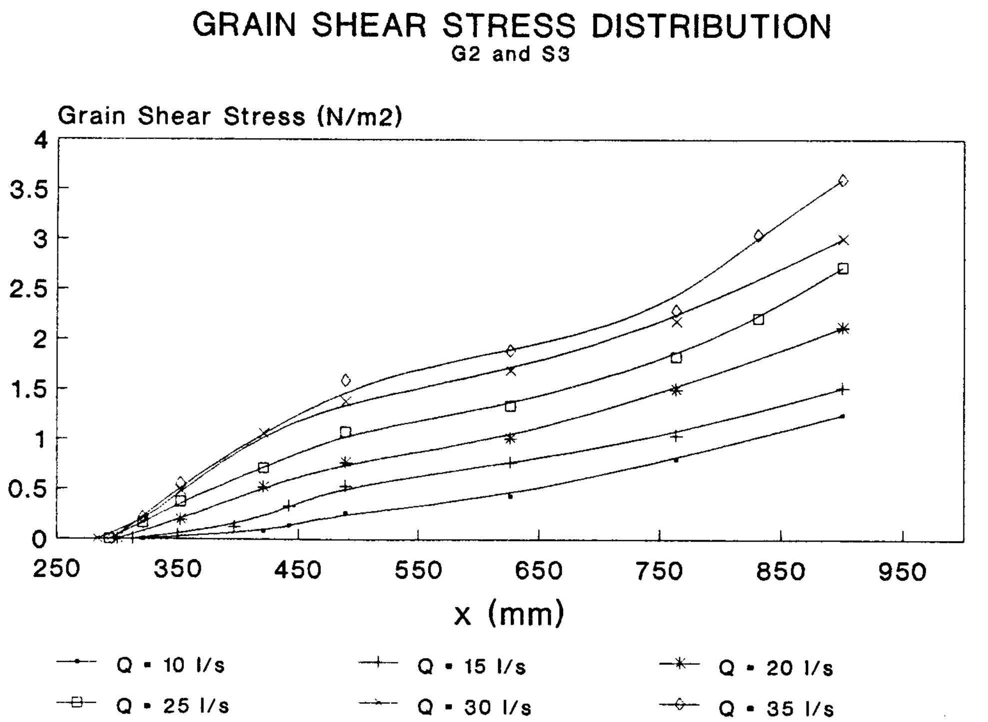
GRAIN SHEAR STRESS DISTRIBUTION
G2 and S3
Grain Shear Stress (N/m2)
4
3.5
3
2.5
2
1.5
1
0.5
0
250
350
450
550
650
750
850
950
x (mm)
Q = 10 l/s
Q = 15 l/s
Q = 20 l/s
Q = 25 l/s
Q = 30 l/s
Q = 35 l/s

GRAIN SHEAR STRESS DISTRIBUTION

G3 and S3

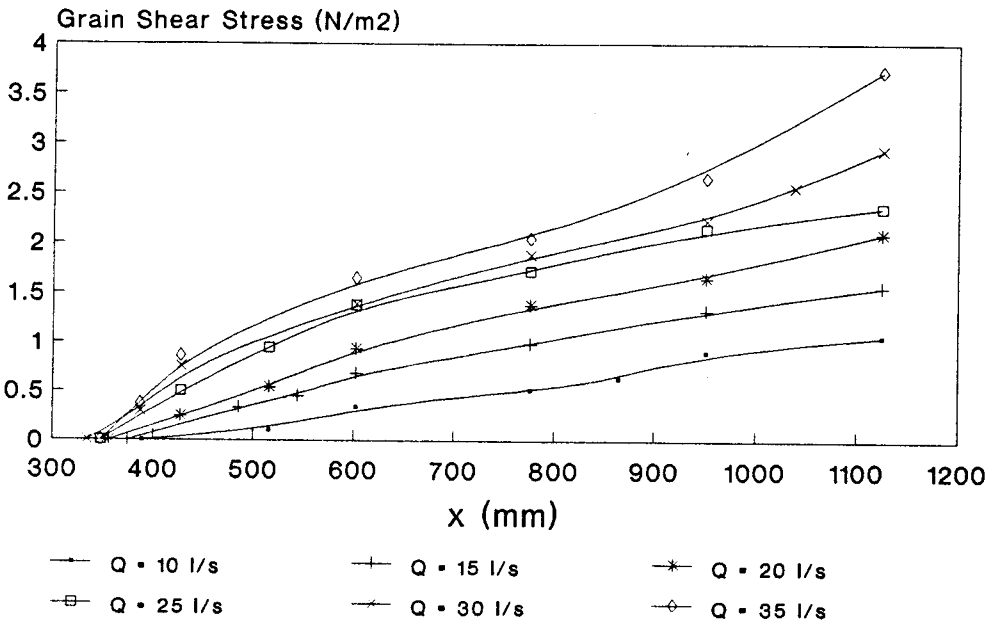

GRAIN SHEAR STRESS DISTRIBUTION

G4 and S3

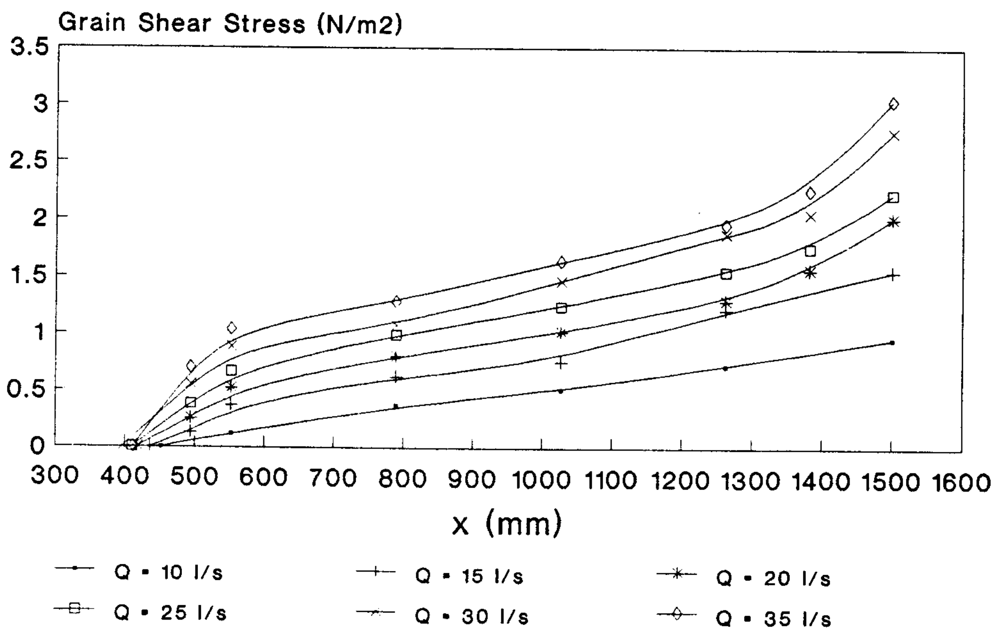

GRAIN SHEAR STRESS DISTRIBUTION

G2 and S1

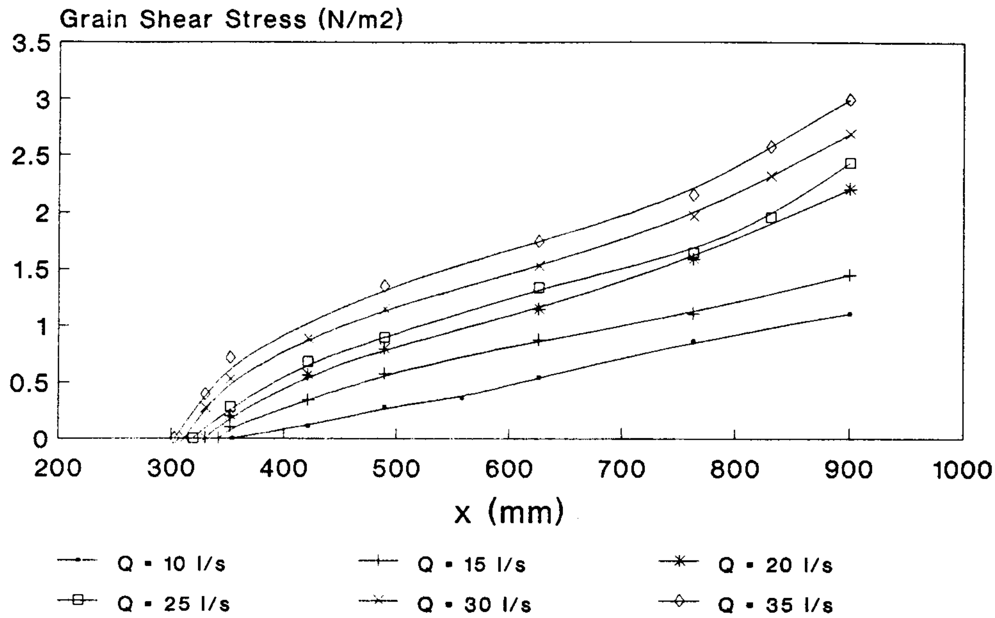

GRAIN SHEAR STRESS DISTRIBUTION

G2 and S2

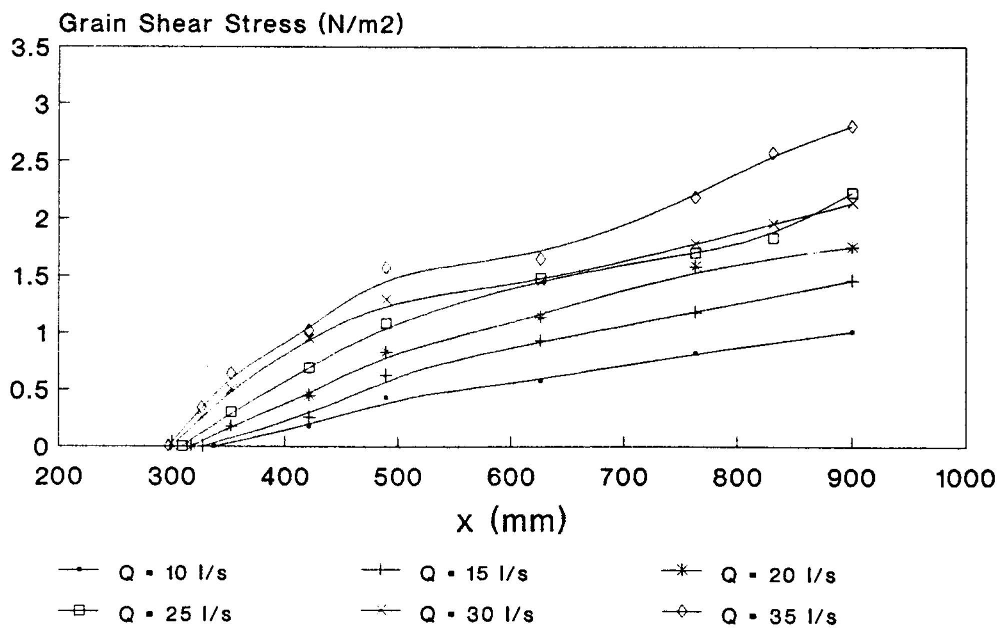

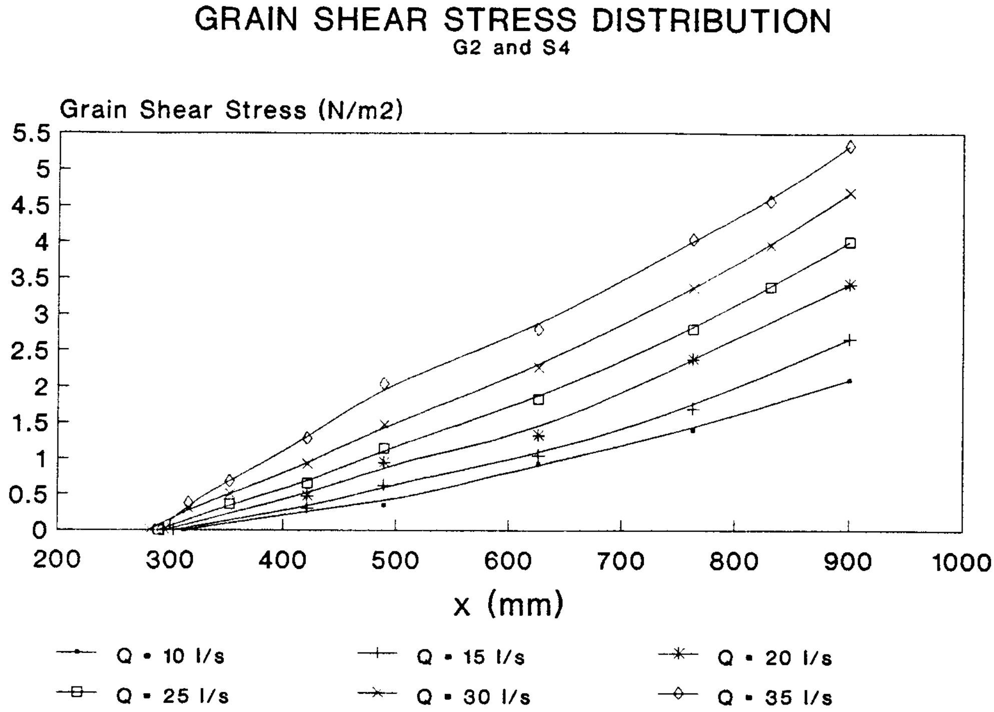
GRAIN SHEAR STRESS DISTRIBUTION
G2 and S4
Grain Shear Stress (N/m2)
5.5
5
4.5
4
3.5
3
2.5
2
1.5
1
0.5
0
200
300
400
500
600
700
800
900
1000
x (mm)
Q • 10 l/s
Q • 15 l/s
Q • 20 l/s
Q • 25 l/s
Q • 30 l/s
Q • 35 l/s

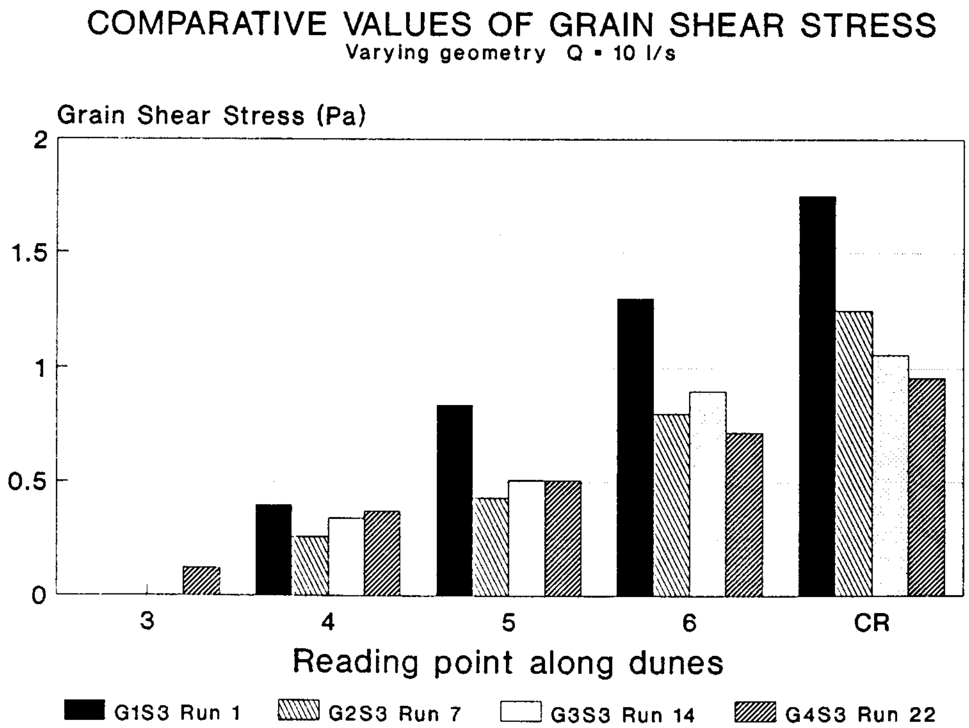
COMPARATIVE VALUES OF GRAIN SHEAR STRESS
Varying geometry Q • 10 l/s
Grain Shear Stress (Pa)
2
1.5
1
0.5
0
3
4
5
6
CR
Reading point along dunes
G1S3 Run 1
G2S3 Run 7
G3S3 Run 14
G4S3 Run 22

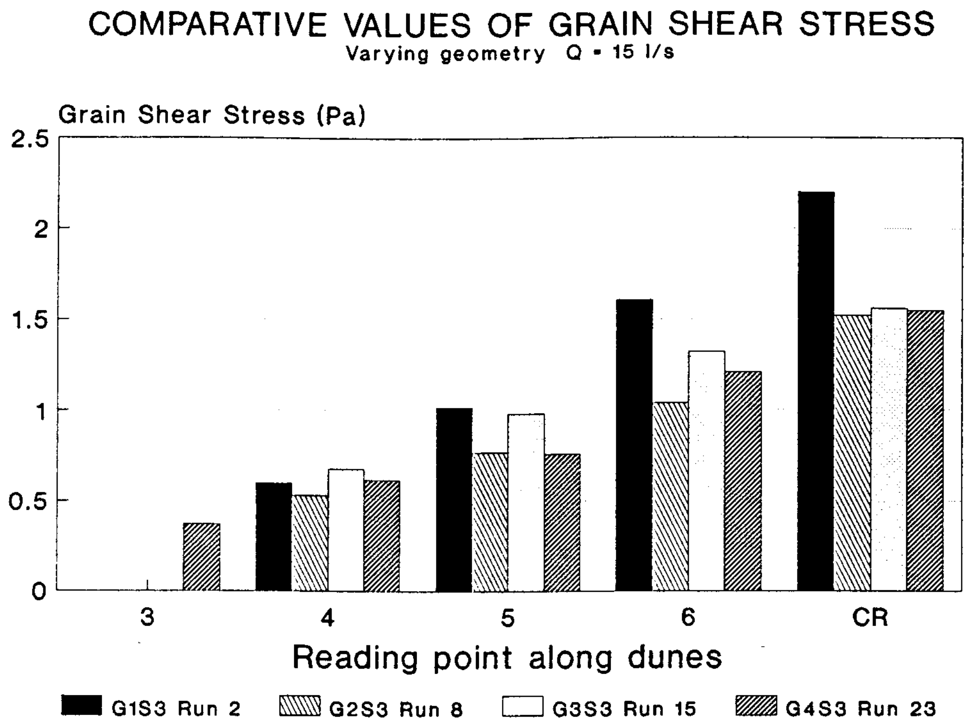
COMPARATIVE VALUES OF GRAIN SHEAR STRESS
Varying geometry Q = 15 l/s
Grain Shear Stress (Pa)
2.5
2
1.5
1
0.5
0
3
4
5
6
CR
Reading point along dunes
G1S3 Run 2
G2S3 Run 8
G3S3 Run 15
G4S3 Run 23

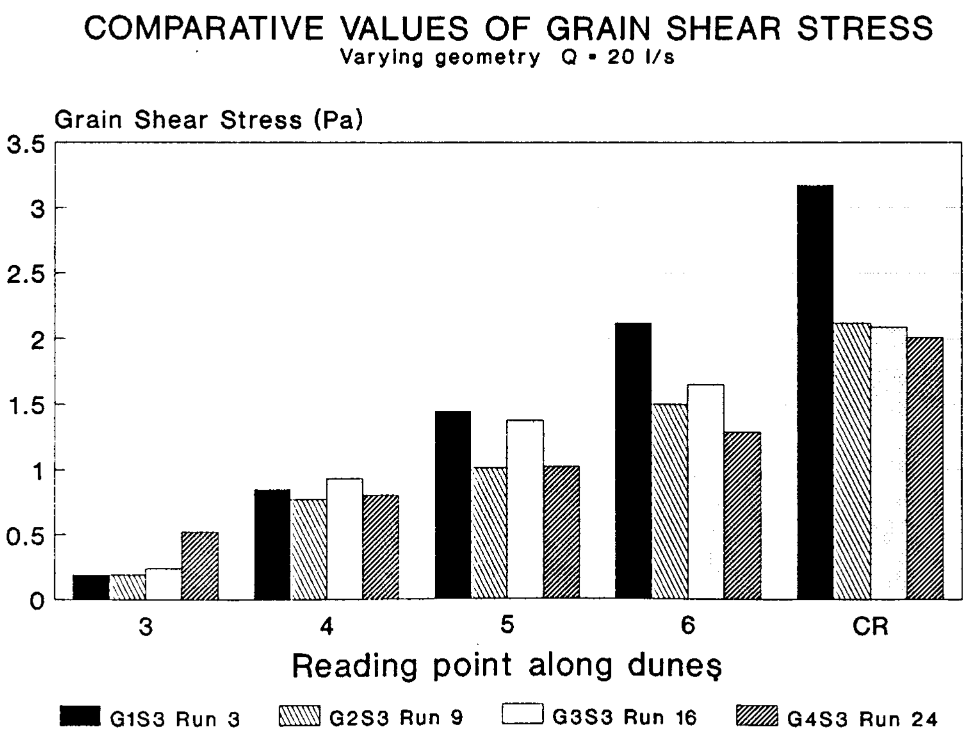
COMPARATIVE VALUES OF GRAIN SHEAR STRESS
Varying geometry Q = 20 l/s
Grain Shear Stress (Pa)
3.5
3
2.5
2
1.5
1
0.5
0
3
4
5
6
CR
Reading point along dunes
G1S3 Run 3
G2S3 Run 9
G3S3 Run 16
G4S3 Run 24

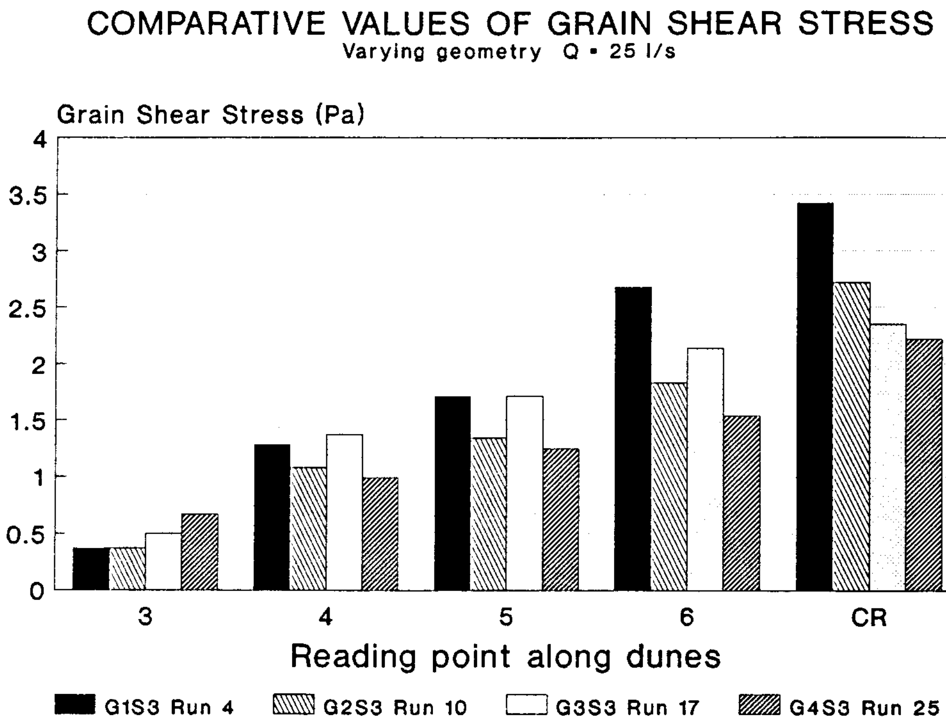

COMPARATIVE VALUES OF GRAIN SHEAR STRESS
Varying geometry Q = 25 l/s
Grain Shear Stress (Pa)
4
3.5
3
2.5
2
1.5
1
0.5
0
3
4
5
6
CR
Reading point along dunes
G1S3 Run 4
G2S3 Run 10
G3S3 Run 17
G4S3 Run 25

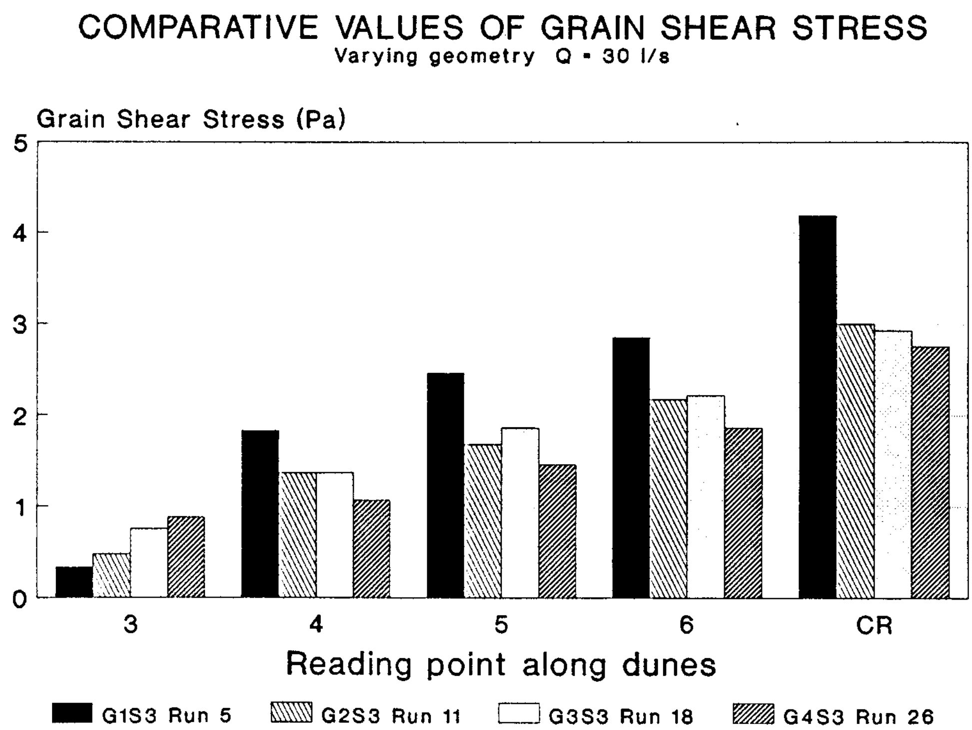

COMPARATIVE VALUES OF GRAIN SHEAR STRESS
Varying geometry Q = 30 l/s
Grain Shear Stress (Pa)
5
4
3
2
1
0
3
4
5
6
CR
Reading point along dunes
G1S3 Run 5
G2S3 Run 11
G3S3 Run 18
G4S3 Run 26

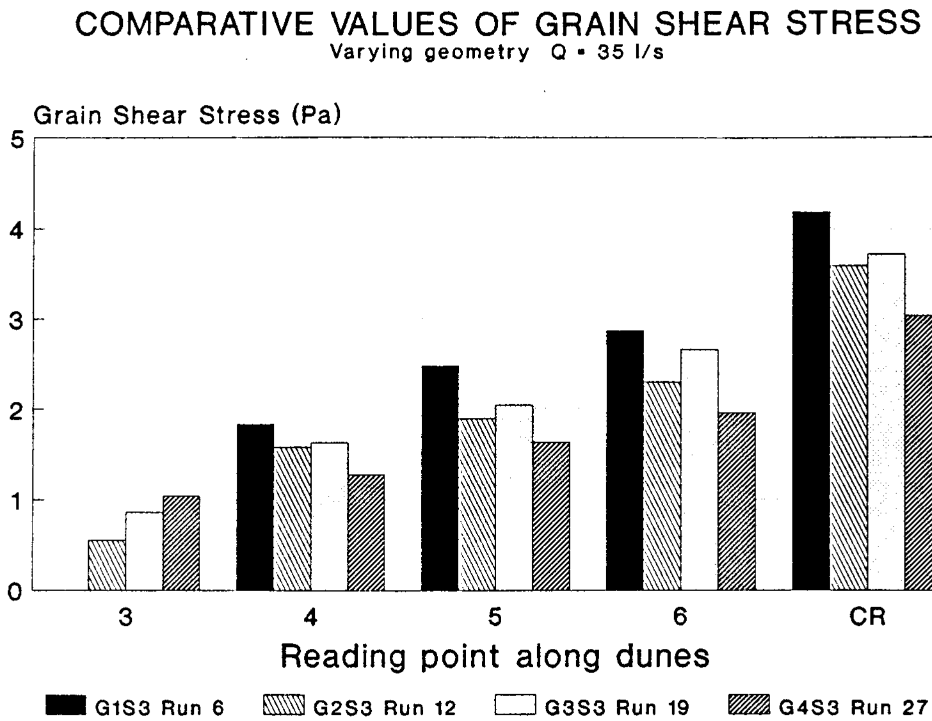
COMPARATIVE VALUES OF GRAIN SHEAR STRESS
Varying geometry Q • 35 l/s
Grain Shear Stress (Pa)
5
4
3
2
1
0
3
4
5
6
CR
Reading point along dunes
G1S3 Run 6
G2S3 Run 12
G3S3 Run 19
G4S3 Run 27

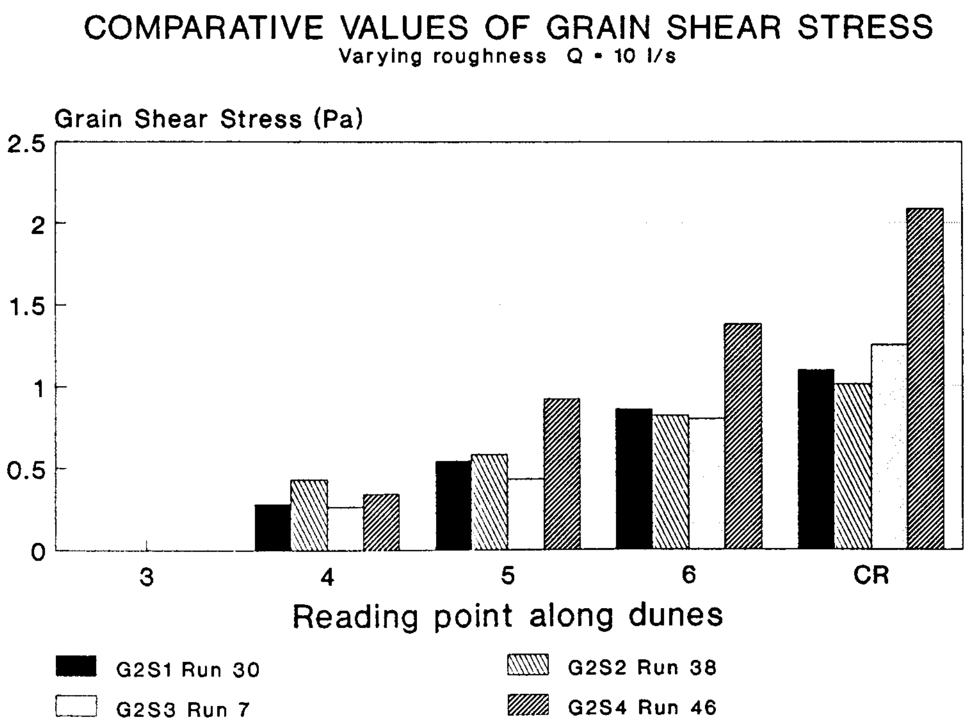
COMPARATIVE VALUES OF GRAIN SHEAR STRESS
Varying roughness Q • 10 l/s
Grain Shear Stress (Pa)
2.5
2
1.5
1
0.5
0
3
4
5
6
CR
Reading point along dunes
G2S1 Run 30
G2S2 Run 38
G2S3 Run 7
G2S4 Run 46

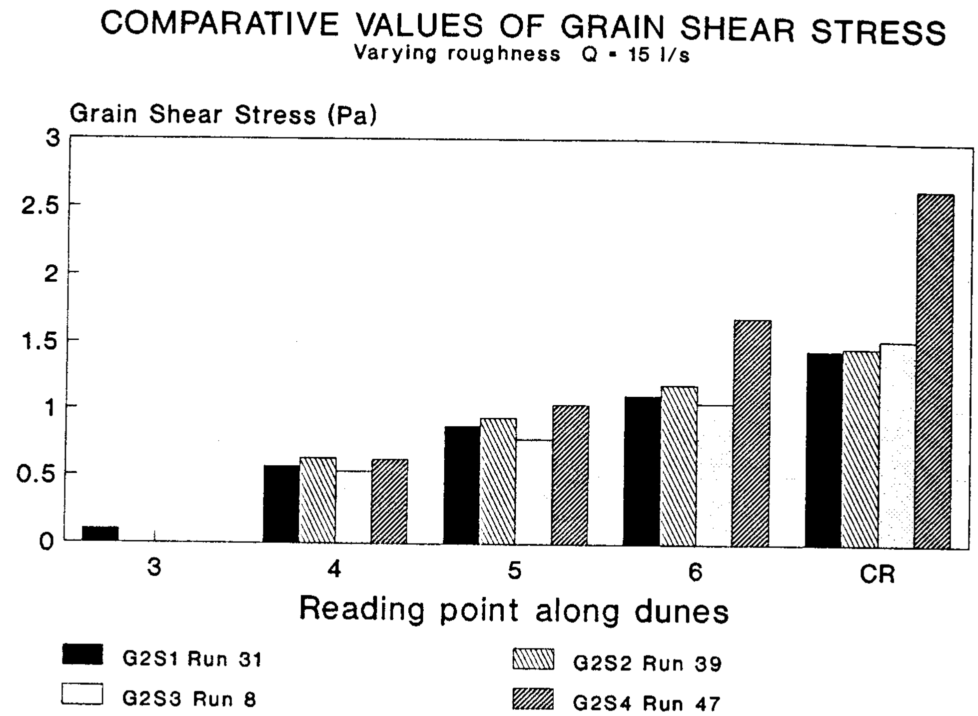
COMPARATIVE VALUES OF GRAIN SHEAR STRESS
Varying roughness Q = 15 l/s
Grain Shear Stress (Pa)
3
2.5
2
1.5
1
0.5
0
3
4
5
6
CR
Reading point along dunes
G2S1 Run 31
G2S3 Run 8
G2S2 Run 39
G2S4 Run 47

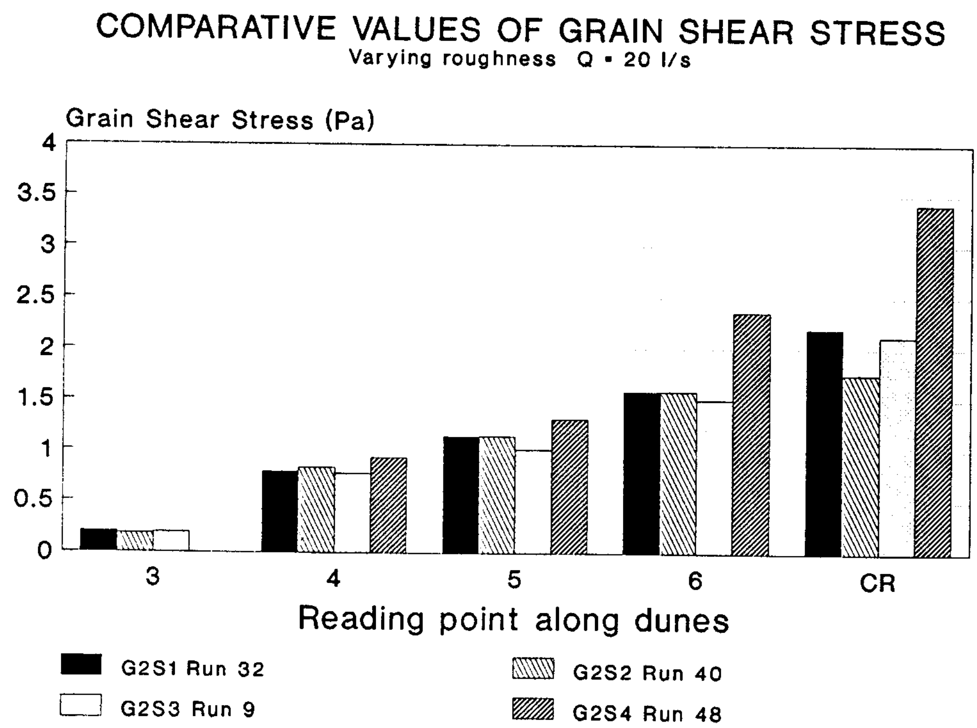
COMPARATIVE VALUES OF GRAIN SHEAR STRESS
Varying roughness Q = 20 l/s
Grain Shear Stress (Pa)
4
3.5
3
2.5
2
1.5
1
0.5
0
3
4
5
6
CR
Reading point along dunes
G2S1 Run 32
G2S3 Run 9
G2S2 Run 40
G2S4 Run 48

COMPARATIVE VALUES OF GRAIN SHEAR STRESS

Varying roughness Q = 25 l/s

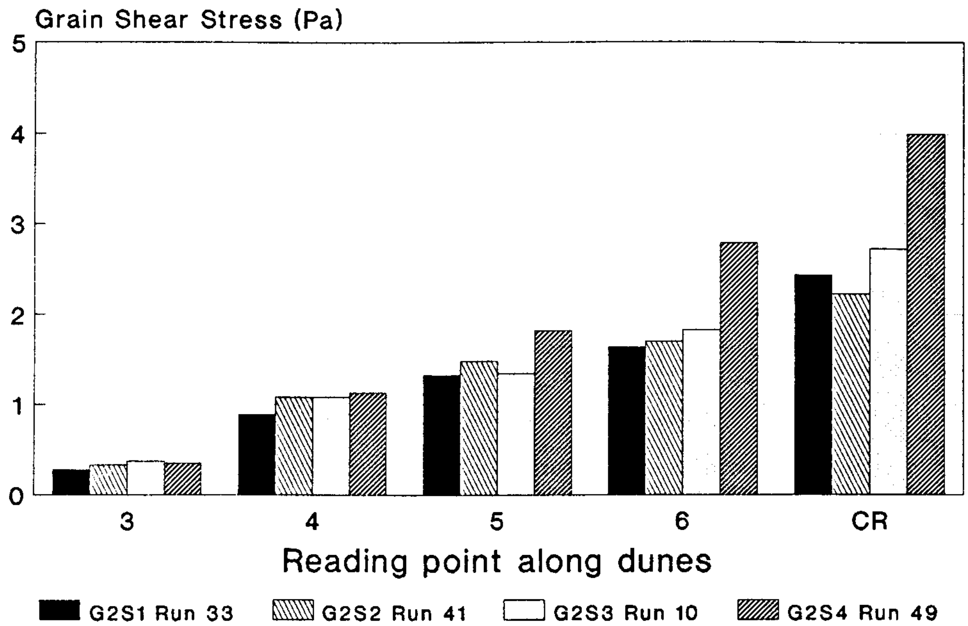

COMPARATIVE VALUES OF GRAIN SHEAR STRESS

Varying roughness Q = 30 l/s

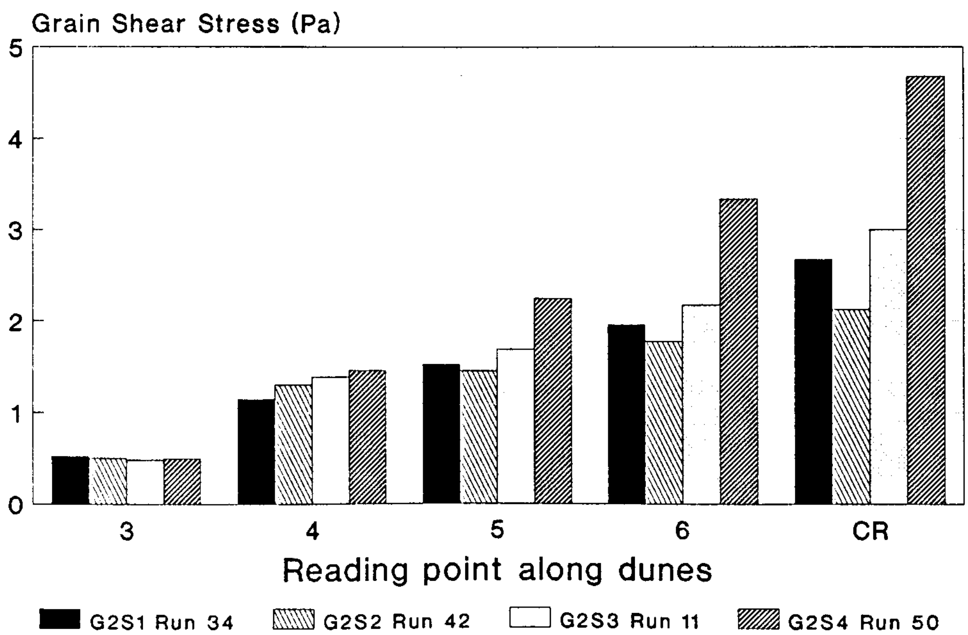

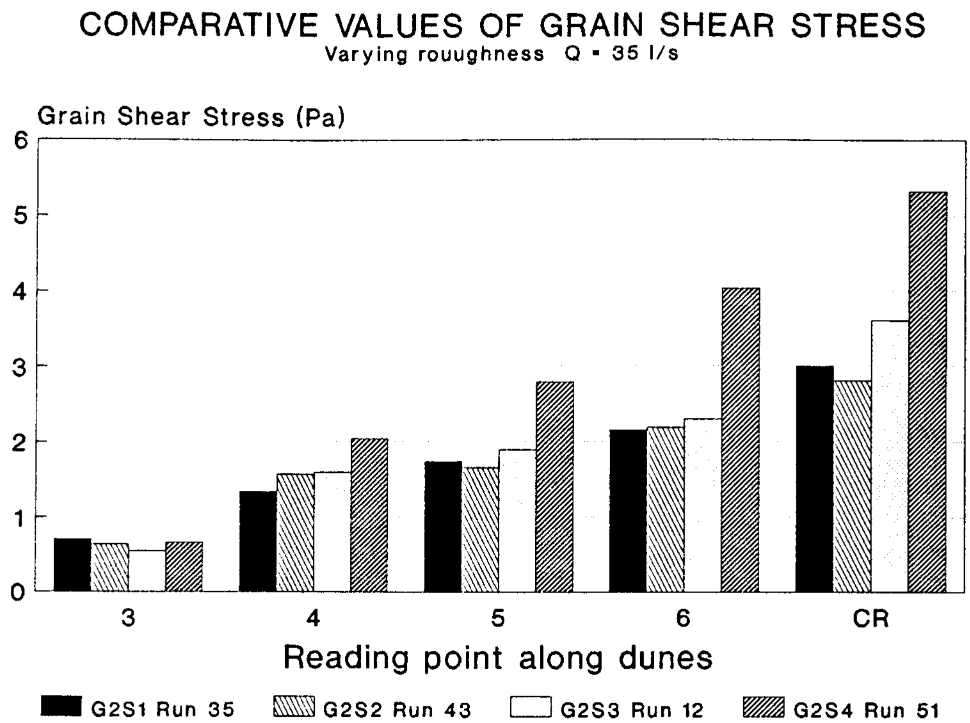
COMPARATIVE VALUES OF GRAIN SHEAR STRESS
Varying rouughness Q = 35 l/s
Grain Shear Stress (Pa)
0
1
2
3
4
5
6
3
4
5
6
CR
Reading point along dunes
G2S1 Run 35
G2S2 Run 43
G2S3 Run 12
G2S4 Run 51

REFERENCES

Ackers, P. , White, W. (1973) " Sediment Transport: New Approach and Analysis " , Journal of the Hydraulics Division , ASCE , Vol. 99, No. HY11 , pp. 2041-2060.

Cardoso, A.H. , Graf, W.H. , Gust, G. (1989) " Spatially Accelerating Flow in Smooth Open Channel " , Proceedings of Technical Session A : Turbulence in Hydraulics - International Association for Hydraulic Research , XXIII Congress : Hydraulics and the Environment , Ottawa, Canada.

Chang, F.F.M. (1970) " Ripple Concentration and Friction Factor " , Journal of the Hydraulics Division , ASCE , Vol. 96 , No. HY2 , pp. 417-430.

Einstein, H.A. (1950) " The Bed-Load Function for Sediment Transportation in Open Channel Flows " , Technical Bulletin No. 1026 , U.S. Department of Agriculture , Washington, D.C.

Einstein, H.A. , Barbarossa, N.L. (1952) " River Channel Roughness " , Transactions ASCE , 117 , pp. 1121-1143.

Engel, P. (1981) " Length of Flow Separation Over Dunes " , Journal of the Hydraulics Division , ASCE , Vol. 107 , No. HY10 , pp. 1133-1143.

Engel, P. , Lau, Y.L. (1980) " Friction Factor for Two-Dimensional Dune Roughness " , Journal of Hydraulic Research , I.A.H.R. , Vol. 18 , No. 3.

Engelund, F. , Fredsøe, J. (1982) " Sediment Ripples and Dunes ", Annual Review of Fluid Mechanics , Vol. 14, pp. 13-37.

Engelund, F. , Hansen, E. (1967) " A Monograph on Sediment Transport in Alluvial Streams ", Teknisk Forlag, Copenhagen , Denmark.

Etheridge, D.U. , Kemp, P.H. (1979) " Velocity Measurements Downstream of a Rearward Facing Step with Reference to Bed Instability " , Journal of Hydraulic Research , I.A.H.R. , Vol. 17, No. 2.

Fehlman, H.M. (1985) " Resistance Components and Velocity Distributions of Open Channel Flows Over Bedforms " , Thesis presented to Colorado State University , at Fort Collins , Colorado, in partial fulfilment of the requirements for the degree of Master of Science.

Fredsøe, J. (1982) " Shape and Dimensions of Stationary Dunes in Rivers " , Journal of the Hydraulics Division , ASCE , Vol. 108 , No. HY8 , pp. 932-947.

Ghosh, S. , Jena, S.B. (1971) " Boundary Shear Distribution in Open Channel Compound " , Proceedings of the Institution of Civil Engineers , London , Vol. 89 , pp. 417-430.

Graf, W.H. (1989) " Flow Resistance Over a Gravel Bed ; Its Consequence on Initial Sediment Movement " , Proceedings of the International Workshop on Fluvial Hydraulics of Mountain Regions , Trento , Italy.

Haque, M.I. , Mahmood, K. (1985) " Geometry of Ripples and Dunes " , Journal of Hydraulic Engineering , ASCE , Vol. 111 , No. 1 , pp. 48-63.

Haque, M.I. , Mahmood, K. (1986) " Analytical Study on Steepness of Ripples and Dunes " , Journal of Hydraulic Engineering , ASCE , Vol. 112 , No. 3 , pp. 220-236.

Head, M.R. , Rechenberg, I. (1972) " The Preston Tube as a Means of Measuring Skin Friction " , Journal of Fluid Mechanics , Vol. 14 , pp. 1-17.

Hey, R.D. (1979) " Flow Resistance in Gravel-Bed Rivers " , Journal of the Hydraulics Division , ASCE , Vol. 105 , No. HY4 , pp. 365-379.

Hinze, J.O. (1975) " Turbulence " , McGraw Hill Book Company, New York.

Hollingshead, A.B. , Rajaratnam, N. (1980) " A Calibration Chart for the Preston Tube " , Journal of Hydraulic Research , I.A.H.R. , Vol. 18 , No. 4 , pp. 313-326.

Hwang, L-S. , Laursen, E.M. (1963) " Shear Measurement Technique for Rough Surfaces " , Journal of the Hydraulics Division , ASCE , Vol. 89 , No. HY2 , pp. 19-37.

Hwang, L-S. , Laursen, E.M. (1964) " Shear Measurement Technique for Rough Surfaces " , Closure to Discussion , Journal of the Hydraulics Division , ASCE , Vol. 90 , No. HY4 , pp. 221-222.

Ippen, A.T. , Drinker, P.A. , Jobin, W.R. , Noutsopoulos, G.K. (1960) " The Distribution of Boundary Shear Stress in Curved Open Channel " , Hydrodynamics Laboratory Report 43 , Massachussets Institute of Technology.

Jackson, R.G. (1976) " Sedimentological and Fluid Dynamic Implications of the Turbulent Bursting Phenomenon in Geophysical Flows " , Journal of Fluid Mechanics , Vol. 77 , pp. 531-560.

Jonys, C.K. (1973) " An Experimental Study of Bed Form Mechanics " , Thesis presented to the University of Alberta , at Edmonton , Alberta , in partial fulfilment of the requirements for the degree of Doctor of Philosophy.

Kamphuis, J.W. (1974) " Determination of Sand Roughness for Fixed Beds " , Journal of Hydraulic Research , I.A.H.R. , Vol. 12 , No. 2, pp. 193-203.

Karahan, M.E. , Peterson, A.W. (1980) " Visualization of Separation Over Sand Waves " , Journal of the Hydraulics Division , ASCE , Vol. 106 , No. HY8 , pp. 1345-1352.

Kennedy, J.F. (1969) " The Formation of Sediment Ripples, Dunes and Antidunes " , Annual Review of Fluid Mechanics , Vol. 1 , pp. 147-168.

Laursen, E.M. , Adams, J.R , Hwang, L.S. , Chen, C.L. (1962) " Pressure and Shear Distribution on Schematic Dunes " , Technical Report No. 2 , Civil Engineering Department , Michigan State University , East Lansing , Michigan.

Leeder, M.R. (1983) " On the Interaction Between Turbulent Flow , Sediment Transport and Bedform Mechanics in Channelized Flows " , Special Publications , International Association of Sedimentology , Vol. 6 , pp. 5-18.

Mahmood, K. (1971) " Flow in Sand Bed Channels ", Water Management Technical Report, No. 11 , Colorado State University , Fort Collins , Colorado.

McLean, S.R. (1976) " Mechanics of the Turbulent Boundary Layer over Sand Waves in the Columbia River " , Thesis presented to the University of Washington , at Seattle , in partial fulfilment of the requirements for the degree of Doctor of Philosophy.

Mendoza-Cabrales, C. (1987) " Refined Modelling of Shallow , Turbulent Flow Over Dunes " , Thesis presented to Colorado State University , at Fort Collins , Colorado , in partial fulfilment of the requirements for the degree of Doctor of Philosophy.

Muller, A. , Gyr, A. (1982) " Visualization of the Mixing Layer Behind Dunes " , Proceedings of Euromech 156 , Conference on the Mechanics of Sediment Transport, Istanbul , Turkey , pp. 41-45.

Nezu, L. , Rodi, W. (1986) " Open Channel Flow Measurements with a Laser Doppler Anemometer " , Journal of Hydraulic Engineering , ASCE , Vol. 112 , No. HY5 , pp. 335-355.

Nikuradse, J. (1950) " Laws of Flow in Rough Pipes " , Translated as Technical Memorandum 1292 , National Advisory Committee for Aeronautics , Washington , D.C.

Patel, V.C. (1965) " Calibration of the Preston Tube and Limitations on its Use in Pressure Gradients " , Journal of Fluid Mechanics , Vol. 23 , Part 1 , pp. 185-208.

Pillai, C.R.S. (1979) " Effective Depth in Channels Having Bed Undulations " , Journal of the Hydraulics Division , ASCE , Vol. 105, No. HY1 , pp. 67-81.

Preston, J.H. (1954) " The Determination of Turbulent Skin Friction by Means of Pitot Tubes " , Journal of the Royal Aeronautical Society , London, England , Vol. 58 , pp. 109-121.

Raudkivi, A.J. (1963) " Study of Sediment Ripple Formation " , Journal of the Hydraulics Division , ASCE, Vol. 89 , No. HY6 , pp. 15-33.

Raudkivi, A.J. (1966) " Bed Forms in Alluvial Channels " , Journal of Fluid Mechanics , Vol. 26 , pp. 507.

Raudkivi, A.J. (1976) " Loose Boundary Hydraulics " , 2nd Edition, Pergamon Press (Inc.) , Elmsford , New York.

Rifai, M.F. , Smith, K.V.H. (1971) " Flow Over Triangular Elements Simulating Dunes " , Journal of the Hydraulics Division , ASCE , Vol. 97 , No. HY7 , pp. 963-976.

Shen, H.W. , Fehlman, H.M. and Mendoza, C. (1990) " Bed Form Resistances in Open Channel Flows " , Journal of Hydraulic Engineering , ASCE , Vol. 116 No. 6 , pp. 799-815.

Simons, D.B. and Richardson, E.V. (1966) " Resistance to Flow in Alluvial Channels " , U.S. Geological Survey, Professional Paper 422-J , Washington, D.C.

Tani, L. (1957) " Experimental Investigation of Flow Separation over a Step " , Symposium Freiburg / BR , International Union of Theoretical and Applied Mechanics, Boundary Layer Research , pp. 26-29.

Vanoni, V.A. , Brooks, N.H. (1957) " Laboratory Studies of the Roughness and Suspended Load of Alluvial Streams " , Report E-68 , Sedimentation Laboratory , California Institute of Technology , Pasadena , California.

Vanoni, V.A. , Hwang, L.S. (1967) " Relation Between Bed Forms and Friction in Streams " , Journal of the Hydraulic Division , ASCE , Vol. 93 , No. HY3 , p. 121.

van Rijn, L.C. (1982) " Equivalent Roughness of Alluvial Bed " , Technical Note , Journal of the Hydraulic Division , ASCE , Vol. 108 , No. HY10, pp. 1215-1218.

van Rijn, L.C. (1984-a) " Sediment Transport Part I : Bed Load Transport " , Journal of Hydraulic Engineering, ASCE , Vol. 110 , No. 10 , pp. 1431-1456.

van Rijn, L.C. (1984-b) " Sediment Transport , Part III : Bed Forms and Alluvial Roughness " , Journal of Hydraulic Engineering , ASCE , Vol. 110 , No. 12 , pp. 1733-1754.

Vittal, N. , Ranga Raju, K.G. , Garde, R.J. (1977) " Resistance of Two Dimensional Triangular Roughness " , Journal of Hydraulic Research , I.A.H.R. , Vol. 15 , No. 1 , pp. 19-36.

Walker, G.R. (1961) " A Study of Two-Dimensional Flow of Turbulent Field Past a Step " , Thesis presented to the University of Auckland , at Auckland , New Zealand , in partial fulfilment of the requirements for the degree of Master of Engineering.

Wang, W.C. , Shen, H.W. (1980) " Statistical Properties of Alluvial Bed Forms " , Proceedings of the Third International Symposium on Stochastic Hydraulics , Tokyo, Japan , pp. 371.

Yalin, M.S. (1964) " Geometrical Properties of Sand Waves " , Journal of the Hydraulics Division , ASCE , Vol. 90 , No. HY5 , pp. 105-119.

Yalin, M.S. (1977) " Mechanics of Sediment Transport " . Pergamon Press , Braunschweig , Germany , 1st edition 1972 , 2nd edition 1977.

Yalin, M.S. (1987) " On the Formation Mechanism of Dunes and Ripples " , Institut für Wasserbau undt Wassermengenwirtschaft und Versuchsanstalt für Wasserbau, Oskar v. Miller - Institut in Obernach , Technische Universität , München , Bericht Nr. 59 , pp. 81-94.

Yalin, M.S. , Karahan, E. (1979) " Steepness of Sedimentary Dunes " , Journal of the Hydraulics Division, ASCE , Vol. 105 , No. HY4 , pp. 381-392 .

Zippe, H.J. , Graf, W.H. (1983) " Turbulent Boundary Layer Flow over Permeable and Non-Permeable Rough Surfaces ", Journal of Hydraulic Research, Vol.21, No. 1

BIBLIOGRAPHY

Hollick, M. (1976) " Boundary Shear Stress Measurement by Preston Tube " , Technical Notes , Journal of the Hydraulics Division , ASCE , Vol. 102 , No. HY7 , pp. 1053-1057.

Krishnappan, B.G. (1984) " Laboratory Verification of Turbulent Flow Model " , Journal of Hydraulic Engineering , ASCE , Vol. 110 , No. 4 , pp. 500-514.